

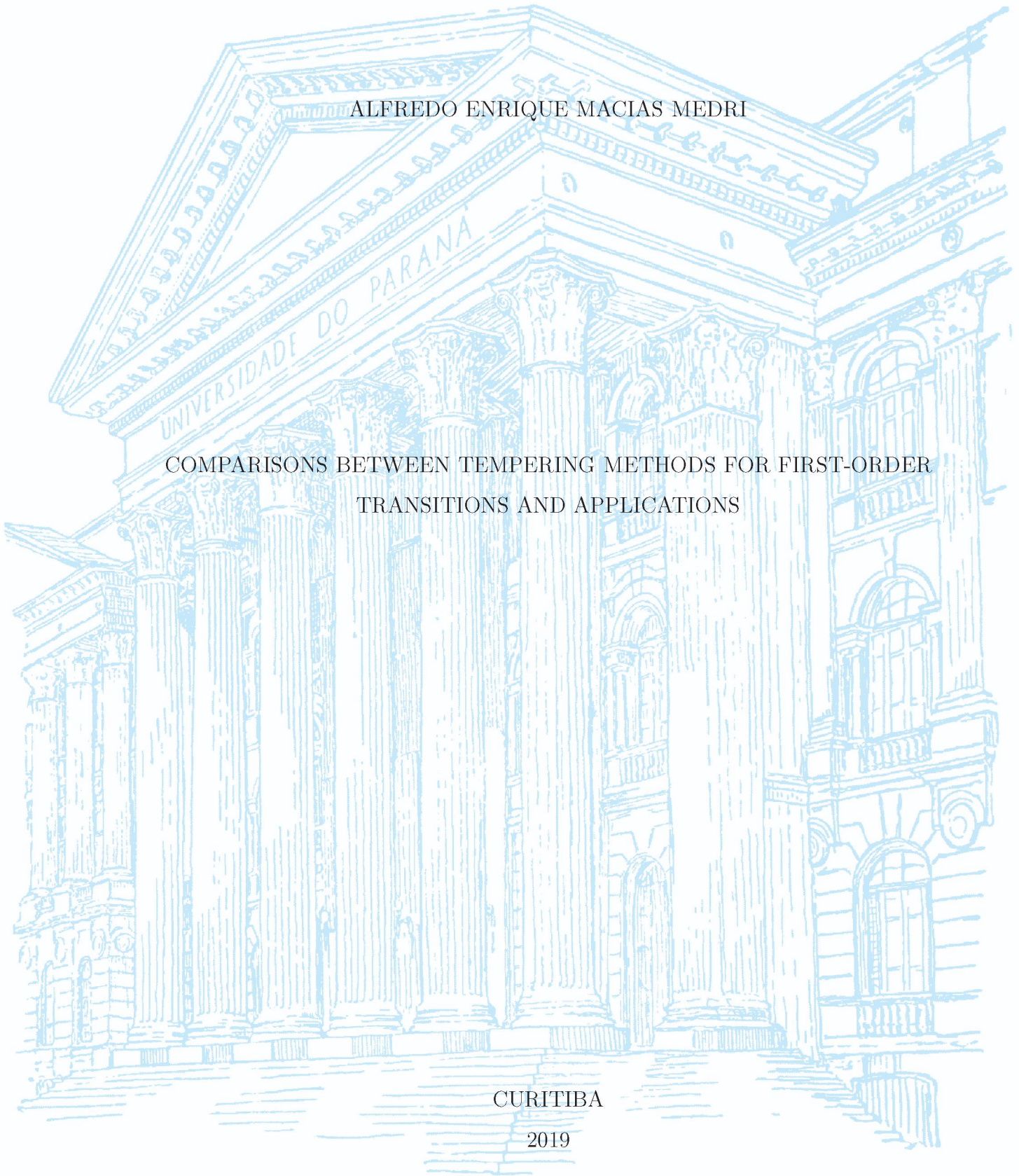
UNIVERSIDADE FEDERAL DO PARANÁ

ALFREDO ENRIQUE MACIAS MEDRI

COMPARISONS BETWEEN TEMPERING METHODS FOR FIRST-ORDER
TRANSITIONS AND APPLICATIONS

CURITIBA

2019



ALFREDO ENRIQUE MACIAS MEDRI

COMPARISONS BETWEEN TEMPERING METHODS FOR
FIRST-ORDER TRANSITIONS AND APPLICATIONS

Tese de doutorado apresentada ao curso de Pós-Graduação em Física, Setor de Ciências Exatas, da Universidade Federal do Paraná, como requisito final para a obtenção do título de Doutor em Física.

Orientador: Prof. Dr. Marcos Gomes E. da Luz
Coorientador: Prof. Dr. Carlos Eduardo Fiore

CURITIBA

2019

Catálogo na Fonte: Sistema de Bibliotecas, UFPR
Biblioteca de Ciência e Tecnologia

M492c

Medri, Alfredo Enrique Macias

Comparisons between tempering methods for first-order transitions and applications [recurso eletrônico] / Alfredo Enrique Macias Medri. – Curitiba, 2019.

Tese - Universidade Federal do Paraná, Setor de Ciências Exatas, Programa de Pós-Graduação em Física, 2019.

Orientador: Marcos Gomes Eleutério da Luz – Coorientador: Carlos Eduardo Fiore.

1. Monte Carlo, Método de. 2. Algoritmos. 3. Gibbs, Energia livre de. 4. Temperatura. I. Universidade Federal do Paraná. II. Luz, Marcos Gomes Eleutério da. III. Fiore, Carlos Eduardo. IV Título.

CDD: 530.15

Bibliotecário: Elias Barbosa da Silva CRB-9/1894

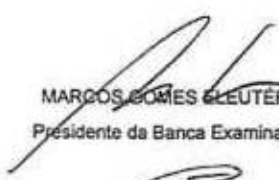



MINISTÉRIO DA EDUCAÇÃO
SETOR SETOR DE CIÊNCIAS EXATAS
UNIVERSIDADE FEDERAL DO PARANÁ
PRÓ-REITORIA DE PESQUISA E PÓS-GRADUAÇÃO
PROGRAMA DE PÓS-GRADUAÇÃO FÍSICA - 40001016020P4


TERMO DE APROVAÇÃO


Os membros da Banca Examinadora designada pelo Colegiado do Programa de Pós-Graduação em FÍSICA da Universidade Federal do Paraná foram convocados para realizar a arguição da tese de Doutorado de **ALFREDO ENRIQUE MACIAS MEDRI** intitulada: "**Comparisons between tempering methods for first-order transitions and applications**", após terem inquirido o aluno e realizado a avaliação do trabalho, são de parecer pela sua aprovação no rito de defesa. A outorga do título de doutor está sujeita à homologação pelo colegiado, ao atendimento de todas as indicações e correções solicitadas pela banca e ao pleno atendimento das demandas regimentais do Programa de Pós-Graduação.

CURITIBA, 28 de Fevereiro de 2019.


MARCOS GOMES CLEUTÉRIO DA LUZ
Presidente da Banca Examinadora (UFPR)


WAGNER FIGUEIREDO
Avaliador Externo (UFSC)


JOAO ANTONIO PLASCAK
Avaliador Externo (UFMG)


RICARDO LUIZ VIANA
Avaliador Interno (UFPR)

AGRADECIMENTOS

À minha família, principalmente meus pais, Alfredo Mario Macías Pérez e Gladys Medri de Macías, pelo estímulo desde o primeiro momento, pelos apoios que foram determinantes em minha caminhada no doutorado, e pelo suporte emocional e material que possibilitaram a minha dedicação à academia. Esta conquista também é de vocês.

Ao meu orientador, Prof. Dr. Marcos Gomes E. da Luz, pelo incentivo, pela confiança, pelo acompanhamento, pela paciência durante esses anos, e pela oportunidade de trabalhar com ele.

Ao meu coorientador, Prof. Dr. Carlos Eduardo Fiore, pelas frutíferas conversas, pelos valiosos ensinamentos que me foi dado, e pela ajuda para implementar os algoritmos.

Aos meus amigos de doutorado, Samuel Domenech de Cândido, Edjan A. da Silva e Carlos Fábio O. Mendes, pelas conversas, pelo companheirismo e pelas dicas. Deixo-lhes o meu sincero desejo de realizações e concretização de projetos profissionais e de vida.

Ao Programa de Pós-Graduação em Física da Universidade Federal do Paraná, pelos grandes ensinamentos, atenções e colaborações na minha formação.

À Organização dos Estados Americanos (OEA) em parceria com a Coordenação de Aperfeiçoamento de Pessoal de Nível Superior (CAPES) pela concessão da bolsa, possibilitando a realização do curso de doutorado e o desenvolvimento deste trabalho.

RESUMO

Nessa tese apresentamos comparações e avaliações dos recentes desenvolvimentos nos métodos de *Simulated-Tempering* (ST) com simulações de Monte Carlo, implementando três modelos de rede: Blume–Emery–Griffiths (BEG), Bell–Lavis (BL) e Potts. O método de ST tem atraído muitos pesquisadores há vários anos, devido a sua capacidade de lidar com sistemas cujo espaço de fase é difícil de amostrar ergodicamente. Implicitamente, existem alguns fatores que otimizam o algoritmo ST, como os pesos probabilísticos $g_r = g(T_r)$ e um conjunto de R réplicas $\Upsilon_R = \{T_1, T_2, \dots, T_R\}$. Para analisar esses fatores, na primeira parte, fazemos uma revisão dos elementos envolvidos durante a coexistência de fase e transições de fase. Também nesta parte, nós introduzimos alguns aspectos sobre o método de Monte Carlo para simular transições de fase de primeira ordem. Dois novos métodos são apresentados e implementados para otimizar as simulações ST: (1) Um esquema para calcular os fatores de peso por meio da integração termodinâmica direta da energia interna, e (2) um novo método para determinar o conjunto de temperaturas Υ_R , com base nas probabilidades de transição do esquema de ST. Posteriormente, apresentamos os modelos de rede BEG, BL e Potts. Finalmente, mostramos alguns resultados com métodos de ST na coexistência de fase e transições de fase de primeira ordem para avaliar a eficiência de cada modelo e método.

Key-words: Métodos de Monte Carlo, algoritmo *Simulated-Tempering*, transições de fase de primeira ordem, integração numérica para a energia livre, réplicas probabilísticas de temperatura.

ABSTRACT

This thesis compares and evaluates recent developments in tempering approaches for Monte Carlo simulations, by implementing three lattice models: Blume–Emery–Griffiths (BEG), Bell–Lavis (BL) and Potts. Simulated Tempering (ST) method has been attracting many researchers for several years, due to its capability to deal with systems whose phase space are difficult to sample ergodically. Implicitly, there are some factors that optimizes the ST-algorithm such as probabilistic weights $g_r = g(T_r)$ and a set of R replicas $\Upsilon_R = \{T_1, T_2, \dots, T_R\}$. In order to analyze these factors, in the first part, we make a review of the elements involved during phase coexistence and phase transitions. We introduce some aspects about the Monte Carlo method to simulate first-order phase transitions in this part also. Two new methods are presented and implemented to optimize ST simulations: (1) a scheme to calculate the weight factors by means of the direct thermodynamic integration of the internal energy, and (2) a new method to determine the set of temperatures Υ_R , based on the transition probabilities of the ST scheme. Later, we present the lattice models BEG, BL and Potts. Finally, we show some results with simulated tempering methods in the phase coexistence and first-order phase transitions to evaluate efficiency for each model and method.

Key-words: Monte Carlo methods, simulated tempering algorithm, first-order phase transitions, numerical integration to obtain the free energy, temperature probabilistic replicas.

List of Figures

2.1	Phase diagram (pressure versus temperature) of a typical substance . . .	25
2.2	Qualitative pressure versus molar volume isotherms predicted by cubic equation of state	26
2.3	Schematic representation and some qualitative results of the Ising model in a square lattice	28
2.4	Phase diagrams for the Ising model for (A) applied magnetic field vs temperature, and (B) lattice magnetization $\langle M \rangle$ vs T with $H = 0$. . .	30
3.1	Illustration of a path in the phase diagram (order parameter versus phase transition parameter control) to avoid crossing a FOPT	43
3.2	Flowchart of the complete algorithm with the ST method and the MA	43
4.1	Exemplification of a contour with a fixed exchange frequency in the T_i-T_j map	52
5.1	Schematic representation of the BL model with some water molecules in the triangular lattice	57
5.2	Two possible orientations of the molecule on a triangular lattice in the BL model, and sublattices	57
6.1	The partition function Z versus temperature T (in J units) for the Ising model with $H = 0$	63
6.2	Contours of the weight difference $g_r - g_{r'}$ values (horizontal axis are T_r and vertical axis are $T_{r'}$) for the Ising model with $H = 0$ and $N = 16 \times 16$	64
6.3	Results obtained for the BEG model by using SA simulations and the TMM, with $K = 3$, $J = 1$, $H = 0$, $\mu = -8$ and $N = 18 \times 18$	65

6.4	Results obtained for the BL model by using SA simulations (10^8 MC steps in each point) and the TMM, with $\epsilon_{\text{hb}} = 1$, $\epsilon_{\text{vdw}} = 0.1$ and $N = 18 \times 18$	66
6.5	Pressure computed by two ways for the three lattice models	67
6.6	Map contours for different exchange frequencies $f_{r \rightarrow r'}$ to the BEG, BL and Potts models between two replicas T_r and $T_{r'}$	69
6.7	The plots show the map contours of logarithm of the exchange probability $\exp(M_{r,r'})$ between two replicas T_r and $T_{r'}$, for the BEG, BL and Potts models	70
6.8	Replicas for the BEG model with two methods: CE and FEF	71
6.9	The same as in Fig.6.8, but for the BL model.	71
6.10	Values of the replicas computed by means of FEP	72
6.11	For the Potts model with $q = 16$, replicas T_r calculated with the DTI method and the three schemes to compute Υ_R (CE, FEF, FEP).	72
6.12	For the BEG model at the phase coexistence ρ and m simulated with the ST algorithm for $\Upsilon_{R=3}$ ($T_1 = 0.5$) obtained from three distinct values of Δs , f and $M_{r,r'}$	73
6.13	Evolutions of ρ and $ m $ in ST simulations for the BEG model ($N = 18 \times 18$) and distinct values of R and with the optimal values of Δs , f and $-M_{r,r'}$	74
6.14	The same as in Fig.6.13, but for the BL model with $T_1 = 0.1$	75
6.15	Long evolutions of ρ and m in the ST simulations ($T_1 = 0.5$, $R = 3, 4, 5$) for the BEG model with TMM and for CE, FEF and FEP methods	76
6.16	The same as in figure 6.15, but for the BEG model with DTI. It can not see a significant difference with respect to the TMM.	76
6.17	The same as in figure 6.15, but for the BL model with TMM, $T_1 = 0.1$ and $R = 5, 6, 7$. The values obtained for the magnetization m turned out to be very small (10^{-7}), and for this reason, we have rescaled these values in the graphs.	77
6.18	The same as in figure 6.17, but for the BL model with DTI.	77
6.19	For BEG model and $R = 3$, the probability distribution histogram of ρ and m in each replica at the coexistence for the CE, FEF and FEP methods	78
6.20	The same as in figure 6.19, but for the BL model with $R = 5$	79

6.21	Recognition of a first order phase transition through the intersection of ρ or u versus μ (BEG and BL) and H (BEG) for three different values of volume $V = N$	80
6.22	For the Potts model ($N = 18 \times 18$), internal energy u versus temperature T . This curve was obtained by through a SA simulation with 200 points of temperature.	81
6.23	For the Potts model, Internal energy versus temperature with the SA method and the MA. Evolutions of ϕ and m in ST simulations with $T_1 = 0.75$ and $R = 3$	81

List of Tables

1	LIST OF ACRONYMS	
2.1	Critical exponents for the Ising model ($\nu, \alpha, \beta, \gamma, \delta$ and η)	31

Table 1: **LIST OF ACRONYMS**

Abbreviation	Meaning	Page(s)
MCM	Monte Carlo Method	3, 24
PRN	Pseudo-Random Number	3
MA	Metropolis Algorithm	3, 27
ST	Simulated Tempering	6, 29
SSPD	Singular Segments in the Phase Diagram	11
FOPT	First-order phase transition	13
MFT	Mean-Field-Theory	17
TMM	Transfer Matrix Method	31
DTI	Direct thermodynamic integration	37
CE	Constant interval of Entropy method	39
FEF	Fixed Exchange Frequency protocol	40
FEP	Fixed Exchange Probability method	41
BEG	Blume-Emery-Griffiths model	44
BL	Bell-Lavis model	45
PP	Physical Principles	7
AC	Algorithm Conditions	7
WSRSS	When the Simulations Reach the Steady State	42

Contents

1	Introduction	14
2	Phase transitions: Basic concepts	21
2.1	Phases, boundaries and transitions	22
2.2	Ferromagnetic Transitions	27
2.3	Order parameters and critical exponents	30
2.4	Transitions close to the coexistence	32
3	Monte Carlo methods	35
3.1	Ergodicity and detailed balance	36
3.2	MA and simulated annealing	38
3.3	Simulated Tempering	40
3.4	Transfer Matrix Method	42
4	New perspectives on ST method	47
4.1	Expected values of the weights	48
4.2	Choosing replicas	50
4.2.1	Constant interval of entropy	50
4.2.2	Fixed Exchange Frequency	51
4.2.3	Fixed exchange probability	52
5	Some lattice models	54
5.1	Blume–Emery–Griffiths model	55
5.2	Bell–Lavis model	57
5.3	Potts model	59

6	Results and Discussions	61
6.1	Ising model	62
6.1.1	Partition function	62
6.1.2	Thermodynamic weights	63
6.2	Entropy for the BEG model	64
6.3	Gibbs–Duhem integration for the BL model	66
6.4	Pressure for the BEG, BL and Potts model	67
6.5	Exchange frequencies and probabilities	68
6.6	Replicas	70
6.7	ST simulations for the BEG and BL models	73
6.8	Probability distributions	78
6.9	FOPT for the BEG and BL models	79
6.10	ST simulations for the Potts model	80
7	Conclusions	82
8	References	85

Chapter 1

Introduction

Advances towards a general understanding and universal analytical characterization of disordered systems and of systems with many degrees of freedom has been limited. The relatively few exact solutions and the restrictions of mean-field approaches¹ call for development of powerful numerical methods to simulate large systems. One special technique comprises computer simulations based on statistical sampling, such as Monte Carlo Methods (**MCMs**). The essential ideas behind MCM were developed by Nicholas Metropolis and coworkers at Los Alamos National Laboratory in the USA during the World War II (for the Manhattan Project) as part of solution to a problem in statistical physics [3]. The mentioned work involved the simulation of probabilistic problems of hydrodynamics concerning the diffusion of neutrons in fission material. In parallel, John von Neumann and Stanislaw Ulam refined the generation of pseudo-random numbers (**PRN**) and methods of task division. Later, in 1948 Enrico Fermi, Metropolis himself and Ulam obtained estimators for the characteristic values of the Schrödinger equation for nuclear neutron capture.

To solve the involving problem of neutrons transport in a complex medium is a clear example of the indispensable necessity of employing stochastic process simulations by means of MCMs, such as the Metropolis Algorithm (**MA**). Before each Monte Carlo sampling with the MA, one particle is chosen randomly and it can change its state through probabilistic rules. From such simulation scheme, the infinite possible

¹In the mean-field theory, each particle is assumed to interact with the mean of all particles. This means that such an approximation can only be valid when fluctuations are unimportant, or when the Hamiltonian includes long-range forces, or when the interacting elements are not punctual (extended particles) (more details in [1]_{§4.5} [2]_{§6.5}).

positions of each neutron are statistically modeled by a large finite set of PRN with density probabilities for capture and scattering states (two simple Markov chains²). Considering appropriate averages, the Los Alamos group was able to determinate the system mean energy, and so, a macroscopic equation of state. It would be almost impossible to obtain a microscopic analytical theory to describe the states for each neutron.

Certainly, MCMs should be implemented mostly when neither analytic nor deterministic methods are workable or efficient. Generally a statistical treatment applied to a system made of N components (e.g., moles, molecules, spins, sites, etc.) leads to quantities whose statistical fluctuations go with $1/\sqrt{\text{number of elements}}$. Therefore, one general domain of application of MCMs is to systems with many degrees of freedom and far from strong perturbative regimes. However, such systems are precisely the ones of interest in quantum field theory and statistical mechanics (the latter subject being the focus of our work). In fact, currently the MCM is used to solve problems in several fields such as statistical physics [5–7], quantum many-body physics [8–10], medical physics [11–13], X-ray imaging [14, 15], chemistry [16, 17], agriculture [18, 19], finance [20], weather prediction [21, 22], solid state physics [23] and other areas (see, for example, [24, 25]).

MCMs are classified —from a classical point of view— as static or dynamic and their applicability depends on the specific problem being analyzed. In static methods, a sequence of statistically independent samples are generated with a desired probability distribution \tilde{p} . The static protocols are extensively used in Monte Carlo numerical integration in spaces of not-too-high dimension [26]_{§5}. But they are inapplicable for most situations in quantum field theory and statistical physics, where \tilde{p} is a constant probability³ specified by the system complicated evolution (for example, determined by high interfacial energies).

In the dynamic MCMs, one can consider for the problem a Markov chain with the state space S having \tilde{p} as its unique equilibrium distribution. So, simulations for

²In a Markov process, the probability distribution of future states depends only upon the present state, namely $\mathcal{P}(\sigma_t|\sigma_{t-1}, \sigma_{t-2}, \dots, \sigma_0) = \mathcal{P}(\sigma_t|\sigma_{t-1})$, where σ_t is the configuration of the system at time t . A Markov chain is a class of Markov process with discrete state space (more details in [4]_{§2}).

³Usually, \tilde{p} is the Gibbs measure which is a generalization of the canonical ensemble to infinite systems, namely, \tilde{p} is equal to equation 1.1 where ψ is a PRN (more details in [27]).

this stochastic process can be implemented (on computer) in principle starting from arbitrary initial configurations. Once the system has reached equilibrium, one can perform time averages, which converge to \tilde{p} -averages. Therefore, with such a numerical protocol we are “creating” an effective stochastic time evolution which somehow emulates the real system. The hope is that at the end we obtain macroscopic quantities correctly describing the properties of the original problem.

One of the most common usage for dynamic MCM is to study the thermodynamics of statistical models defined on a “lattice”, usually obeying an excluded volume constraint [28]. Thus, the simulated particles occupy only the positions of lattice nodes. The classical or quantum states of each particle (occupational, orientational, multiple spin-values or more complex states) are modeled through different variables contained in a Hamiltonian. From these classes of problems, it is possible to model anti/ferromagnetic systems (Ising model [29] [5]_{§2.1}), spin glass (a particular case with the Blume–Emery–Griffiths model is studied in Refs. [30, 31], but the general properties are described by means of the XY model [32]), fluid phase of water (Bell–Lavis model [33, 34]), crystalline solids [35], lattice polymers [36], molecular self-assemblies [37], soluble systems [38], dissemination of culture [39], charge transport [23], and others.

Most simulation studies considering MCMs (for example MA) and molecular dynamics work with the canonical ensemble, assuming microscopic states $\{\psi_1, \psi_2, \dots\} = \psi$ distributed according to the Boltzmann distribution

$$\tilde{p}[\psi] = Z^{-1} \exp\left(-\frac{\mathcal{H}[\psi]}{k_B T}\right), \quad (1.1)$$

where Z is the canonical partition function, \tilde{p} is probability to each distinct microstate, \mathcal{H} is the Hamiltonian of the system, k_B is the Boltzmann constant and T is the absolute temperature. Although this choice (equation 1.1) relies on strong and well grounded physical concepts, many applications aimed at a reliable computation of free energies end up resulting in poor estimates [40]_{§3.2.1}. Also, problems with quasi-ergodicity are observed for canonical Boltzmann sampling (see, for example, [41] and [40]_{§8}). Even worse, high correlation time can lead to a relative slow evolution (spinodal decomposition, for example) when canonical methods are considered (a simple instance is

illustrated in [42]).

Given this scenario, a variety of numerical methods have been proposed to overcome these drawbacks, such as Cluster Monte Carlo Algorithms [43] [44]_{§2} and multicanonical simulations [45–47]. In the first case, the configurations of particles in the lattice are implemented through non-local samplings by means of cluster algorithms, hence differing from the MA. Nonetheless, the growth of the cluster size has a specific algorithm for each application with a particular phase space, thus being far from an universal approach.

For systems with high free energy barriers, the multicanonical approach can be used. The multicanonical method uses a different choice for the probabilities, namely,

$$\tilde{p}[\psi] = \frac{1}{\mathcal{D}(\mathcal{H}[\psi])}, \quad (1.2)$$

which thus depend on the density of states function \mathcal{D} . In fact, the Wang and Landau algorithm [48] is normally used to obtain the density of states $\mathcal{D}(\mathcal{H})$ during the simulation. So, the generated states are equally distributed on the phase space and the simulation cannot see any “rough energy landscape”, because every energy is treated equally. Subsequently, the original canonical distribution is reobtained after a reweighting process. The drawback is that this last step often involves certain difficulties in the case of large systems.

Recently, more straightforward stochastic methods, such as Parallel Tempering [49] and Simulated Tempering (**ST**) [50], have been employed for systems with rough energy landscapes. Actually, in order to generate ergodic paths at low temperatures, both tempering protocols use relevant information at higher temperatures. The main idea of these approaches is based on the fact that it is easier to visit distinct regions of the phase space when the temperature is increased. In this way, a back and forth increment of the temperature along a run avoids the simulation to remain in local minima (or temporally homogeneous Markov process [4]_{§2}). In the Parallel Tempering algorithm, the configurations of N parallel systems are exchanged between two or more different temperatures, whereas the temperature becomes a dynamic parameter discreetly changing for each iteration in the ST-algorithm.

In ST implementations, the probability of temperature change $\mathcal{P}_{r \rightarrow r'}$ depends

on thermodynamic weights $g_{r'} - g_r = g(T_{r'}) - g(T_r)$ (with $r, r' = 1, 2, \dots, R$) and on a finite set of pre-fixed temperature (replicas) $\Upsilon_R = \{T_1, T_2, \dots, T_R\}$. Usually, the numerical convergence of the order parameter \mathcal{W} strongly depends on the exact Υ_R and the number of iterations. Presently, there are some procedures proposed in the literature to calculate the main ingredients, namely, the g_r 's, the number of replicas R , and the temperature values T_r . In each method to establish Υ_R is defined and used a control parameter ξ , whereby the T_r 's are determined (it is explained in detail in section 4.2). The linear searching of the ξ -value with which one gets the best tunneling, say ξ_* , should be performed by means of N_ξ ST-simulation series (for ξ ranging from ξ_i to ξ_f), which might involve high computational effort if the mentioned ingredients are not fine tuned.

A frequency-based protocol to obtain the replica values T_r was recently published by Valentim [51, 52]. In the procedure indicated therein, the number of replicas R and the T_r 's were determined by the direct sighting of a fixed exchange frequency $\xi \rightarrow \nu_{r,r'}$ between two temperature values T_r and $T_{r'}$. Nevertheless, the method implies that a previous ST-simulation series must be run before to perform the search for the optimal value $\nu_{r,r'} = \nu_*$. In other schemes, such as the constant entropy method, the procedures to compute Υ_R are implemented without previous simulations. However, these approaches are less efficient than Valentim's protocol.

In the constant entropy method, the control parameter is an entropy interval $\xi = \Delta s$, and the T_r 's are computed by using the entropy as a function of the temperature $s(T)$. On the other hand, as it is common in generalized-ensemble simulations, the weights g_r are not a-priori known and their estimator has to be calculated. One way to do so is through the transfer matrix method, and only when g_r and the internal energy are obtained, then the entropy can be inferred from thermodynamic relationships.

From the above, it becomes clear the following. First, (i) the ST is an important method to address different systems having more complicated phase space landscapes (in special to study aspects related to phase transitions). Second, (ii) there are different technical issues involved in the ST general approach (e.g., number of replicas, how to calculate the thermodynamical weights, the correct setting of the temperatures) which once proper established, in principle can lead to higher computational performance. And third, (iii) for the protocol implementation itself (i.e., the principles used to set

the temperatures T_r and to promote the jumps between them) there are mainly two different ways to go. One based on physical principles (**PP**) (for instance, to choose the T_r 's considering thermodynamical quantities like entropy). The other based just on algorithm conditions (**AC**), say, defining the T_r 's simply from procedural considerations (like to fix a certain frequency of changes between the replicas).

An extremely pertinent question is then to identify how from (i)-(iii) one can improve the ST method efficiency, getting better numerical results with less computational effort. In particular, the point (iii) relates to a fundamental question in computational physics, namely, which type of rules in a given simulational method could yield superior outcomes, those from PP or from AC? As we have mentioned, on one hand the PP protocols try to mimic actual physical processes (for instance, choosing the temperatures for the ST replicas so to correspond to effective increases of the system entropy). On the other hand, the AC protocols rely on pure probabilistic rates of configurations shifts. It might seem that PP would be better since the simulation code is somehow closer to the real dynamics of the system [53–55]. Nevertheless, “generic” algorithms (i.e., logic- and probabilistic-based ones) can present a greater performance in solving certain statistical physics problems [56–58] as well as some problems with a collective behavior similar to natural processes, but in fact outside the physics realm [59–61].

Therefore, our general goal in the present work is to investigate the points (i)–(iii) above, looking for more appropriate implementations of the ST method. More concretely, since $\mathcal{P}_{r \rightarrow r'}$ strongly depends on g_r , here an exact thermodynamic-based approach to compute $g_{r'} - g_r$ is introduced and implemented, in such a way that the TMM no longer is required. Also, we present a novel method to calculate Υ_R . It is based on exchange probabilities which are directly derived from endowing optimal values for $\mathcal{P}_{r \rightarrow r'} \mathcal{P}_{r' \rightarrow r}$. Further, we consider the issues related to (iii) and compare the efficiency of the ST method implemented through the PP and AC guidelines. At least for the models studied in this contribution, we find that the AC protocol tends to give better results.

To these purposes, this Doctoral Thesis is organized as the following. Chapter 2 gives a background on the study of phase transitions and applications in ferromagnetic systems. In Chapter 3 we describe the standard Monte Carlo method and some of its variations to simulate first order phase transitions. In Chapter 4 is presented the two

main contributions of this work: the calculations of $g_{r'} - g_r$ with a thermodynamic approach, and the novel method to compute Υ_R by a probabilistic scheme. In Chapter 5 a review is made on three models to be implemented in MCMs with ST-algorithm: Blume–Emery–Griffiths, Bell–Lavis and Potts. The Chapter 6 presents the results and discussions about Ising-model, Blume–Emery–Griffiths, Bell–Lavis and Potts. Finally, in Chapter 7, we drawn the conclusions of this thesis highlighting our most important findings and briefly mentioning perspectives for future developments.

Chapter 2

Phase transitions: Basic concepts

Phase transition is a change in a structural feature of a physical system (for instance, readjustment of the spatial organization of the system constituents), commonly involving the emission or absorption of energy and resulting in a transformation to another “state”. Transitions between states of matter (eutectic, eutectoid and peritectic transformations) are present in thermodynamic systems, where the density of mass is a transition parameter that change with temperature, pressure, and/or others macroscopic variables. In other systems such as semiconductor alloys, magnetic materials, complex fluids, granular matter, etc, the transition can be described via order parameters (from the Landau Theory) characterizing the local order in the system. Depending on the physical system, the order parameters can statistically indicate the existence of one or more phases when some thermodynamic parameters are fixed. In this case, the phase coexistence occurs at the same time, and its is separated by a boundary surface called interface. In complex fluids like emulsions, foams, aerosols and particle dispersions, the interfacial energy is several orders of magnitude higher than the bulk energy [62]_{§11}. So, the study of coexistence of phases is very important to understand natural and industrial processes, given that these phenomena are ubiquitous in nature and involved in innumerable industrial transformations production processes (food, metallurgy, drugs, etc).

One of the most important applications of MCMs in condensed matter physics is the study of phase transitions (see for example [5]_{§2.1.2}, [40]_{§7.3} and [63]): one wishes to estimate for which parameter values a phase transition occurs; one wishes to distinguish

whether a transition is of first order or of second order; and one wishes to characterize precisely the properties of a transition. For a second order transition, this means the estimation of the critical exponents and critical amplitudes [5]_{§2.1.2.3} [64]; for a first order transition, this means the estimations of the magnitudes of jump of various first derivatives of the free energy at the transition [5]_{§2.1.2.3} [1]_{§2.5}, such as order parameter or energy (latent heat), for instance.

This chapter describes the main features of phase transitions from the mean-field-theory (**MFT**) point of view. As an illustration, we will consider phase transitions in the Ising model, one of the simplest, yet not trivial [65], system in theoretical statistics physics (see Figure 2.3). Exact solutions for the Ising model will be a reference to test the accuracy of the results obtained in this thesis.

2.1 Phases, boundaries and transitions

Generally the system of interest is specified as some spatial region $\Omega[\varphi]$ (with volume V_Ω and surface S_Ω), for φ the set of all microstates. It is reasonable to consider that $V_\Omega \propto L^d$ and $S_\Omega \propto L^{d-1}$, where L is some characteristic linear size and d is the dimensionality of the system. From a statistical mechanics point of view, in the region Ω the classical Hamiltonian can be defined as

$$\beta\mathcal{H}_\Omega = -\sum_n \Lambda_n \Theta_n, \quad \text{where } \beta^{-1} \equiv k_B T, \quad (2.1)$$

$k_B \approx 1.38 \times 10^{-23} J/K$ is the Boltzmann constant, T is the temperature (in Kelvin scale, K), Λ_n are the coupling constants and the Θ_n are the energies corresponding to a particular process in the system (usually given as combinations of the dynamical degrees of freedom which are summed over in the partition function). The Λ_n constants are the external parameters, such as fields, exchange interaction parameters, temperature, etc. In finite systems with strong potential energies, the Hamiltonian \mathcal{H}_Ω can be computed as a sum of N_I contributions where each one involves a type of interaction. As an example, in the Ising model we have $\beta\mathcal{H}_\Omega \rightarrow \mathcal{H}$, $N_I = 2$, $\Theta_1 = \sum_i \sigma_i$, $\Theta_2 = \sum_{\langle i,j \rangle} \sigma_i \sigma_j$, $\Lambda_1 = H$, and $\Lambda_2 = J$, where H is a external magnetic field and J is the energy interaction between spins (see figure 2.3).

In lattice models with N_Ω particles, the degrees of freedom are the spins σ_i on the lattice sites i , where $1 \leq i \leq N_\Omega = V_\Omega$. Thus the Θ_n are built out of combinations of the σ_i . In this context, the partition function for a canonical ensemble itself is given by

$$Z_\Omega(\Lambda_1, \Lambda_2, \dots) \equiv Z_\Omega[\Lambda] = \sum_{\sigma_1} \sum_{\sigma_2} \sum_{\sigma_3} \dots \sum_{\sigma_{N_\Omega}} e^{-\beta \mathcal{H}_\Omega}. \quad (2.2)$$

Each sum is over all states of each particle, so that Z_Ω contains a sum over all combinations of states of the system. Also, in the canonical ensemble, the free energy is defined by

$$F_\Omega[\Lambda] = -\beta^{-1} \ln Z_\Omega[\Lambda]. \quad (2.3)$$

Information on the thermodynamic properties of the system Ω is contained in the derivatives $\partial F_\Omega / \partial \Lambda_n$, $\partial^2 F_\Omega / \partial \Lambda_n \partial \Lambda_m$, etc, which include bulk effects (in the uniform matter), surface effects (in the heterogeneous matter), and finite-size effects (see for example reference [66]). However, if Ω is finite, there is no information about phase transitions or phases.

On the other hand, it is expected that the free energy will be extensive for large systems, namely

$$F_\Omega \approx V_\Omega f + S_\Omega \tilde{f} + O(L^{d-2}), \quad (2.4)$$

where f is the bulk free energy per unit volume or bulk free energy density and \tilde{f} is the surface free energy per unit area. We can give a precise definition of these important quantities as follows

$$f[\Lambda] \equiv \lim_{V_\Omega \rightarrow \infty} \frac{F_\Omega[\Lambda]}{V_\Omega}, \quad \tilde{f}[\Lambda] \equiv \lim_{S_\Omega \rightarrow \infty} \left\{ \frac{F_\Omega[\Lambda] - V_\Omega f[\Lambda]}{S_\Omega} \right\} \quad (2.5)$$

when the limits exist and are independent of Ω . For a system defined on a lattice, with N_Ω lattice sites, the bulk free energy per site are the same but with $V_\Omega = N_\Omega$. The limits in the above equation are known as the *thermodynamic limit*, and it means a consideration of the asymptotic statistical properties of a model system in which the linear dimensions are allowed to become infinite. Sometimes, an auxiliary constraint is imposed simultaneously to this limit. For example, in fluid systems, taking the limit $V_\Omega \rightarrow \infty$ is senseless unless one simultaneously takes the limit that the number of

particles N_Ω in the fluid also tends to infinity, in such a way that the density N_Ω/V_Ω stays constant.

Let us suppose that there are D coupling constants. The axes of the phase diagram are $\Lambda_1, \Lambda_2, \dots, \Lambda_D$, and hence the dimension of the phase diagram is D . Regions of analyticity of $f[\Lambda]$ are called **phases**. The possible non-analyticities of $f[\Lambda]$ are Singular Segments in the Phase Diagram (**SSPD**) (points, lines, planes, hyperplanes, etc) which have a dimensionality associated with them ($D_s = 0, 1, 2, \dots, D - 1$ respectively). An important invariant for each type of SSPD is the codimension $C \equiv D - D_s$. SSPD of codimension $C = 1$ (i.e. SSPD which separate phases) are called **phase boundaries**.

Since f is everywhere continuous with respect to Λ_n (a thermodynamic proof is presented in [62]_{§6.1}), transitions across the phase boundaries (varying Λ_n) can be classified as

1. **First-order phase transition (FOPT)**: One or more $\partial f/\partial\Lambda_n$ are discontinuous across a phase boundary.
2. **Continuous phase transition**: The only other remaining possibility for non-analytic behavior is that all $\partial f/\partial\Lambda_n$ are continuous across a diffuse phase boundary. This transition type is always defined with a thermodynamic critical point^{1,2}. If, in addition to that, one or more $\partial^2 f/\partial\Lambda_n^2$ are discontinuous, then this event is named as a **second-order phase transition** (following the so called Ehrenfest classification).

The definitions of phase transitions given above are ambiguous, because there may exist a path along which $f[\Lambda]$ is analytic going from one side of a phase boundary to the other. An example is the liquid–gas–solid phase diagram, shown in figure 2.1. Although it is not possible to pass from fluid to solid without encountering a phase

¹For example, a critical point is a point at the end of a biphasic curve. The most classical example is the liquid-vapor critical point. The end point of the pressure-temperature curve designates the final condition under which a liquid and its vapor can coexist.

²For example, one of the interesting phenomena occurring in a continuous phase transition is **critical opalescence**. At the critical point the compressibility $\kappa_T = -\frac{1}{V} \frac{\partial V}{\partial P}|_T$ (T =temperature, V =volume, P =pressure) is infinite and close to the critical point it is very large. So that, small fluctuations in the pressure P will cause large fluctuations in ρ , inducing tiny droplet formation that scatter light.

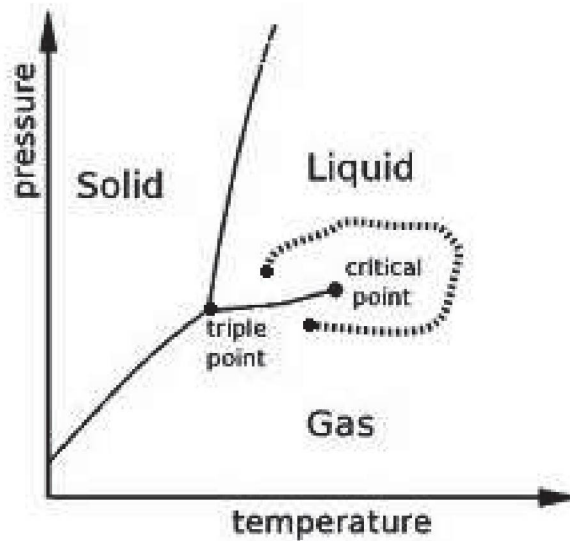


Figure 2.1: Phase diagram (pressure P vs temperature T) of a typical substance. For this case, both in the triple point and in the critical point, the codimension is $C = 2$. The solid–liquid phase boundary ($C = 1$) extends to arbitrarily high pressure, whilst the gas–liquid phase boundary ends at the critical point. The dashed curve represents a trajectory in the phase diagram along which no phase transition is encountered, even though a change of phase has apparently taken place.

transition, it is possible to choose a path in p – T space which goes from liquid to gas without encountering any singular behavior of the thermodynamic quantities.

The phase boundaries are commonly called coexistence curves in thermodynamics of fluids, because two phases can coexist in equilibrium when pairs of conjugate variables such as pressure and volume or chemical potential and number of particles are fixed. In a continuous medium, the phase coexistence as function of the position \vec{r} is usually described by means of a free energy functional as³ [68]_{§6.1,§6.2} [69, 70] [71]_{§2.3.1}

$$\mathcal{F}(\vec{r}) = \int \left\{ f(\rho) + \frac{\kappa}{2} |\nabla \rho|^2 \right\} d\vec{r}. \quad (2.6)$$

Here, ρ is the density of particles, $f(\rho)$ is the bulk free energy density and κ is the influence parameter which measures the effect of density gradients on the free energy of inhomogeneous systems [62]_{§11.1.4}. By minimizing equation 2.6, the resulting $\rho(\vec{r})$ should describe the density profile in the region comprising the interfacial energy.

³When the spatial density variations are not too strong, the scattering fority differences in the free energy functionals can be expanded in a Taylor’s series and truncated after a few terms. The result is that the distribution equation becomes a nonlinear differential equation instead of a nonlinear integral equation. This methodology is known as *density gradient theory*, and equation 2.6 is a result of the expansion. In order to obtain appropriate values of κ , experimental procedures measuring interfacial tension and wetting can be performed (see for example [62]_{§13.5} [67]).

For biphasic fluids (for example, van der Waals model) the coexistence *phase1-phase2* (for example, *liquid-gas*) presents spatial interfaces that separate clusters between phases with a free interfacial energy \tilde{f} (see equation 2.4) and characterized by the interfacial tension $\gamma_s \propto \kappa$ [62]_{§8.4} [72, 73]. When the temperature T is constant, theoretical values for the density of the bulk phases ρ_1 and ρ_2 can be computed by the conditions of thermodynamic equilibrium [62]_{§6.1} [2]_{§5.2}

$$P(\rho_1, T) = P(\rho_2, T), \quad \mu(\rho_1, T) = \mu(\rho_2, T), \quad (2.7)$$

$$P(\rho, T) = -f + \rho\mu, \quad \mu(\rho, T) = \left. \frac{\partial f}{\partial \rho} \right|_T, \quad (2.8)$$

where P and μ are the pressure and chemical potential at the bulk phases. As a consequence of equations 2.7 and 2.8, the Maxwell Construction Method is obtained (see Figure 2.2). So, a complete equilibrium thermodynamic description can be ob-

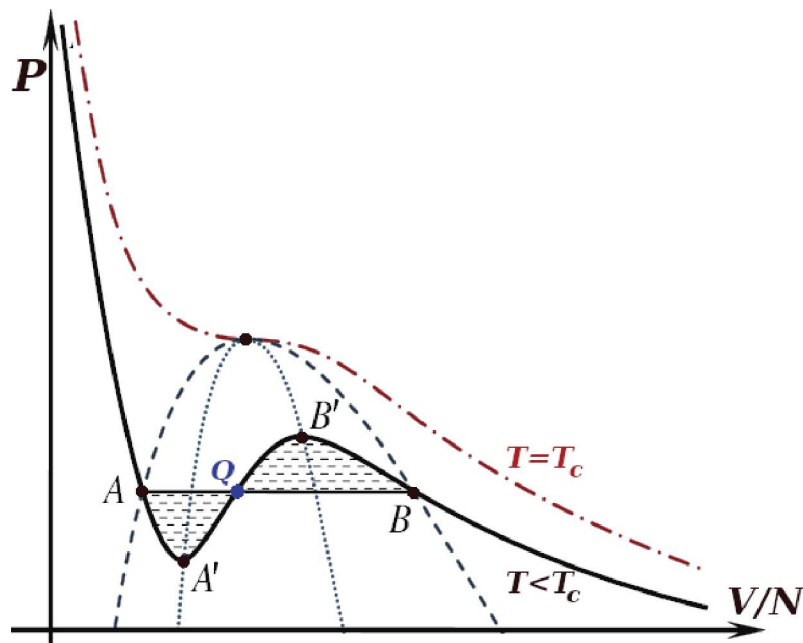


Figure 2.2: Qualitative pressure P versus molar volume V/N isotherms (constant T) predicted by cubic equation of state in V/N . N is the number of particles and its density is equal to $\rho = N/V$. The P - V states between A' and B' on the $T < T_c$ isotherm (solid line) are thermodynamically unstable. For $T = T_c$ (critical isotherm shown in dot-dashed line) and $T > T_c$ only a state can be found when P and V/N are fixed. There are also Maxwell construction for the binodal (dashed line) as well as spinodal (dotted line). The Maxwell construction method is based on the Gibbs–Duhem equation $SdT - VdP + Nd\mu = 0$ in thermodynamic equilibrium ($dT = 0$). Namely, one obtains $\mu_A - \mu_B = \int_A^B (V/N)dP = 0$, where equation 2.7 has been used. This integral implies a simple geometric construction (the area designated as $[AA'Q]$ has to be equal to $[QB'B]$) for finding two-phase equilibrium states.

tained once the bulk free energy $f(\rho, T)$ is known or determined. If each microscopic interaction between particles (given by a Hamiltonian \mathcal{H} like equation 2.1) is known, a classical statistical mechanics treatment to determine the partition function Z and, later, the relationship between f , ρ and T , can be developed.

Insomuch as the total number of configurations or combinations of microstates which assemble a macrostate, is $n_s^{N_\Omega}$ (where n_s is the number of possible microstate of a particle), Z turns out very difficult or even impossible to determine if n_s or N_Ω is a relatively large number. In this case, an alternative approach to calculate Z , once \mathcal{H} is known, is by means of numerical methods and using reasonable approximations. That is, if one can homogeneously discretize time and space such that a finite number of particles occupy a finite volume and microstate transitions take place during a reasonable time interval, then a simplified total internal energy $U = \langle \mathcal{H} \rangle$ can be computed as function of ρ and T . The relation $f(U)$ is described in section 4.1.

In this sense, the transformation of the free energy from a continuous system to a mean-field-theory approach results from [74]_{§6.5}

$$\int f(\rho) d\vec{r} \rightarrow \sum_i f(\rho_i) \quad \text{and} \quad \int |\nabla \rho|^2 d\vec{r} \rightarrow \sum_{\langle i,j \rangle} (\rho_i - \rho_j)^2. \quad (2.9)$$

2.2 Ferromagnetic Transitions

A ferromagnetic material without external magnetic field H is characterized by presenting a **spontaneous magnetization** at temperatures below a certain critical temperature T_c . When $H \neq 0$, the magnetization $\langle M \rangle$ versus magnetic field curve shows hysteresis, i.e. the ability to store information of which direction a sufficiently strong external magnetic field last pointed before dropping to zero field. That is why ferromagnets are widely used in computer memories, among other applications.

Toward the end of the 19th century the ferromagnetic transition was investigated quantitatively as a function of temperature by P. Curie at the University of Paris. He found experimentally that the susceptibility $\chi = \frac{\partial \langle M \rangle}{\partial H}$ of a ferromagnet depends on the temperature according to the simple law $\chi(T) = \frac{C}{T - T_c}$ where C is a constant (the Curie constant), and T_c is a critical temperature below which spontaneous magnetization shows up (Curie temperature). Physically, below T_c , the spontaneous symmetry begins

to break and magnetic moments become aligned with their neighbors. So, the Curie temperature is the temperature at the critical point in a second-order phase transition. The magnetic susceptibility is (theoretically) infinite and domain-like spin correlations fluctuate at all length scales.

Simulations of ferromagnetic phase transitions, especially via the Ising model (Figure 2.3), had a significant impact on the development of statistical physics. The two-dimensional Ising model [29] [5]_{§2.1} exhibits cooperative phenomena and has the attractive feature that it can be solved exactly. It has a direct bearing on order-disorder transitions occurring in alloys and ferromagnetic materials. It is composed of a square lattice whose sites can be occupied by magnetic spins that can be oriented up (\uparrow) or down (\downarrow). In the classical MA, the interactions between spins are calculated only including the nearest neighbors (four neighbors in a square lattice). In more complex

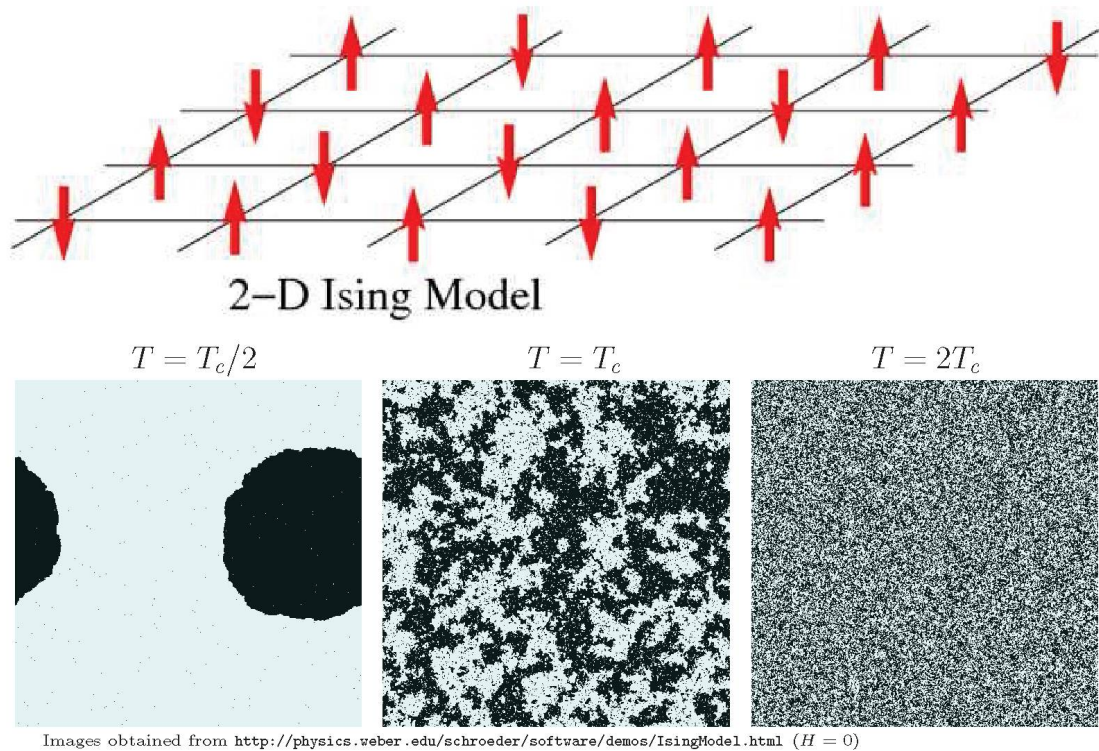


Figure 2.3: Schematic representation (upper figure) and some qualitative results of the Ising model (inferior panels) in a square lattice. As in the figure, the orientation of the spins (represented by arrows) are disordered ($T > T_c$), and therefore, the system is in a paramagnetic state. If spins are aligned in a regular pattern with neighboring spins pointing in opposite directions, the state is called antiferromagnetic. For example, in a one-dimensional lattice the antiferromagnetic state is $\cdots \uparrow\downarrow\uparrow\downarrow\uparrow\downarrow \cdots$. The inferior panels show qualitatively the steady state of simulations with the Metropolis algorithm for three temperatures. The system is ordered as the temperature increases (from left to right).

lattices the phase transitions can be distorted, where the critical exponents seem to vary with the disorder strength [75]. The total energy can take values according to the Hamiltonian $\mathcal{H} = -J \sum_{\langle i,j \rangle} \sigma_i \sigma_j - H \sum_i \sigma_i$, where J is the interaction energy, H is an external magnetic field, $\langle i, j \rangle$ are pairs of nearest neighbor and σ_i is the value of spin ± 1 . The probability $\tilde{p} = \exp(-\beta\mathcal{H})$ (where $1/\beta = k_B T$) is used in MA for a single flip spin. Macroscopic observables are computed once the equilibrium state is reached, such as internal energy $u = \langle \mathcal{H} \rangle$ and the lattice magnetization $\langle M \rangle = \frac{1}{N} \sum_{i=1}^N \sigma_i$. It is obtained $\langle M \rangle = 0$ for $\beta J \leq \beta_c J = [\ln(1 + \sqrt{2})]/2$ (critical temperature), and $\langle M \rangle \approx \pm 1$ for $T \approx 0$, when $H = 0$. Other quantities of interest such as the heat capacity $C = \frac{\partial u}{\partial T}$ or the magnetic susceptibility $\chi = \frac{\partial \langle M \rangle}{\partial H}$ can be computed indirectly. Even though \mathcal{H} is very simple for this ferromagnetic model, calculations of $\langle M \rangle$ at $T \approx T_c$ can be relatively imprecise, such as shown in recent studies [76].

It was first clearly shown that mean field theory approaches failed to predict the correct behavior at T_c . In the phase diagram of the Ising model there are five distinguishable regions:

- $\Omega_{<}^<$, at $T < T_c$ and $H < 0$: ferromagnetic phase with $\langle M \rangle < 0$,
- $\Omega_{<}^=$, at $T < T_c$ and $H = 0$: phase boundary of $\langle M \rangle$,
- $\Omega_{<}^>$, at $T < T_c$ and $H > 0$: ferromagnetic phase with $\langle M \rangle > 0$,
- $\Omega_{=}$, at $T = T_c$: ferromagnetic–paramagnetic critical point,
- $\Omega_{>}$, at $T > T_c$: paramagnetic phase (disorder),

If the value of applied magnetic field is gradually changed from H to $-H$ at $T < T_c$ (Figure 2.4.A), a first order phase transition takes place where the phase boundary is $\Omega_{<}^=$. In this case, the magnetization change abruptly $\langle M \rangle \rightarrow -\langle M \rangle$, the free energy remains constant $f \rightarrow f$, and the coexistence of domains (of \uparrow and \downarrow) are present in $\Omega_{<}^=$. If T is gradually changed from $T < T_c$ to $T > T_c$ (or otherwise), a continuous phase transition takes place. In this other case, the transition between the ferromagnetic (order) and paramagnetic (disorder) phases is diffuse at the phase boundary $\Omega_{=}$. The magnetization $\langle M \rangle$ is zero above the transition and is non-zero below the transition temperature. A quantity which varies in this way is referred to as an order parameter (see Figure 2.4.B).

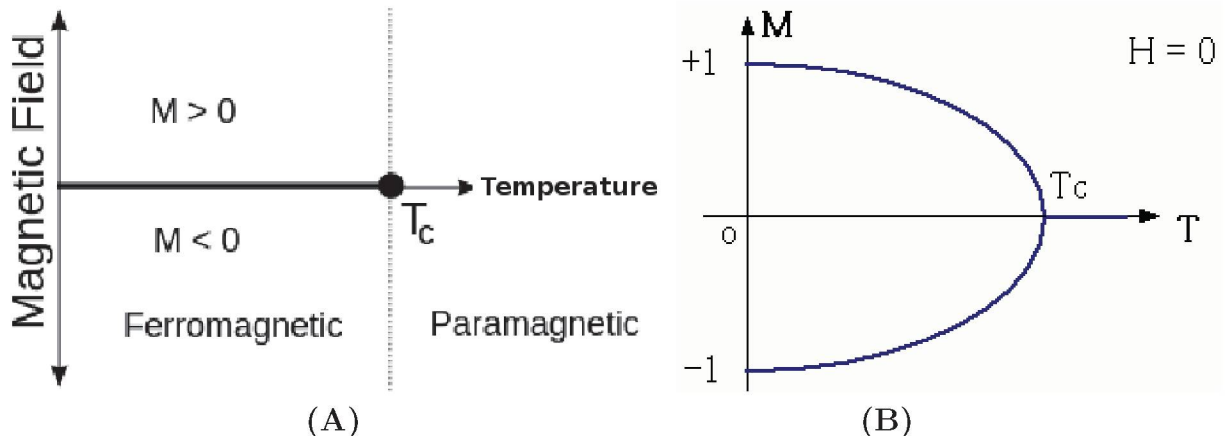


Figure 2.4: Phase diagrams for the Ising model for **(A)** applied magnetic field H vs temperature T , and **(B)** lattice magnetization $\langle M \rangle$ vs T with $H = 0$. The phase coexistence curve (at $H = 0$ and $T < T_c$) is shown in **(A)** as the line on the T -axis from $T = 0$ to $T = T_c$, which equilibrium values of $\langle M \rangle$ are shown in **(B)**. For $H \neq 0$ and $T < T_c$, the system exhibits ferromagnetic behaviors (ordered phase); while a paramagnetic behavior is observed for $T \geq T_c$ (disordered phase). For $H = 0$, spontaneous magnetization behavior as a function of T is present in the system of spins. The symmetry behavior of M (image **(B)**) for $T < T_c$) is a consequence of the no-preference of microstates $\uparrow\downarrow$ in the absence of any external magnetic field.

2.3 Order parameters and critical exponents

Mean-field theory (**MFT**) can give the so-called classical values for the critical exponents if one expands the equation of state near the critical point [1]_{§4}. The expansion parameter is the spontaneous magnetization in the case of a ferromagnetic system and the half-width of the coexistence curve in the case of a fluid system (see for example [62]_{§4.4}). Both quantities exhibit the same temperature dependence, and are good examples for the concept of an order parameter.

The order parameter for a given system is not unique. Any thermodynamic variable that is zero in the disordered phase and non-zero in an adjacent phase (on the phase diagram), is a possible choice for an order parameter (such adjacent phase is usually called the ordered phase). In a first-order phase transition, the order parameter \mathcal{W} changes abruptly in a specific range of some intensive parameter (example: H in the Ising model or μ in fluids). Whereas that in a continuous phase transition, the behavior of $\mathcal{W}(T)$ is smooth from $T = 0$ to $T = T_c$. For biphasic fluids (for example, van der Waals model) an appropriate order parameter considered in the Landau theory is $\Delta\rho \propto |\rho - \rho_c|$ where ρ is the volumetric mass density of the fluid, $2\rho_c \equiv \rho_l + \rho_g$, and

ρ_l and ρ_g are the mass densities of the liquid and gas at the coexistence, respectively. In this case ρ is non-zero in the disordered phase ($T > T_c$), but $\Delta\rho = 0$ because $\rho = \rho_l = \rho_g$.

The behavior of the order parameter, as well as of other thermodynamic quantities, has an universal character in the vicinity of the critical point. From Onsager's solution [77] (exact solution for the Ising model to an infinite square lattice), we know the power rules obeyed by several thermodynamic variables close to T_c (Table 2.1). Since for the correlation length we have $h \sim |\epsilon|^{-\nu}$ with $\nu = 1$ (where $\epsilon \equiv 1 - T/T_c$), then obviously h diverges near T_c in the thermodynamic limit. However, it is reasonable to assume that the correlation length has the same order of magnitude of finite lattices. Often, h is a measure of the cluster sizes when the system reaches equilibrium (for the Ising model, see images in Figure 2.3). From such analysis, it can be considered

Table 2.1: Critical exponents for the Ising model (ν , α , β , γ , δ and η). Here $\langle M \rangle$ is the magnetization, H is an applied magnetic field and $\epsilon \equiv (T - T_c)/T_c$. The correlation length h establishes a measure of some degree of interaction or "how far the interactions reach". If one flips a single spin from say \downarrow to \uparrow , h describes how far away will that flip affect the probabilities for finding other spins \downarrow or \uparrow . As a consequence, the correlation length diverges at the critical points ($h \rightarrow +\infty$ with $T \rightarrow T_c$), because the spins are strongly correlated when the phases are coexisting. On other hand, the correlation function $G(r)$ is a measure of the order in a system, which describe how microscopic variables at different positions are related. Even in the disordered phase, particles at different positions are correlated. Namely, if $r \ll \lambda$ ($r =$ distance between particles/spins, $\lambda =$ length scale), the interaction will yield some correlation between particles. At relatively high temperatures asymptotic and exponentially-decaying correlations are observed with increasing distance $G(r) \approx \exp(-r/\lambda)/r^{d-2+\eta}$.

Quantity	Behavior	Value of the exponents		
		$d = 2$ [65]§7.12	$d = 3$ [78]	MFT [2]§6.3
Correlation length	$h \sim \epsilon ^{-\nu}$	1	0.629	1/2
Specific heat	$C_V \sim \epsilon ^{-\alpha}$	logarithmic	0.113	jump
Order parameter	$\langle M \rangle \sim \epsilon ^\beta$	1/8	0.324	1/2
Susceptibility	$\chi \sim \epsilon ^{-\gamma}$	7/4	1.238	1
Equation of state	$\langle M \rangle \sim H^{1/\delta}$	15	4.82	3
Correlation function	$G(r) \sim 1/r^{d-2+\eta}$	1/4	0.031	0

that $h \approx L$ in finite systems when $T \approx T_c$. As a consequence, one obtains

$$|\epsilon| \sim L^{-1/\nu} \quad \Rightarrow \quad \left\{ \begin{array}{l} \frac{\partial u}{\partial T} \Big|_V = C_V \sim L^{\alpha/\beta} \\ \langle M \rangle \sim L^{-\beta/\nu} \\ \frac{\partial \langle M \rangle}{\partial H} \Big|_V = \chi \sim L^{\gamma/\nu} \end{array} \right. \quad (2.10)$$

The numbers α , β and γ are known as critical exponents of the system [79,80], and as an example, Table 2.1 gives the critical exponents for the Ising model.

According to modern statistical mechanics theory, quantities such as γ_s , κ_T and $\Delta\rho$ approach zero through universal scaling laws

$$\gamma_s \sim |\omega|^\zeta, \quad \kappa_T \sim |\omega|^{-\nu}, \quad \Delta\rho \sim |\omega|^\eta, \quad \omega = \left| \frac{\xi^* - \xi}{\xi^*} \right|, \quad (2.11)$$

where $\xi = \Lambda_n$ is a thermodynamic field variable (T for example), ξ^* is the value of ξ at its critical point (T_c for example), γ_s is the interfacial tension, κ_T is the compressibility and the constants ζ , ν and η are the critical exponents characterizing the fluid system.

2.4 Transitions close to the coexistence

As explained above, both the correlation length h and $\frac{\partial \mathcal{W}}{\partial \xi}$ (\mathcal{W} is the order parameter and $\xi = \Lambda_n$ is an external parameter) diverge to infinity in very large (or infinite) systems during a FOPT (see also [80]). In the previous cases, we had $\mathcal{W} = \langle M \rangle$ for the Ising model and $\mathcal{W} = \Delta\rho$ for a biphasic fluid. In other words, when the value of a thermodynamic field variable ξ is such that leads to a divergence, then we have a critical point at $\xi = \xi^*$. Nevertheless, in finite systems this condition is not met, and a different strategy is needed to find ξ^* .

The approach we present below was explained and applied by Fiore and da-Luz [81,82] to find the SSPD at $\xi \approx \xi^*$ in finite systems. However, the method is equally useful in the thermodynamic limit $V \rightarrow \infty$.

At low temperatures, the partition function can be expressed as [83,84]

$$Z = \sum_{n=1}^{\mathcal{N}} \alpha_n \exp(-\beta V f_n) + Z_u. \quad (2.12)$$

Z_u is associated to unstable phases (exponentially negligible), \mathcal{N} is the number of phases, $f_n = f_n(\xi)$ is the bulk free energy density of the n th phase, α_n are the degeneracy parameters from possible spatial symmetries and V is the volume.

On the other hand, it is noted that usually the starting point to calculate distinct order parameter is⁴

$$\mathcal{W}(\xi) \equiv -\frac{1}{\beta V} \frac{\partial}{\partial \xi} \ln Z = \frac{\sum_{n=1}^{\mathcal{N}} \alpha_n g_n \exp(-\beta V f_n)}{\sum_{n=1}^{\mathcal{N}} \alpha_n \exp(-\beta V f_n)} \quad (2.13)$$

where

$$g_n = T \frac{\partial}{\partial \xi} \left(\frac{f_n}{T} \right). \quad (2.14)$$

Now, suppose that other intensive parameters are kept fixed with proper values at the phase coexistence, such that the bulk free energies are single functions of ξ . Consequently, a first order series expansion around $y = \xi - \xi^* \approx 0$ for each f_n is

$$f_n \approx f^* + f_n'^* y, \quad f^* = f_n(\xi^*), \quad f_n'^* = \left. \frac{\partial f_n}{\partial \xi} \right|_{\xi=\xi^*}. \quad (2.15)$$

Thus, substituting equation 2.15 into equations 2.14 and 2.13 yields ($T_c = T^*$)

$$g_n \approx f_n'^* - \frac{f^*}{T_c} \frac{\partial T}{\partial \xi} \quad (2.16)$$

$$\mathcal{W}(\xi) \approx \frac{\sum_{n=1}^{\mathcal{N}} \alpha_n g_n \exp(-\beta V f_n'^* y)}{\sum_{n=1}^{\mathcal{N}} \alpha_n \exp(-\beta V f_n'^* y)} \frac{\exp(+\beta V f_1'^* y)/\alpha_1}{\exp(+\beta V f_1'^* y)/\alpha_1},$$

$$\mathcal{W}(\xi) \approx \frac{b_1 + \sum_{n=2}^{\mathcal{N}} b_n \exp(-a_n y)}{1 + \sum_{n=2}^{\mathcal{N}} c_n \exp(-a_n y)}, \quad (2.17)$$

$$a_n = (f_n'^* - f_1'^*) V \beta, \quad c_n = \frac{\alpha_n}{\alpha_1}, \quad b_n = c_n g_n.$$

The coefficients a_n , b_n and c_n are independent of ξ , but depend on ξ^* , $f_n'^*$, T and other system parameters. Note that only the a_n 's are functions of V (linearly). So, during the phase coexistence ($y = 0$) all the curves $\mathcal{W}(\xi \neq V)$ should cross at $\xi = \xi^*$, which

⁴Typically relevant thermodynamic quantities have that form. For example: if $\xi = \mu$, the density follows directly from $\rho = -\mathcal{W}$, if $\xi = \beta$, the energy per volume is $u = \beta \mathcal{W}$, and if $\xi = V$ then the pressure is $P = -\mathcal{W}/V$.

regarding the values of \mathcal{W}^* , correspond to

$$\mathcal{W}^* = \mathcal{W}(\xi^*) = \frac{\sum_{n=1}^{\mathcal{N}} b_n}{\sum_{n=1}^{\mathcal{N}} c_n} = \sum_{n=1}^{\mathcal{N}} \tilde{c}_n f_n^* - \frac{f^*}{T_c} \frac{\partial T}{\partial \xi}, \quad \tilde{c}_n = \frac{c_n}{\sum_{n=1}^{\mathcal{N}} c_n} \quad (2.18)$$

In a symmetric two-phase system ($\mathcal{N} = 2$ and $\alpha_1 = \alpha_2$), we have

$$\mathcal{W}^* \approx \frac{1}{2} \left(\left. \frac{\partial f_1}{\partial \xi} \right|_{\xi=\xi^*} + \left. \frac{\partial f_2}{\partial \xi} \right|_{\xi=\xi^*} \right) - \frac{f^*}{T_c} \frac{\partial T}{\partial \xi}. \quad (2.19)$$

From equation 2.19, the lattice magnetization for the Ising model can be calculated with $\xi = H$ and $\mathcal{W} = \langle M \rangle$, namely

$$\langle M \rangle^* = \left. \frac{1}{2} \frac{\partial (f_- + f_+)}{\partial H} \right|_{H=H^*}, \quad (2.20)$$

where f_{\pm} are the free energy densities when all spin are \uparrow or \downarrow . The values of f_{\pm} are determined at $T = 0$ as⁵

$$f_{\pm} = \left. \frac{F_{\pm}}{V} \right|_{T=0} = \left. \frac{U_{\pm} - TS_{\pm}}{V} \right|_{T=0} = \langle \mathcal{H} \rangle_{\pm} = - \left(\frac{z}{2} J \pm H \right) \quad (2.21)$$

F_{\pm} are the volumetric free energies, U_{\pm} are the internal energies, $S_{\pm} = 0$ are the entropies and z is the number of nearest neighbors for each node or **the coordination number**⁶. Finally, we obtain $\partial f_{\pm} / \partial H = \mp 1$ that implies $\langle M \rangle^* = 0$.

Obviously, there are other methods to characterize phase transitions of lattice models (see for example [85]). But the approach here discussed is very appropriate for the purposes of the present work.

⁵Here, we have assumed stable phases and we have used

$$\mathcal{H} = -J \sum_{\langle i,j \rangle} \sigma_i \sigma_j - H \sum_i \sigma_i$$

with

$$\langle \sum \sigma_i \sigma_j \rangle = z/2, \quad \langle \sum \sigma_i \rangle = \pm 1.$$

⁶The coordination number of a central particle is the number bonded to it. The usual value of the coordination number for a given structure refers to a particle in the interior of a lattice with z neighbors in all directions. For example, in 2D lattices, $z = 4$ for a rectangular and $z = 6$ for a triangular.

Chapter 3

Monte Carlo methods

Monte Carlo methods (**MCMs**) are a broad class of computational approaches based on stochastic procedures to solve distinct problems. The method is mainly used in mathematical and/or physical problems that might be deterministic in principle. It finds many usages involving optimization, numerical integration, and generating draws from distinct probability distributions. MCMs are particularly useful in lattice models to simulate specific physical systems (characterized by Hamiltonians).

Computational algorithms with very simple structures are implemented in all MCMs. The first step in any Monte Carlo algorithm is to generate a set of N realizations $r_1(t), r_2(t), \dots, r_N(t)$ of the Markov process $\Theta(t)$. For a given value of t , these realizations are just sample values of the random variable $\Theta(t)$. Since the probability density function $\mathcal{P}(r, t|r_0, t_0)$ of $\Theta(t)$ is usually not known, we cannot expect to generate these sample values by subjecting $\mathcal{P}(r, t|r_0, t_0)$ to any of the conventional random number generating methods. Practical Monte Carlo simulation schemes produce sample values of $\Theta(t)$ by more complex procedures, that essentially emulate the actual time evolution of the process. That is, the i -th realization of the process $\Theta(t)$ generally consists of a set of sample values $r_i(t_0), r_i(t_1), r_i(t_2), \dots$ of the process at successive instants t_0, t_1, t_2, \dots . Once a set of realizations $\{r_i(t)\}$ has been generated, then virtually any dynamical quantity can be numerically estimated (by using time averages for example).

3.1 Ergodicity and detailed balance

The MCM is a method using probability arguments and PRNs to perform calculations. In treating physical systems, it provides estimates of observables, such as the internal energy and magnetization. In the canonical ensemble, the thermal average is expressed as

$$\langle Q \rangle = Z^{-1} \sum_{\varphi_1, \varphi_2, \dots} Q_n e^{-\beta E_n}, \quad Z = \sum_{\varphi_1, \varphi_2, \dots} e^{-\beta E_n}, \quad (3.1)$$

where $\{\varphi_1, \varphi_2, \dots\}$ is a set of all configurations of the system, $E_n = E(\varphi_n)$ is the energy of the system in n -state, $Q_n = Q(\varphi_n)$ is the value of the corresponding observable, $e^{-\beta E_n}$ is the Boltzmann weight and Z is the partition function. The state space might be huge in the thermodynamic limit because there are infinite states. But, if we were to choose states from the phase space according to some probability $\tilde{p}_n = \tilde{p}(\tilde{\varphi}_n)$ (with $\tilde{E}_n = E(\tilde{\varphi}_n)$ and $\tilde{\varphi}_n = \tilde{\varphi}_n[\varphi_n]$), we would get

$$\langle \tilde{Q} \rangle = \frac{\sum_{\tilde{\varphi}_1, \tilde{\varphi}_2, \dots} \tilde{Q}_n e^{-\beta \tilde{E}_n} / \tilde{p}_n}{\sum_{\tilde{\varphi}_1, \tilde{\varphi}_2, \dots} e^{-\beta \tilde{E}_n} / \tilde{p}_n}, \quad (3.2)$$

and for $\tilde{p}_n \propto e^{-\beta \tilde{E}_n}$ (**importance sampling**) we obtain

$$\langle \tilde{Q} \rangle \rightarrow \langle Q \rangle = \frac{1}{\mathcal{M}} \sum_{m=1}^{\mathcal{M}} Q_m, \quad (3.3)$$

where \mathcal{M} is the number of configurations with probability \tilde{p}_m . Here, the gain is that the estimate of $\langle Q \rangle$ does not include states contributing little to the average, since there are rarely picked by \tilde{p}_m .

In order to construct a Markov process with the **transition probabilities** $\mathcal{P}_{m \rightarrow m'}$ (from m -microstate to m' -microstate) according to \tilde{p}_m , we need two conditions to be fulfilled: ergodicity and detailed balance. The ergodicity condition¹ (or property) is satisfied only if

$$\mathcal{P}_{m \rightarrow m'} > 0, \quad \text{and} \quad \mathcal{P}_{m' \rightarrow m} > 0, \quad m \neq m' = 1, \dots, \mathcal{M}, \quad (3.4)$$

¹An ergodic dynamical system is one that has the same behavior averaged over time and space of all the states in the phase space. In other words, a random process is ergodic if the time average is the same as the average over the probability space, known as the ensemble average. As a consequence, the final state of an ergodic process is independent of its initial state.

This means that it is possible for the system to reach any microstate from any other microstate. An ergodic process is necessary to ensure that the algorithm can pass through all states if one runs long enough simulations, such that $\langle Q \rangle$ includes every states with \tilde{p}_m probability.

The detailed balance ensures that the Markov process reaches the equilibrium distribution. At first glance, one may think that the equilibrium state is already achieved if the total probability balance holds true, namely,

$$\sum_m \tilde{p}_m \mathcal{P}_{m \rightarrow m'} = \sum_{m'} \tilde{p}_{m'} \mathcal{P}_{m' \rightarrow m}.$$

Unfortunately, this condition can also lead to non-equilibrium limit cycles or dynamic equilibriums. These possibilities are running out when for each term pair of microstates m and m' we have [26]^{§9.3}

$$\tilde{p}_m \mathcal{P}_{m \rightarrow m'} = \tilde{p}_{m'} \mathcal{P}_{m' \rightarrow m}, \quad m \neq m' = 1, \dots, \mathcal{M}. \quad (3.5)$$

Equation 3.5 is called **detailed balance**² The ratio of the transition probabilities reads

$$\frac{\mathcal{P}_{m \rightarrow m'}}{\mathcal{P}_{m' \rightarrow m}} = \frac{\tilde{p}_{m'}}{\tilde{p}_m} = e^{-\beta(E_{m'} - E_m)}. \quad (3.6)$$

Since MC iterations involve two stages to change the microstate of a particle, the total probability should contain two contributions. A general expression for $\mathcal{P}_{m \rightarrow m'}$, which contains both selection and acceptance/rejection processes, is [86]

$$\mathcal{P}_{m \rightarrow m'} = \mathcal{S}_{m \rightarrow m'} \mathcal{A}_{m \rightarrow m'}. \quad (3.7)$$

The selection probability $\mathcal{S}_{m \rightarrow m'}$ is used to choose a new possible microstate and the acceptance probability $\mathcal{A}_{m \rightarrow m'}$ is implemented to accept or reject the microstate. If the possible combinations of the selection probability have reversal symmetries $\mathcal{S}_{m \rightarrow m'} =$

²A rigorous deduction is in [4]^{§6.4.A}. In summary, equation 3.5 is obtained by minimizing $\frac{\partial}{\partial t} \mathcal{P}_{m \rightarrow m'}$, where $\mathcal{P}_{m \rightarrow m'} = \sum_{n=-\infty}^{n=+\infty} \mathcal{P}_{m \rightarrow n} \mathcal{P}_{n \rightarrow m'}$ is the **Chapman-Kolmogorov equation** and $m = m(t)$ is the numbered configuration at time t .

$\mathcal{S}_{m' \rightarrow m}$, equation 3.6 is simplified as

$$\frac{\mathcal{A}_{m \rightarrow m'}}{\mathcal{A}_{m' \rightarrow m}} = e^{-\beta(E_{m'} - E_m)}. \quad (3.8)$$

Also, the values of $\mathcal{S}_{m \rightarrow m'}$ should be normalized, namely

$$\sum_{m' \neq m=1}^{\mathcal{M}} \mathcal{S}_{m \rightarrow m'} = 1. \quad (3.9)$$

Equation 3.9 warrants that the system try to visit all the possible combinations of microstates. However, the change of internal energy of the system is performed with a probability given by the equation 3.8.

3.2 MA and simulated annealing

One of the most widely used and simplest MCMs is the Metropolis Algorithm (**MA**). This section presents the “plain” MA in the case of a single spin update, i.e. only one spin can be flipped at each attempt. It is important to mention that the MA is not restricted to this type of dynamics, because it can handle multiple updates. But in the context of single updates, the MA establishes a direct way to choose $\mathcal{P}_{m \rightarrow m'}$. Generating new configurations by single spin updates create successive samplings that are strongly correlated; however, it is necessary to perform many iterations for a significant evolution of the system.

Let's suppose that each spin (not necessarily on a lattice) can take the discrete values³

$$\sigma_i = \sigma_{(v)}, \quad i = 1, \dots, N, \quad v = 1, \dots, q. \quad (3.10)$$

N is the number of particles and q is the number of possible values. Since just one spin is flipped, the energy difference $E_{m'} - E_m = \mathcal{H}_{(v')} - \mathcal{H}_{(v)}$ depends only on the possible spin state change. Note that the values of the symmetric selection probabilities are given by $\mathcal{S}_{(v) \rightarrow (v')} = \mathcal{S}_{(v') \rightarrow (v)} = 1/(q-1)$. So, the transition probability between two

³For the Ising model $q = 2$ and $\sigma_{(v)} = 2v - 3$, for BEG $q = 3$ and $\sigma_{(v)} = v - 2$, for Potts $\sigma_{(v)} = v - 1$, and for BL $q = 3$ and $(\sigma\tau)_{(v)} = v - 2$.

states of a chosen spin is

$$\mathcal{P}_{(v)\rightarrow(v')} = \left(\frac{1}{q-1} \right) \min\{1, e^{-\beta[\mathcal{H}_{(v')} - \mathcal{H}_{(v)}]}\}, \quad (3.11)$$

where $\mathcal{H}_{(v)}$ is the Hamiltonian of the original configuration. The equation 3.11 satisfies the detailed balance, since

$$\frac{\mathcal{P}_{(v)\rightarrow(v')}}{\mathcal{P}_{(v')\rightarrow(v)}} = \frac{\frac{1}{q-1} \min\{1, e^{-\beta[\mathcal{H}_{(v')} - \mathcal{H}_{(v)}]}\}}{\frac{1}{q-1} \min\{1, e^{-\beta[\mathcal{H}_{(v)} - \mathcal{H}_{(v')}]}\}} = e^{-\beta[\mathcal{H}_{(v')} - \mathcal{H}_{(v)}]}, \quad (3.12)$$

for any case of $\mathcal{H}_{(v)}$ and $\mathcal{H}_{(v')}$. Also, note that the ergodicity condition (equation 3.4) is satisfied. Therefore, one Monte Carlo step for the MA can be implemented as follows:

1. Randomly choose a spin with value $\sigma_i = \sigma_{(v)}$ (in a lattice, one needs choose a node).
2. If $q > 2$, randomly choose a possible new state $v' \neq v$ with selection probability $\frac{1}{q-1}$.
3. Calculate the energy difference $\Delta\mathcal{H} = \mathcal{H}_{(v')} - \mathcal{H}_{(v)}$, where $\mathcal{H}_{(v')}$ is calculated supposing that the chosen spin has changed its state to $\sigma_{(v')}$.
4. If $\Delta\mathcal{H} \leq 0$, then σ_i changes from $\sigma_{(v)}$ to $\sigma_{(v')}$. Otherwise, a normalized PRD φ_1 is generated, and if $\varphi_1 \leq e^{-\beta\Delta\mathcal{H}}$, then σ_i changes from $\sigma_{(v)}$ to $\sigma_{(v')}$.

For one Monte Carlo iteration, one step (Monte Carlo step) should be executed N times in order to obtain an average evolution of the system (N is the number of particles or nodes in a lattice). It is expected that after “many” iterations, the system will reach a reasonable equilibrium condition or a steady state, which can be quantified by means of the discrete-time autocorrelation function⁴ [52]_{§3.2}. If we shall

⁴When a simulation is run from $t = 0$ to $t = N_{MC}$ iterations (MC steps), the discrete-time autocorrelation function C_t for the t MC steps is given by [87]

$$C_t = \frac{1}{(N_{MC} - t)(\langle Q^2 \rangle - \langle Q \rangle^2)} \sum_{k=1}^{N_{MC}-t} (Q_k - \langle Q \rangle)(Q_{k+t} - \langle Q \rangle),$$

where $t < N_{MC}$, $\langle Q^2 \rangle - \langle Q \rangle^2$ is the variance and $\langle Q \rangle$ is the average of the observable Q . This estimator C_t is a measurement of how strongly Q is correlated in the time (iteration), or it is an indicator about how Q_{k+t} depends on Q_k . If $Q_k \approx \langle Q \rangle$ for several values of k , the autocorrelation is drastically decreased. So, the condition $C_t \rightarrow 0$ is good indicator of the steady state.

obtain the curve $\langle Q \rangle_\xi = \mathcal{W}(\xi)$, it will be necessary to perform several simulations varying $\xi = \xi_1, \xi_2, \dots$ to get $\mathcal{W} = \mathcal{W}_1, \mathcal{W}_2, \dots$

In this sense, we can take advantage of the fact that the configuration of equilibrium $\varphi_l(t \rightarrow \infty)$ of the simulation- l with a fixed value $\xi = \xi_l$ can be introduced as a initial configuration of the system $\varphi_{l'}(t = 0)$ into another simulation- l' with $\xi = \xi_{l'}$, where t is the current Monte Carlo step. Namely, if $\xi_1 < \xi_2 < \dots < \xi_{N_\xi}$ or $\xi_1 > \xi_2 > \dots > \xi_{N_\xi}$, then $\varphi_{l+1}(t = 0) = \varphi_l(t \rightarrow \infty)$ from $l = 0$ to $l = N_\xi - 1$, where $\varphi_0(t = 0)$ is the unique start configuration and N_ξ is a number of intervals of ξ . This procedure is commonly known as **simulated annealing (SA)** [44]_{§10}. For example, if $\xi = T$ and $N_T = \frac{T_{N_T} - T_0 + 1}{\Delta T}$, where T_{N_T} , T_0 and ΔT are pre-fixed values of temperatures, then

$$\begin{aligned} \varphi_0 &= \varphi_{[T_{N_T}]}, \\ \varphi_1 &= \varphi_{[T_{N_T-1}]}, \\ &\dots \\ \varphi_l &= \varphi_{[T_{N_T-l}]}, \\ &\dots \\ \varphi_{N_T} &= \varphi_{[T_0]}. \end{aligned}$$

Later, we would start the simulations with a random configuration for φ_0 (disordered system). Whereas that the remaining simulations should be initialized as $\varphi_l(t = 0) = \varphi_{[T_{N_T-l}]}(t \rightarrow \infty)$ where $\varphi_{[T_{N_T-l}]}(t \rightarrow \infty)$ is the configuration obtained from a simulation with “many” iterations.

3.3 Simulated Tempering

The SA-algorithm is used as a statistical predictor for only one global minimum of \mathcal{H} , i.e. we can compare the values of the energy after many SA runs and if the probability of ending at the global minimum is not too small in a given instance, the SA may be considered a rather efficient algorithm for that instance. However, if the absolute minimum has a small basin of attraction and is separated from the large local minima by very high barriers, the SA may not be a good choice of some simulation protocol.

As an illustration, in the Ising model we can observe that there are two values of the lattice magnetization (see Figure 2.4.B) at the phase coexistence (region $\Omega_{\pm}^{\bar{}}$). Therefore, by using only one SA simulation it is almost impossible to obtain the two phases at low values of T because the barrier to change from $\langle M \rangle = f_{\pm}$ to f_{\mp} is very high (see equation 2.21). Even though the MA is ergodic, the algorithm would remain fixed in just one global minimum ($\langle M \rangle = f_{+}$ or $\langle M \rangle = f_{-}$). Only when a sufficiently large set of SA simulation are performed, we would observe $\langle M \rangle = f_{\pm}$ with the same statistics.

The method we explain in this section is meant to overcome these difficulties. Also constituting in a distinct scheme to the minimize free energy. The main idea of the Simulated Tempering (**ST**) method [50] consists of changing the temperature while remaining at equilibrium: This contrasts with the SA method, where every change of the temperature drives the system out of equilibrium.

First of all, in this scheme the space of configurations is enlarged by assuming the temperature T as a dynamic variable of the system. It can range through a set of ordered values $\Upsilon_R = \{T_1, T_2, \dots, T_R\}$ where $T_n < T_{n+1}$ and R is the number of **replicas**. For some replica r (at $\beta_r = 1/k_B T_r$), the physical system is described by the dimensionless Hamiltonian

$$\bar{\mathcal{H}}_r[\sigma] \equiv \beta_r \mathcal{H}[\sigma] - g_r, \quad (3.13)$$

where $\sigma = \{\sigma_1, \sigma_2, \dots, \sigma_N\}$ is the configuration of the system and g_r are weights related to free energy (see section 3.4), which must be calculated or a-priori assigned.

The exact form of equation 3.13 follows from supposing the probability distribution $\mathcal{P}_r[\sigma]$ to be proportional to $\exp(-\bar{\mathcal{H}}_r[\sigma])$. Therefore, the probability of having a given value of r goes with

$$\mathcal{P}_r \propto Z_r e^{g_r} \equiv \exp(-\beta_r f_r + g_r), \quad (3.14)$$

where the Z_r are the partition functions at given β_r , and the f_r are the corresponding free energies [62]_{§2.5}. Notice that if $g_r = \beta_r f_r$ all replicas have the same probability.

Along the simulations the temperature changes (from r to r') can take place considering a transition probability given by the equations 3.6, 3.14 and $\mathcal{H}[\sigma] = T_r S[\sigma] + f_r$,

or

$$\mathcal{P}_{r \rightarrow r'} = \mathcal{S}_{r \rightarrow r'} \min\{1, e^{(\beta_r - \beta_{r'})\mathcal{H}[\sigma] + g_{r'} - g_r}\}, \quad (3.15)$$

where the selection probability $\mathcal{S}_{r \rightarrow r'}$ values depend on the number of replicas during one transition (see below). So, a complete ST algorithm is generally implemented as three steps procedure, repeated a given number of times:

1. At a temperature T_r the MA is used to promote the transition of the configuration $\sigma = \{\sigma_1, \sigma_2, \dots, \sigma_N\} \rightarrow \{\sigma'_1, \sigma'_2, \dots, \sigma'_N\} = \sigma'$. After N_* iterations performed, the system is expected to reach a state close to the steady one.
2. Randomly, it is chosen the next possible replica. For example, $r' \rightarrow r + 1$ or $r' \rightarrow r - 1$ with the same probability and so $\mathcal{S}_{r \rightarrow r'} = 0.5$ (note that transitions to temperatures lower than T_1 and greater than T_R are automatically rejected since T_R and T_1 are the maximum and minimum temperatures in Υ_R).
3. An attempt to change the replica temperature (from T_r to $T_{r'}$) is made according to the acceptance probability. For so
 - (a) We need to calculate $-\Delta\bar{\mathcal{H}} \equiv (\beta_r - \beta_{r'})\mathcal{H}[\sigma] + g_{r'} - g_r$.
 - (b) If $\Delta\bar{\mathcal{H}} \leq 0$, then the temperature changes from T_r to $T_{r'}$. Otherwise, a normalized PRD φ_2 is generated. If $\varphi_2 \leq e^{-\Delta\bar{\mathcal{H}}}$, the temperature changes from T_r to $T_{r'}$.

The goal of this algorithm is to get out from a local minimum of energy to land into another too many times, in such a way as to avoid crossing directly a FOPT (see Figure 3.1). Whenever the simulation jumps to a local minimum, the algorithm will be able to measure order parameters. The complete algorithm (joining MA and the ST method) is shown in the flowchart in figure 3.2.

3.4 Transfer Matrix Method

In this thesis, one of our goals is to compare ST implementations using either the transfer matrix method or direct calculations of the statistical weights for the probabilities.

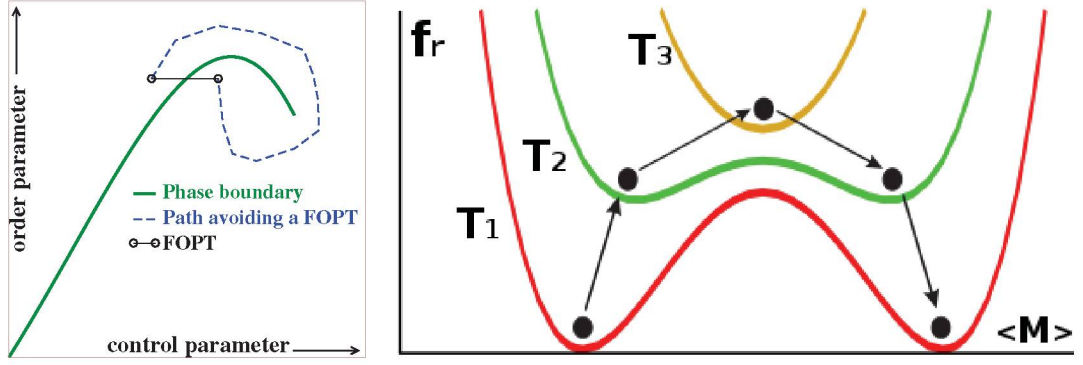


Figure 3.1: *Left*: Illustration of a path (dashed line) in the phase diagram \mathcal{W} (order parameter) versus ξ (phase transition control parameter) to avoid crossing a FOPT. The solid line represents the coexistence curve, where a FOPT takes place. *Right*: Example of the temperature exchange mechanism used in the ST algorithm for the Ising model (taken from the reference [52]), where f_r is the free energy and $\langle M \rangle$ is the magnetization.

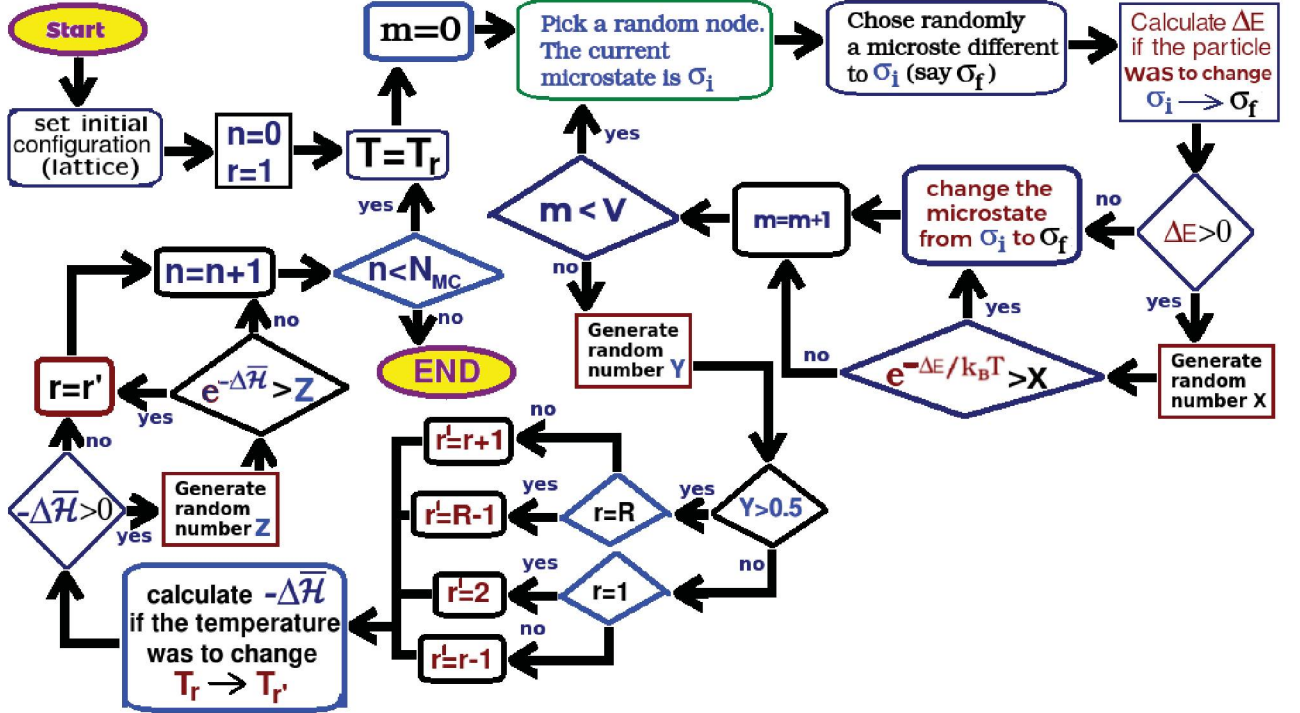


Figure 3.2: Flowchart of the complete algorithm with the simulated tempering method and Metropolis algorithm (MA). There are three PRN, which are generated in order to try to change the spin microstate (X), calculate the selection probability (Y) and try to change the temperature (Z).

Thus, in this section it is worth to present an overview of the transfer matrix method (TMM) [88] and how this method is used to compute Z in lattice models.

A general Hamiltonian of a regular lattice, with spins distributed as σ_{ij} , can be

written as

$$\mathcal{H}[\varphi] = \sum_{k=1}^K \mathcal{H}[\mathcal{L}_k, \mathcal{L}_{k+1}], \quad (3.16)$$

$$\mathcal{L}_k \equiv \{\sigma_{1,k}, \sigma_{2,k}, \dots, \sigma_{L,k}\}, \quad \varphi = \{\mathcal{L}_1, \mathcal{L}_2, \dots, \mathcal{L}_K\},$$

where \mathcal{L}_k is the state configuration of the k th layer, K is number of layers in the lattice, L is the number of nodes in each layer and $\mathcal{L}_{K+1} = \mathcal{L}_1$ (periodic boundary condition). Generally, as “layers” we mean parallel hyperplanes composed by all the sites along that spatial region of the lattice. The K layers hence comprise the entire collection of the system sites.

In the canonical ensemble, the probability $P[\varphi] = P[\mathcal{L}_1, \mathcal{L}_2, \dots, \mathcal{L}_K]$ for the layer 1 to have the configuration \mathcal{L}_1 , for the layer 2 to \mathcal{L}_2 , and so on, is given by $P[\varphi] = Z^{-1} e^{-\beta \mathcal{H}[\varphi]}$, or

$$ZP[\mathcal{L}_1, \mathcal{L}_2, \dots, \mathcal{L}_K] = \prod_{k=1}^K e^{-\beta \mathcal{H}[\mathcal{L}_k, \mathcal{L}_{k+1}]} \quad (3.17)$$

Now, we can define the transfer matrix \mathcal{T} such that its elements

$$\mathcal{T}[\mathcal{L}_k, \mathcal{L}_{k'}] \equiv \mathcal{T}_{k,k'} = e^{-\beta \mathcal{H}[\mathcal{L}_k, \mathcal{L}_{k'}]}, \quad \Rightarrow \quad ZP[\mathcal{L}_1, \mathcal{L}_2, \dots, \mathcal{L}_K] = \prod_{k=1}^K \mathcal{T}_{k,k+1}. \quad (3.18)$$

Since

$$\sum_{\mathcal{L}_1} \sum_{\mathcal{L}_2} \dots \sum_{\mathcal{L}_K} P[\mathcal{L}_1, \mathcal{L}_2, \dots, \mathcal{L}_K] = 1, \quad \Rightarrow \quad Z = \sum_{\mathcal{L}_1} \sum_{\mathcal{L}_2} \dots \sum_{\mathcal{L}_K} \prod_{k=1}^K \mathcal{T}_{k,k+1}. \quad (3.19)$$

$$\sum_{\mathcal{L}_k} \mathcal{T}_{k',k}^n \mathcal{T}_{k,k''} \equiv \mathcal{T}_{k',k''}^{n+1}, \quad \Rightarrow \quad Z = \sum_{\mathcal{L}_1} \mathcal{T}_{1,1}^K = \text{Tr}(\mathcal{T}^K). \quad (3.20)$$

So, we can introduce an orthonormal basis of the eigenvectors for \mathcal{T}^K , $\{|\lambda_\ell\rangle\}$, to get

$$Z = \text{Tr}(\mathcal{T}^K) = \sum_{\ell} \langle \lambda_\ell | \mathcal{T}^K | \lambda_\ell \rangle = \sum_{\ell} \lambda_\ell^K. \quad (3.21)$$

For the limit $K \rightarrow \infty$ (thermodynamic limit), equation 3.21 gives

$$Z = \lambda_0^K, \quad (3.22)$$

where λ_0 is the largest eigenvalue of \mathcal{T} .

The marginal probabilities for the layer 1 to have the configuration \mathcal{L}_1 and for layers 1 of 2 to have configurations \mathcal{L}_1 of \mathcal{L}_2 are

$$ZP[\mathcal{L}_1] = Z \sum_{\mathcal{L}_2} \cdots \sum_{\mathcal{L}_K} P[\mathcal{L}_1, \mathcal{L}_2, \cdots, \mathcal{L}_K] \equiv \mathcal{T}_{1,1}^K, \quad (3.23)$$

$$ZP[\mathcal{L}_1, \mathcal{L}_2] = Z \sum_{\mathcal{L}_3} \cdots \sum_{\mathcal{L}_K} P[\mathcal{L}_1, \mathcal{L}_2, \cdots, \mathcal{L}_K] \equiv \mathcal{T}_{1,2}^1 \mathcal{T}_{2,1}^{K-1}. \quad (3.24)$$

For $|\ell\rangle$ being the eigenvector associated to the eigenvalue λ_ℓ of \mathcal{T} , one has that the usual spectral expansion of an operator, $\mathcal{T} = \sum_\ell \lambda_\ell |\ell\rangle\langle\ell|$, yields

$$\mathcal{T}_{k,k'} = \langle\lambda_k|\mathcal{T}|\lambda_{k'}\rangle = \sum_\ell \lambda_\ell \langle\lambda_k|\ell\rangle\langle\ell|\lambda_{k'}\rangle = \sum_\ell \lambda_\ell \phi_\ell[\mathcal{L}_k] \phi_\ell^*[\mathcal{L}_{k'}], \quad (3.25)$$

where $\phi_\ell[\mathcal{L}_k] = \langle\lambda_k|\ell\rangle$ is an element of $|\ell\rangle$ in the representation of the layer configuration \mathcal{L}_k . In consequence, equations 3.23 and 3.24 for arbitrary layers ($\mathcal{L}_1 \rightarrow \mathcal{L}_k$ and $\mathcal{L}_2 \rightarrow \mathcal{L}_{k'}$) become

$$\begin{aligned} P[\mathcal{L}_k] &= \frac{\sum_\ell \lambda_\ell^K \phi_\ell[\mathcal{L}_k] \phi_\ell^*[\mathcal{L}_k]}{\sum_\ell \lambda_\ell^K} \\ &= \frac{\phi_0[\mathcal{L}_k] \phi_0^*[\mathcal{L}_k] + \sum_{\ell \neq 0} \left(\frac{\lambda_\ell}{\lambda_0}\right)^K \phi_\ell[\mathcal{L}_k] \phi_\ell^*[\mathcal{L}_k]}{1 + \sum_{\ell \neq 0} \left(\frac{\lambda_\ell}{\lambda_0}\right)^K}, \end{aligned} \quad (3.26)$$

$$\begin{aligned} P[\mathcal{L}_k, \mathcal{L}_{k'}] &= \frac{\mathcal{T}_{k,k'}^1 \sum_\ell \lambda_\ell^{K-1} \phi_\ell[\mathcal{L}_k] \phi_\ell^*[\mathcal{L}_{k'}]}{\sum_\ell \lambda_\ell^K} \\ &= \frac{\lambda_0^{-1} \mathcal{T}_{k,k'}^1 (\phi_0[\mathcal{L}_k] \phi_0^*[\mathcal{L}_{k'}] + \sum_{\ell \neq 0} \left(\frac{\lambda_\ell}{\lambda_0}\right)^{K-1} \phi_\ell[\mathcal{L}_k] \phi_\ell^*[\mathcal{L}_{k'}])}{1 + \sum_{\ell \neq 0} \left(\frac{\lambda_\ell}{\lambda_0}\right)^K}. \end{aligned} \quad (3.27)$$

Taking the limit $K \rightarrow \infty$, equations 3.26 and 3.27 can be approximated by

$$P[\mathcal{L}_k] = \phi_0[\mathcal{L}_k] \phi_0^*[\mathcal{L}_k], \quad P[\mathcal{L}_k, \mathcal{L}_{k'}] = \lambda_0^{-1} \mathcal{T}_{k,k'}^1 \phi_0[\mathcal{L}_k] \phi_0^*[\mathcal{L}_{k'}], \quad (3.28)$$

and therefore

$$\lambda_0 = \frac{\mathcal{T}_{k,k} P[\mathcal{L}_k]}{P[\mathcal{L}_k, \mathcal{L}_k]} = \frac{\sum_{\mathcal{L}_k} \mathcal{T}_{k,k} P[\mathcal{L}_k]}{\sum_{\mathcal{L}_k} (\sum_{\mathcal{L}_{k'}} \delta_{\mathcal{L}_k, \mathcal{L}_{k'}} P[\mathcal{L}_k, \mathcal{L}_{k'}])} = \frac{\langle \mathcal{T}_{k,k} \rangle}{\langle \delta_{\mathcal{L}_k, \mathcal{L}_{k'}} \rangle} \quad (3.29)$$

This expression enables one to calculate the largest eigenvalue λ_0 of \mathcal{T} in terms of the

averages $\langle \mathcal{T}_{k,k} \rangle$ and $\langle \delta_{\mathcal{L}_k, \mathcal{L}_{k'}} \rangle$, with $\delta_{\mathcal{L}_k, \mathcal{L}_{k'}} = 1$ or 0 if the layers \mathcal{L}_k and $\mathcal{L}_{k'}$ are equal or different, respectively. Finally, the computed values of λ_0 will be used to determine the thermodynamic weights g_r by the equation [88,89]

$$g_r = \beta_r \psi_r = \beta_r \left(-\frac{\ln Z}{\beta_r V} \right) = -\frac{\ln(\lambda_0^K)}{V} = -\frac{\ln(\lambda_0)}{L}, \quad (3.30)$$

$$\psi_r = u_r - T_r s_r, \quad (3.31)$$

$$V = LK, \quad (3.32)$$

where ψ_r is the free energy density, u_r is the internal energy density, s_r is the entropy density, V is the volume or number of nodes in the lattice and λ_0 is given by the equation 3.29. Consequently, the surface pressure p_r becomes [34,90]

$$p(T_r) \equiv p_r = -\psi_r = -\frac{g_r}{\beta_r}. \quad (3.33)$$

In order to build a suitable ST algorithm, r -values of $g_r = g(T_r)$ should be computed previously using equation (3.30). For example, simulated annealing methods can be implemented to obtain an average for each value of g_r and the internal energy

$$U(T_r) = U_r = \langle \mathcal{H}(T_r) \rangle. \quad (3.34)$$

We observe that equations 3.30-3.34 are going to be used for different lattice models in chapter 5.

On the other hand, the correlation length h (see section 2.3) can be calculated as $1/h = \ln(\lambda_1/\lambda_0)$ [65,91], where λ_1 is the second largest eigenvalue of the transfer matrix. This expression gives h correctly for relatively large systems in a disordered phase, and diverges $\propto \sqrt{V}$ at a second order phase transition, in accord with scaling theory (more details in [92]_{§7.6}).

Chapter 4

New perspectives on ST method

We have realized that the correct implementation of the temperature transitions in the ST method (equation 3.15) could depend on two factors

1. The accuracy of the weight values, namely $g_r = g(T_r)$, by means of which the equation $\psi_r - g_r/\beta_r = 0$ is satisfied (where ψ_r is the grand potential free energy density), and by means of which the exchange probability $\mathcal{P}_{r \rightarrow r'}(g_r, g_{r'})$ is computed correctly, and
2. The appropriate choice of the set of temperatures Υ_R such that (a) allows to arrive at disordered states enough times (high temperatures) to obtain all phases at low temperatures, and (b) the system keeps the temperature T_1 enough so that the steady-state is reached.

With respect to the first factor, the TMM [51, 87], internal energies at the steady state [93, 94] and transmission matrices of Markov chains [95], were used to compute the weight difference $g_{r'} - g_r$. In each implementation mentioned above, different types of accuracy were found. Concerning the second factor, there are some methodologies to determine Υ_R [52]. One of those methodologies is the *exchange frequency* protocol, which is the most efficient method. However, this method requires additional computational effort, because the exchange frequencies are previously calculated.

Taking into account these two factors, we decided to develop and implement new methodologies in order to get another point of view, which could help to understand the influence of weights and replicas in the ST method.

4.1 Expected values of the weights

The TMM provide a useful framework to compute g_r while simulations are running. However, it is necessary to clarify that equations 3.22 and 3.28 are not-so-good computationally approximations, because the thermodynamic limit is far from being fulfilled. Usually, periodic boundary conditions in lattices can greatly simulate the thermodynamic limit, but that is not always true. Some ground states can require certain periodicity to reach thermodynamic stability, such as crystals [96] or molecular self-assembly systems [97]. Even more, when the physical model contains a considerable number of indistinguishable micro-states, the probability to find two identical consecutive layers is drastically reduced from relatively not-low temperatures, namely $\langle \delta_{\mathcal{L}_k, \mathcal{L}_{k'}} \rangle \rightarrow 0$ (see equation 3.29). In such case, values of g_r and p could be inaccurate and inappropriate to be implemented in tempering methods.

For this reason we will perform simulations using two types of methods to calculate $g_{r'} - g_r$ (see equation 3.15). As the first one, we will use the TMM by applying equations 3.30 and 3.29; and as second method, we will calculate the weights by direct thermodynamic integration (**DTI**) of the ensemble average for the energy $U(T)$, which is assumed to be known. That is, the definitions of free energy F and U are

$$\Psi - \Psi_o = (\psi - \psi_o)V \equiv -\beta^{-1} \ln Z, \quad (4.1)$$

$$U - U_o = (u - u_o)V \equiv -\frac{\partial \ln Z}{\partial \beta}, \quad (4.2)$$

where ψ is the free energy, $u_o = \psi_o = -p_o$ is a reference energy such that $Z \approx \text{constant}$ (for example $u_o = u(T = 0)$). The direct integration of equation 4.2 results

$$\begin{aligned} -\int_{\beta_r}^{\beta_{r'}} (u - u_o) d\beta &= \frac{\ln Z(\beta_{r'})}{V} - \frac{\ln Z(\beta_r)}{V} \\ &= -\beta_{r'}(\psi_{r'} - \psi_o) + \beta_r(\psi_r - \psi_o) \equiv -g_{r'} + g_r, \end{aligned} \quad (4.3)$$

or equivalently

$$g_{r'} - g_r = -\frac{1}{k_B} \int_{T_r}^{T_{r'}} \frac{u - u_o}{T^2} dT. \quad (4.4)$$

The equation 4.4 represents the expected thermodynamic values of the weights. The

weight differences $g_{r'} - g_r$ ($r, r' = 1, 2, \dots, R$) depends only on $u(T)$ -curve from T_r to $T_{r'}$ and the fundamental state u_o . It is not possible to compute only g_r -value without knowing another values. However, in simulated tempering implementations, the knowledge of $g_{r'} - g_r$ is enough.

On the other hand, using the integration by parts in equation 4.4 one obtains

$$k_B(g_{r'} - g_r) = \frac{u_{r'} - u_o}{T_{r'}} - \frac{u_r - u_o}{T_r} + \int_{u_r - u_o}^{u_{r'} - u_o} \frac{d(u - u_o)}{T}. \quad (4.5)$$

or

$$s_{r'} - s_r = - \int_{u_r - u_o}^{u_{r'} - u_o} \frac{du}{T}, \quad (4.6)$$

where

$$s(T_r) = s_r = \frac{u_r - u_o}{T_r} - k_B g_r, \quad (4.7)$$

is the entropy per volume. Since it is always satisfied $S(T = 0) = 0$, then (from equation 4.6)

$$s_{r'} = - \int_0^{u_{r'} - u_o} \frac{du}{T}, \quad \text{or} \quad s[u(T)] = - \int_0^{u - u_o} \frac{du}{T}. \quad (4.8)$$

In this same sense, when $T_r = T_o$ and $T_{r'} = T$, the surface pressure $p(T)$ can be calculated from equation 4.3 to take the form

$$p(T) = -u_o + T \int_{T_o}^T \frac{u - u_o}{T^2} dT. \quad (4.9)$$

The value of u_o needed to calculate the weights $g_{r'} - g_r$ and the entropy s_r can be determined analytically by means of the TMM. Here, there is no problem about finding two identical consecutive layers, because

$$\langle \delta_{\mathcal{L}_k, \mathcal{L}_{k'}} \rangle_o = 1, \quad \text{and} \quad \langle \mathcal{T}_{k,k} \rangle_o = e^{-\beta L u_o}, \quad (4.10)$$

at the steady-state. So, u_o depends on the average of the transverse elements of the decomposed Hamiltonian $\mathcal{H}[\mathcal{L}_k, \mathcal{L}_k]$, namely $\langle \mathcal{T}_{k,k} \rangle = \exp(-\beta \mathcal{H}[\mathcal{L}_k, \mathcal{L}_k])$. In the next chapter, we will determine the values of u_o for three lattice models.

4.2 Choosing replicas

In this section we shortly describe three methods to determine the set of temperatures

$$\Upsilon_R = \{T_1, T_2, \dots, T_R\}, \quad \text{where} \quad T_1 < T_2 < \dots < T_R, \quad (4.11)$$

where R is the number of replicas. In all methods, the first temperature value of the set Υ_R (namely T_1) should be established. In the ST method, this value represents the temperature from which the steady-state is reached. Therefore, the value of T_1 should be sufficiently low.

In this thesis, the last method presented in this section (subsection 4.2.3) is an original contribution to the ST method. The goal here is to have a comparative idea of different approaches followed to determine Υ_R that could produce different efficiencies in ST simulations.

4.2.1 Constant interval of entropy

The more thermodynamic-oriented scheme to determine Υ_R is the constant entropy (**CE**) method, proposed in Refs. [98, 99] and implemented to some lattice models in Ref. [89]. It consists of choosing intermediate T_r values so as to lead to a same fixed difference of entropy Δs between successive temperatures. In order to do this, the $s(T)$ -curve should be known or computed by equation 4.7 or 4.6. For example, by performing SA simulations one can obtain the $U(T)$ and $g(T)$ curves, and so on, $s(T)$ consequently.

Once known $s(T)$, the reciprocal function $T[s]$ can be build, in such a way the T_r values take the form

$$T_r = T[s(T_1) + (r - 1)\Delta s], \quad r = 2, 3, \dots, R. \quad (4.12)$$

Since thermodynamically $TdS = CdT$ (where S is the entropy and C is the heat capacity), this choice of temperatures (equation 4.12) implies

$$\int_{T_r}^{T_{r+1}} \frac{C}{T} dT = \Delta s, \quad (\text{a constant volume}). \quad (4.13)$$

Thus, equation 4.13 furnishes a means for generating a specific tempering ensemble. In other words, one first integrates some model of $C(T)$ from $T = T_1$ to $T = T_R$ to obtain the total entropy change $(R - 1)\Delta s$ and then solves for the successive temperatures T_2, T_3, \dots, T_{R-1} that satisfy equation 4.13. This approach can be used either as an iterative procedure where successive estimates of $C(T)$ are used to refine the quality of the ensemble selection.

4.2.2 Fixed Exchange Frequency

This method is mini-scheme of simulation, because Υ_R is obtained through previous simulations with relatively low computational effort [51, 52]. Here, the replicas are determined by means of a fixed exchange frequency (**FEF**) prescription. Given R , it consists in determining the T_r 's such that the exchange frequency between any pair of adjacent temperatures is f . The protocol is as follows: Once fixing T_1 , it is chosen $T_1 < T_2 < T_3 < \dots < T_R$ in such a way that resulting exchange frequencies $f_{r+1,r}$ between any two successive temperatures T_r and T_{r+1} are all equal to some value f . Then, it is defined $f_{r+1,r} = N_{r+1,r}/N_{MC}$, with N_{MC} the number of time steps in a Monte Carlo run and $N_{r+1,r}$ as the number of times that the temperature change happened.

The methodology applied in this thesis to use the exchange frequencies was to build a 2D-map where the horizontal axis represents a temperature T_i and the vertical axis represents another temperature T_j . The values contained in the map (with resolution $n_* \times n_*$) would be the frequencies for each pair (T_i, T_j) , namely $f_{i,j}$. Thus, by using a linear interpolation in the map, contours with $f_{r,r+1} = f$ can be obtained to determine T_2, T_3, \dots, T_R (see figure 4.1). In order to not lose precision through the linear interpolation, the resolution or number of discrete temperatures for T_i and T_j (namely n_*) must be relatively large.

Also, it is important to mention that some numerical work is necessary to determine $f_{i,j}$, but such a process demands relatively short simulations (e.g. it is not necessary to evolve the system until full convergence). But evidently, the computing of $n_* \times n_*$ values contained in the frequency map implies a high computational effort.

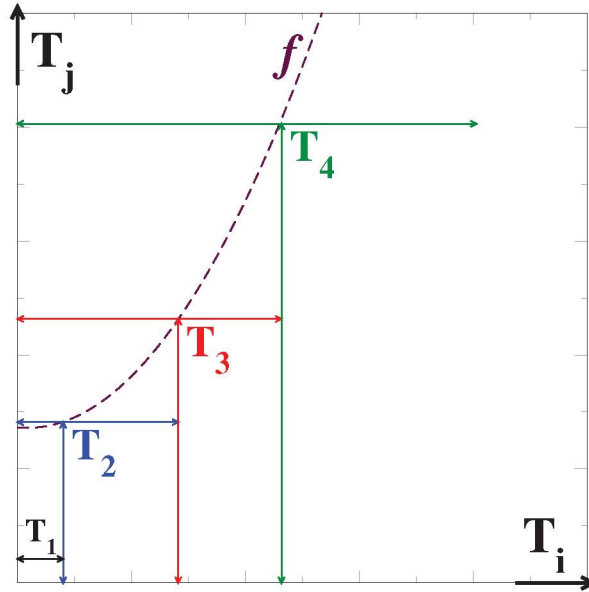


Figure 4.1: Exemplification of a contour with a fixed exchange frequency f (dashed line) in the T_i - T_j map. The value of temperature $T_{r+1} = T_j$ is determined by the intersection between a vertical line at $T_i = T_r$ with the contour. This procedure was a methodology implemented in this work to determine Υ_R . However, in other works [52,94] the replicas are computed without the use of maps. That is, the T_r -values are calculated through an iterative search process [51]_{§2.3}.

4.2.3 Fixed exchange probability

Similarly to CE and FEF, the main idea of this new method is to keep constant some variable by means of which Υ_R can be determined. In the CE, the difference of entropy $\Delta s = s_r - s_{r-1}$ (where $s_r = -g_r + \beta_r u_r$) is kept constant when T_r is computed, whereas the exchange frequency f_r takes this role in the FEF. In the last one, short ST simulations with N_{MC} Monte Carlo steps (MCSs) between T_r and T_{r+1} should be performed to compute the number of times of temperature changes (N_r) given by the probability $\mathcal{P}_{r \rightarrow r+1}$, and thus determine $f_{r+1,r} = N_{r+1,r}/N_{MC}$. By contrast with FEF and CE, in this work we have to consider a fixed exchange probability (**FEP**) to compute Υ_R , as described following.

In Monte Carlo simulations, the goal of ST algorithms is to exhibit all stationary phases through discrete temperature changes $T_{r'} \rightarrow T_{r''}$ with an associate probability $\mathcal{P}_{r' \rightarrow r''}$. This method allows the jump between energy trappings and guarantee uniform visits of the phase space. That advantages would be impossible by using standard simulation models, namely computational methods that do not implement temperature-dependent transitions.

In each MCS the $\mathcal{P}_{r' \rightarrow r''}$ -values are computed as follows (see section 3.3)

$$\ln \mathcal{P}_{r' \rightarrow r''} = \min(0, \omega_{r' \rightarrow r''}) \quad (4.14)$$

$$\omega_{r' \rightarrow r''}(\mathcal{H}) = (\beta_{r'} - \beta_{r''})\mathcal{H} + (g_{r''} - g_{r'})V, \quad (4.15)$$

where $\mathcal{H} = \mathcal{H}[\sigma] = \mathcal{H}_{\sigma_1, \sigma_2, \dots, \sigma_V}$ is the volumetric energy as function of the set of micro-states $[\sigma]$, V is the discrete volume of the lattice and $g_r = g(T_r)$ are pre-fixed weights. When $g_r = \beta_r \psi_r$, being ψ_r the free energy of the system at temperature T_r , the evolution of the system should uniformly visit all replicas. Due to $\omega_{r' \rightarrow r''}$ is dependent on $g_{r''} - g_{r'}$, it is strictly necessary to diversify strategies to obtain consistent and efficient values of $\mathcal{P}_{r' \rightarrow r''}$, two of which are presented below.

By using equations (4.14) and (4.15), we have defined the exchange probability between two replicas (forward and reverse) as

$$\mathcal{P}_{r' \rightarrow r''} \mathcal{P}_{r'' \rightarrow r'} = \exp(M_{r', r''}), \quad (4.16)$$

where (see equations 4.14 and 4.15)

$$\begin{aligned} M_{r', r''} &\equiv \min(0, \omega_{r' \rightarrow r''}) + \min(0, \omega_{r'' \rightarrow r'}) \\ &\approx \omega_{r' \rightarrow r''}(U_{r'}) + \omega_{r'' \rightarrow r'}(U_{r''}) \\ &= (\beta_{r'} - \beta_{r''})(U_{r'} - U_{r''}), \end{aligned} \quad (4.17)$$

and it was assumed that the final tunneling states are such that the internal energy takes values according to steady state for each replica. Note that $\exp(M_{r', r''})$ is similar to the probability $\mathcal{P}_{r' \leftrightarrow r''}$ used to establish the temperature switching in the parallel tempering method (PTM) [82,87] and it is not depending on weights. This fact implies that only knowing $U(T)$ will be enough to determine Υ_R .

A 2D-map of exchange probabilities can be built in the same way as figure 4.1, but by substituting $f \rightarrow -M_{r', r''}$. However, there is a remarkable difference between the FEF and FEP maps: The values of exchange frequencies $f_{r', r''}$ should be determined by means of short ST simulations between two temperatures $T_{r'}$ and $T_{r''}$, whereas that the values of probabilities $\exp(M_{r', r''})$ are calculated only by the equation 4.17.

Chapter 5

Some lattice models

Before we proceed to describe some lattice models, it is appropriate to explain a few remarks about the role of models in statistical physics. There are two diametrically opposing guidelines about the way models are applied. From a traditional viewpoint, one constructs a faithful representation of the system, including as many fine details as possible. When theory is unable to explain the results of an experiment, the response is to fine-tune or to add new parameters if necessary.

On the other hand, such fine detail may not be needed or relevant to describe a particular phenomenon of interest. Usually, the directly measurable quantities form dimensionless numbers, or even universal functions, which (in a good approximation) do not depend on microscopic details. In these cases, it is only important to start with the correct minimal model and all of the microscopic physics is subsumed into as few phenomenological parameters as possible.

In this order of ideas, this chapter presents three lattice models that contain the minimum elements to reproduce FOPTs. These models will be applied to reproduce all the results of this thesis. In the lattice models presented here, we have defined the average over the \mathcal{N} equilibrium phases of the order parameter \mathcal{W}_{ss} in the ground state ($T \approx 0$) (and when the simulations reaches the steady state, **WSRSS**) as

$$\mathcal{W}_{ss} \equiv \frac{1}{\mathcal{N}} \sum_{n=1}^{\mathcal{N}} \mathcal{W}_n, \quad (5.1)$$

where \mathcal{W}_n is the order parameter of the n -phase in the ground state (or in the lowest temperature).

5.1 Blume–Emery–Griffiths model

Researches of multi-component Bose-Fermi/Fermi-Fermi mixtures are an active area of studies in the field of ultracold atoms (see for example [100]), and a simple lattice model that reproduces a similar phase diagram of such mixtures is the Blume–Emery–Griffiths (BEG) model. The BEG model is one of the simplest models known to exhibit both a continuous phase transition and a FOPT. Because of this feature, the model has been studied extensively as a scheme of many diverse systems, including states of ^3He - ^4He mixtures (the original system for which Blume, Emery and Griffiths first devised their model [101]) as well as solid-liquid-gas fluids [102], antiferromagnetic systems [103], microemulsions [104], etc¹.

The BEG model is a generalization of the Ising model, where the spin can take three values $\sigma_i = 0, \pm 1$. The Hamiltonian presents four terms²

$$\mathcal{H} = - \sum_{\langle i,j \rangle} (J\sigma_i\sigma_j + K\sigma_i^2\sigma_j^2) - \sum_i (H\sigma_i - D\sigma_i^2) \quad (5.2)$$

where J and K are interactions energies, $\mu = -D$ is the chemical potential and H is an external field. For low temperatures and $K/J \approx 3.3$ [88], a FOPT separates liquid ($\rho \rightarrow 1$) and gas ($\rho \ll 1$) phase for high and low μ , respectively (see for example [107]). The order parameter is the particle density

$$\rho = \langle \sigma_i^2 \rangle = \frac{1}{N} \sum_{n=1}^N \sigma_n^2. \quad (5.3)$$

At the ground state ($T \approx 0$) the system presents two liquid phases $\rho_{1,2} \approx 1$ coexisting with one gas phase $\rho_g \approx 0$. WSRSS, they have equal statistical weights, and therefore,

¹The XY model or plane-rotator model is a better model to simulate helium fluids [32,105]. Here, the micro-states of each particle on the lattice can take continuous values θ_i which are related with the polar angle of the spin in the lattice plane. The Hamiltonian is given by

$$\mathcal{H} = -J \sum_{\langle i,j \rangle} \cos(\theta_i - \theta_j) - H \sum_i \cos \theta_i.$$

This scheme is particularly important in 2D, where it shows a peculiar phase transition through the vortex formations (so called Kosterlitz Thouless transition). This kind of transition is experimentally observed in liquid crystals, thin films of liquid helium, layered high temperature superconductors, etc.

²The Blume–Capel model [106] is a special case of the BEG for $K = 0$.

equation 5.1 with $\mathcal{W} = \rho$ results

$$\rho_{ss} = \frac{(-1)^2 + 0^2 + 1^2}{3} = \frac{2}{3}, \quad \text{when } T \approx 0. \quad (5.4)$$

Furthermore, the lattice magnetization can be measured by

$$m = \langle \sigma_i \rangle = \frac{1}{N} \sum_{n=1}^N \sigma_n, \quad \Rightarrow \quad m_{ss} = 0, \quad (5.5)$$

which can be tested to observe continuous phase transitions [108].

From equation 5.2, the bilayer Hamiltonian for a square lattice results

$$\mathcal{H}[\mathcal{L}_k, \mathcal{L}_{k+1}] = \sum_{i=1}^L \left\{ -J\sigma_{i,k}(\sigma_{i+1,k} + \sigma_{i,k+1}) - K\sigma_{i,k}^2(\sigma_{i+1,k}^2 + \sigma_{i,k+1}^2) - H\sigma_{i,k} + D\sigma_{i,k}^2 \right\}, \quad (5.6)$$

and setting $\mathcal{L}_{k+1} = \mathcal{L}_k$, the diagonal elements of \mathcal{T} become

$$\mathcal{T}_{k,k} = \exp \left(\beta \sum_{i=1}^L \left\{ (H + J\sigma_{i+1,k})\sigma_{i,k} + [J - D + K(1 + \sigma_{i+1,k}^2)]\sigma_{i,k}^2 \right\} \right). \quad (5.7)$$

Insomuch as all particles have the same spin-value σ_o at the ground state, the average of equation 5.7 becomes (see equation 4.10)

$$\langle \mathcal{T}_{k,k} \rangle_o = e^{\beta L \sigma_o [H + (2J - D + 2K)\sigma_o]}. \quad (5.8)$$

Thus, the internal energy at the steady-state is (for $\sigma_o = 0, \pm 1$)

$$u_o(\sigma_o) = -\sigma_o [H + (2J - D + 2K)\sigma_o], \quad (5.9)$$

or $u_o(0) = 0$ and $u_o(\pm 1) = \mp H - 2J + D - 2K$. These are the three values of internal energy in the ground state ($T = 0$) for the BEG model. The coexistence condition can be obtained when $u_o(0) = u_o(+1) = u_o(-1)$, because each energy correspond to each order parameter value in the ground state. So, the coexistence occurs when

$$H = 0 \quad \text{and} \quad D/2 = J + K. \quad (5.10)$$

5.2 Bell–Lavis model

The Bell-Lavis (**BL**) model [109] was proposed in 1970 to consider a two-dimensional bonded fluid, emphasizing the orientational property of the hydrogen bond on triangular lattices (see figure 5.1). Particles are represented by occupational variables with $\sigma_i = 0, 1$, for empty or occupied sites, respectively. Orientation may be described in terms of bonding and nonbonding “arms”, which are represented by variables $\tau_i = \pm 1$ (figures 5.1.a and 5.1.b) for the arm of particle i that points to particle j (nonbonding $\tau_i^{ij} \tau_j^{ji} = 0$, or bonding $\tau_i^{ij} \tau_j^{ji} = 1$). Thus, two next neighbor molecules are considered

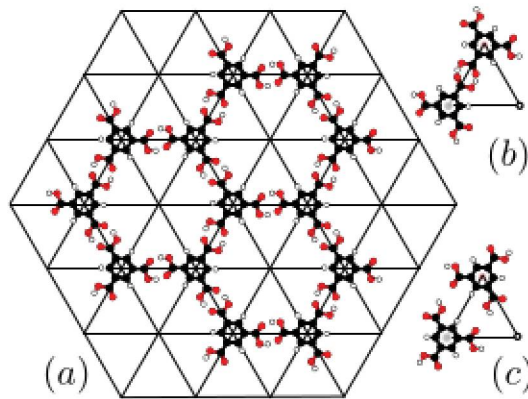


Figure 5.1: Schematic representation of the BL model with some water molecules in the triangular lattice (taken from the reference [110]). (a) A portion of the lattice illustrating how the particles can assembly in the gas-phase (one of the ordered phases). (b) Two close coupled molecules with van der Waals and hydrogen bond interaction ($-\epsilon_{\text{vdw}} - \epsilon_{\text{hb}}$). (c) Two molecules that only have van der Waals interaction.

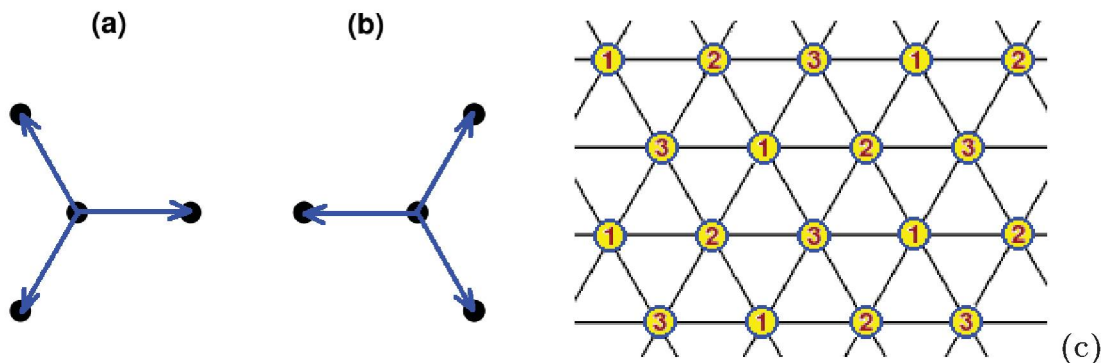


Figure 5.2: (a) and (b) denote the two possible orientations of the molecule on a triangular lattice in the BL model. They are designed as states $\tau_i = +1$ and $\tau_i = -1$ of a spin-one model. (c) The convention adopted for labelling the three sublattices 1, 2 and 3.

to interact via van der Waals forces and hydrogen bonds through the Hamiltonian

$$\mathcal{H} = - \sum_{\langle i,j \rangle} \sigma_i \sigma_j (\epsilon_{\text{hb}} \tau_i^{ij} \tau_j^{ji} + \epsilon_{\text{vdw}}) - \mu \sum_i \sigma_i \quad (5.11)$$

where ϵ_{hb} is the hydrogen bond energy, ϵ_{vdw} is the van der Waals interaction energy and μ is the chemical potential.

In order to get statistical values according to the system symmetries, the observables should be measured in three periodic sublattice [34, 110] (see figure 5.2.c), since high order structures can form in the lattice. This observables are the particle density and the orientation, defined respectively as

$$\rho_s = \frac{3}{N} \sum_{l_s=1}^{N/3} \sigma_{l_s}, \quad m_s = \frac{3}{N} \sum_{l_s=1}^{N/3} \pi_{l_s} \sigma_{l_s}, \quad s = 1, 2, 3, \quad (5.12)$$

where \sum_{l_s} is over each node of the s -sublattice, in such a way that $3\rho = \rho_1 + \rho_2 + \rho_3$ and $3m = m_1 + m_2 + m_3$. At zero temperature, the model presents two dense phases, which depend on the relation $\zeta \equiv \epsilon_{\text{vdw}}/\epsilon_{\text{hb}}$. One of them is obtained with $\zeta < 1/3$ (figure 5.1.a), where $\rho_1 = \rho_2 = 1$, $m_1 = -m_2 = \pm 1$ and $\rho_3 = m_3 = 0$; while the other phase (the same but with a particle in the center of each hexagon) is achieved with $\zeta > 1/3$, where $\rho_1 = \rho_2 = \rho_3 = 1$, $m_1 = -m_2 = \pm 1$ and $m_3 = 0$.

The diagonal elements of the transfer matrix are calculated as

$$\mathcal{H}[\mathcal{L}_k, \mathcal{L}_{k+3}] = \sum_{i=1}^L \left\{ -\sigma_{i,k} (\sigma_{i,k} + \sigma_{i+1,k} + \sigma_{i+1,k+3}) [\epsilon_{\text{vdw}} + \epsilon_{\text{hb}} \tau_{i,k} (\tau_{i,k} + \tau_{i+1,k} + \tau_{i+1,k+3})] - \mu \sigma_{i,k} \right\},$$

$$\mathcal{T}_{k,k} = \exp \left(\beta \sum_{i=1}^L \sigma_{i,k} [(\sigma_{i,k} + 2\sigma_{i+1,k}) (\epsilon_{\text{vdw}} + \epsilon_{\text{hb}} \tau_{i,k} \tau_{i+1,k}) + \mu] \right), \quad (5.13)$$

where $\mathcal{T}_{k,k}$ was obtained by $\mathcal{H}[\mathcal{L}_k, \mathcal{L}_{k+3} = \mathcal{L}_k]$ (see equation 3.19).

The homogeneous state at the ground state is assumed through two possible configurations: (1) an empty lattice $\sigma_i = 0$, and (2) hexagonal structures with periodicity in three sublattices. In other words, in the ground state the molecules can organize themselves in hexagonal and periodical structures, which total energy bonding is maximum. In this state, two-thirds of the sites in the lattices are occupied with molecules which all arms are bonded with neighboring molecules. Thus, u_o can take

two possible values, $u_o(\sigma_i = 0) = 0$ and (from equation 5.11)

$$u_o(1) = -\frac{2}{3} \times \left[\frac{1}{2} \times 3 \times (\epsilon_{hb} + \epsilon_{vdw}) + \mu \right]. \quad (5.14)$$

Then, the coexistence condition is determined as ($u_o(0) = u_o(1)$)

$$\mu = -\frac{3}{2} (\epsilon_{hb} + \epsilon_{vdw}). \quad (5.15)$$

In the same sense, the averages over for this model are (WSRSS)

$$\rho_{ss} = \frac{0 + 3 \times \frac{2}{3}}{1 + 3} = \frac{1}{2}, \quad m_{ss} = \frac{0 + 3 \times 0}{1 + 3} = 0. \quad (5.16)$$

5.3 Potts model

Widely studied in statistical mechanics, both numerically and analytically, the Potts [111] [65]_{§12} is a simple spin lattice model for which the variable σ_i ($i = 1, \dots, N$) takes the integer values $0, 1, \dots, q - 1$. Adjacent sites i and j have a non-null interaction energy of $-J$ whenever $\sigma_i = \sigma_j$. The full Hamiltonian of the problem reads

$$\mathcal{H} = -J \sum_{\langle i,j \rangle} \delta_{\sigma_i \sigma_j} - A \sum_i \delta_{\sigma_i \sigma_*}, \quad (5.17)$$

where A is an external field and its the direction is specified by the spin variable σ_* .

For low temperatures the system is ordered and becomes disordered as T increases. The transition point is exactly given by

$$\frac{1}{k_B T_c} = \ln(1 + \sqrt{q}), \quad \text{with } A = 0. \quad (5.18)$$

In 2D, for $q \leq 4$ the phase transition is second-order and discontinuous if $q \geq 5$. A proper order parameter is

$$\phi = \frac{q(V_{max}/V) - 1}{q - 1}, \quad (5.19)$$

where V_{max} is the volume occupied by the spins of the state s of largest population and $V = N$ is the number of nodes in the lattice.

For the Potts model in a square lattice, the layered elements of the Hamiltonian

result

$$\mathcal{H}[\mathcal{L}_k, \mathcal{L}_{k+1}] = - \sum_{i=1}^L \left(J \left[\delta_{\sigma_{i,k}\sigma_{i+1,k}} + \delta_{\sigma_{i,k}\sigma_{i,k+1}} \right] + A \delta_{\sigma_{i,k}\sigma_*} \right). \quad (5.20)$$

Therefore, the diagonal elements of the transfer matrix yield

$$\mathcal{T}_{k,k} = \exp \left(\beta \sum_{i=1}^L \left\{ J \left[1 + \delta_{\sigma_{i+1,k}\sigma_{i,k}} \right] + A \delta_{\sigma_{i,k}\sigma_*} \right\} \right). \quad (5.21)$$

Finally, when $\sigma_{i,k} = \sigma_{i,k+1} = \sigma_*$, the ground states becomes

$$u_o = -(2J + A). \quad (5.22)$$

Also, we have defined the magnetization for this lattice model as³

$$m = \frac{1}{N} \sum_{n=1}^N \sigma_n. \quad (5.23)$$

At the ground state with $A = 0$, the system can reach q homogeneous phases with the same probability. So, the average of equation 5.23 over all of phase at the ground state is (WSRSS and $A = 0$)

$$m_{ss} = \frac{0 + 1 + 2 + \dots + (q-1)}{q} = \frac{0 + (q-1)(q-1+1)/2}{q} = \frac{q-1}{2}. \quad (5.24)$$

It is necessary to clarify that, for this lattice model, this quantity is achieved only when the MA is used. Other algorithms, such as the Wolff algorithm [43]_{§4} [82]_{§II.B}, change the cluster-spin value with a probability equal to 1, for this lattice model. In this way, the equilibrium of the $\langle \sigma \rangle$ is never reached and m_{ss} is not valid.

³This estimator is very simple and useful to ascertain the phase coexistence ($A = 0$). However, if the number of microstates q is relatively high ($q > 5$) then, the magnetization will be not a good predictor, because some combinations different to $\sigma_n = 0, 1, \dots, q-1$ can yield the same average.

Chapter 6

Results and Discussions

This chapter presents the results of the numerical simulations obtained for the four lattice models discussed in the previous chapters (Ising, BEG, BL and Potts). In this sense, we need to clarify some details regarding the results.

1. Some results contain simulated annealing (**SA**) simulations to thermodynamically valid or/and to determine the accuracy of simulation methods involved in the weights calculation: transfer matrix method (TMM) and direct thermodynamic integration (DTI).
2. The total of ST simulations to evaluate the combination of methods by calculation of the weights $g_{r'} - g_r$ (TMM and DTI), by determining the replicas Υ_R (CE, FEF and FEP) and by implementing the three lattice models (BEG, BL and Potts), is not complete. The idea here is to show some cases where a combination of methods can be implemented to obtaining some tunneling efficiency of the order parameter \mathcal{W} . Namely, we are interested in knowing what methods should be used for identifying phase coexistence and FOPTs when the evolution of $\langle \mathcal{W} \rangle$, in ST simulations, converges to an expected value.
3. The selected pseudorandom number generator to compute all probabilities (in the Metropolis Algorithm and the Simulated Tempering method) was the Mersenne Twister code (64-bits) with an internal alteration to optimize the performance. In order to be clearer, the operations to mixture the old vector of numbers were replaced with pointers. Benchmarks generating 10^9 pseudorandom numbers with

Intel processors threw more than 15 percent of time profit.

4. All algorithms presented in this work were programmed in `C Language` and they were run in nodes of the server `hoggar.fisica.ufpr.br`.

6.1 Ising model

Note that from equation 5.2 one can obtain the Hamiltonian for the Ising model. Namely, setting $K = D = 0$ and $\sigma_{i,k}^2 = 1$ in equation 5.7, it follows that

$$\mathcal{T}_{k,k} = \exp\left(\beta \sum_{i=1}^L \left\{ J(1 + \sigma_{i,k}\sigma_{i+1,k}) + H\sigma_{i,k} \right\}\right). \quad (6.1)$$

So, by taking the average for this equation, the internal energy at ground state results¹ $u_{o\pm} = \mp H - 2J$ and the coexistence condition $H = 0$, as shown in figure 2.4.A.

The results presented in the following subsections correspond to SA simulations (without performing ST runs) in order to evaluate the TMM accuracy when it is implemented in the most simple lattice model, such as the Ising model.

6.1.1 Partition function

In order to verify equation 6.1 computationally, numerical calculations have been performed for $H = 0$, as shown in figure 6.1. By implementing equations 3.22, 3.29 and 6.1 into SA simulations, the partition function Z was numerically computed for each fixed value of T (in units of J). The exact solution of Z for 2D Ising model (with volume equal to $L \times K$) is presented in reference [112], and it is shown in figure 6.1 with points. The equations used for this case were

$$Z(T) = \frac{1}{2} \left(2 \sinh 2\tilde{\beta}\right)^{LK/2} \sum_{r=1}^4 \prod_{k=0}^{K-1} 2\mathcal{K}_{kr}(\tilde{\beta}), \quad \tilde{\beta} \equiv \frac{J}{k_B T}, \quad (6.2)$$

$$\vec{\mathcal{K}}_k \equiv \left\{ \cosh \frac{m\gamma_{2k+1}}{2}, \sinh \frac{m\gamma_{2k+1}}{2}, \cosh \frac{m\gamma_{2k}}{2}, \sinh \frac{m\gamma_{2k}}{2} \right\}, \quad (6.3)$$

$$\gamma_0 = 2\tilde{\beta} + \ln \tanh \tilde{\beta}, \quad (6.4)$$

$$\cosh \gamma_l = \left(\cosh 2\tilde{\beta} \right) \left(\coth 2\tilde{\beta} \right) - \cos(l\pi/K), \quad l \neq 0 \quad (6.5)$$

¹This result is the same one used in section 2.4 (see equation 2.21) for $z = 4$ (the coordination number for a 2D rectangular lattice).

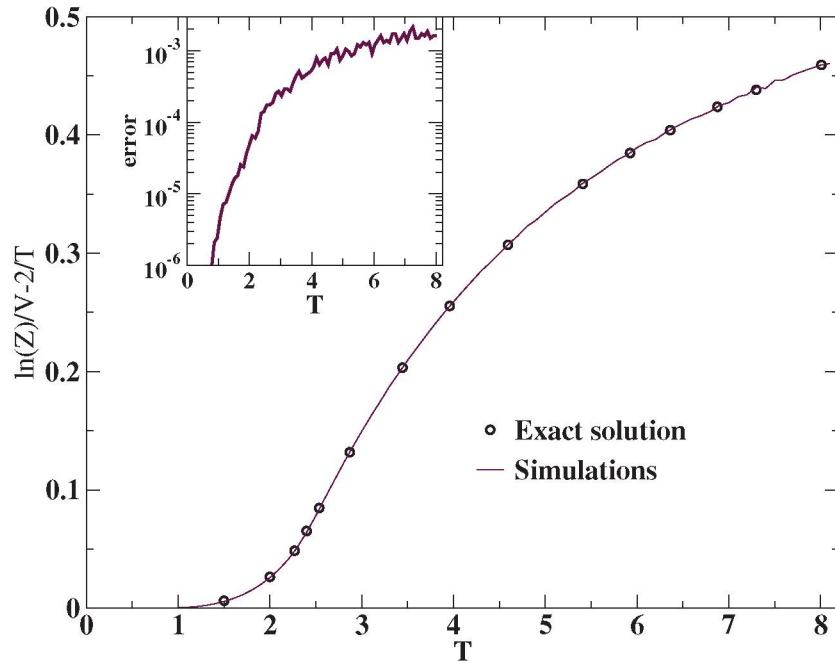


Figure 6.1: Logarithm of the partition function Z or weights (see equation 3.30) versus temperature T (in J units) for the Ising model with $H = 0$. The simulations (solid line containing 81 points) were performed in a square lattice of $N = 16 \times 16$ sites or nodes with periodic border conditions. Each numerical value of $Z(T)$ was computed in steady state (10^5 Monte Carlo iterations) and averaged over 10^4 configurations. The theoretical values shown in points were calculated using the reference [112] (see also reference [65]_{§7.12}).

The agreement is remarkable, indicating that even for relatively small systems ($V = 16 \times 16$), Z and therefore f are relatively close to their values at the thermodynamic limit. Since $\langle \delta_{\mathcal{L}_k, \mathcal{L}_{k'}} \rangle$ is increasingly inaccurate with T , a small numerical noise for relatively high temperatures ($T > 7$) is observed.

6.1.2 Thermodynamic weights

In order to have a clear estimation of the difference $g_{r'} - g_r$ computed by the TMM and by the thermodynamic approach developed in section 4.1 (DTI), we have to calculate such quantity in two ways (see figure 6.2). First, we start by taking values of $Z_r = Z(T_r)$ and $Z_{r'} = Z(T_{r'})$ and then we compute g_r and $g_{r'}$ by means of equation 3.30. Second, we numerically integrate equation 4.4 with the help of the $U(T)$ -curve obtained from SA simulations, where the internal energy per volume is given by $U = \langle \mathcal{H} \rangle N$. A relative disagreement is observed at $T_r < 4$ and $T_{r'} \approx T_r$: The values obtained by TMM and by DTI are always the same except in a small temperature region, where their values disagree by around 6%; to be more precise the TMM gives lower values than the one

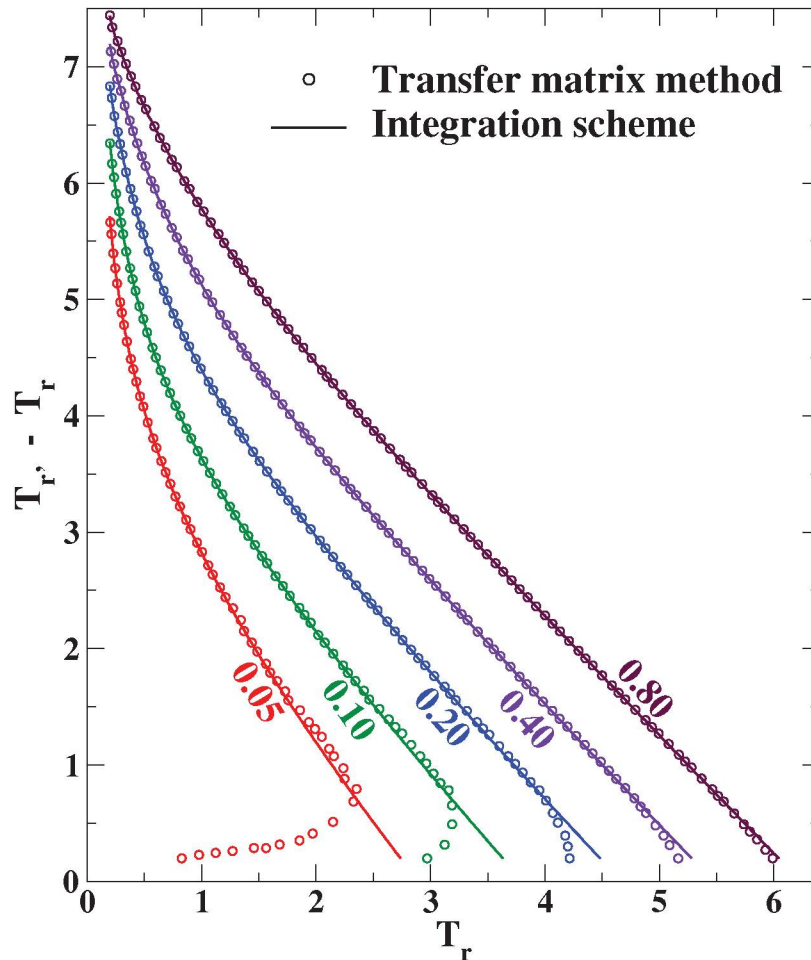


Figure 6.2: Contours of the weight difference $g_r - g_{r'}$ values for the Ising model with $H = 0$ and $N = 16 \times 16$. Results in lines are the exact values given by equation 4.4, whilst in circles we show the difference calculated by means of the TMM.

obtained from the exact approach (DTI). The reason why this happens is the same one mentioned in the previous subsection: the term $\langle \delta_{\mathcal{L}_k, \mathcal{L}_{k'}} \rangle$ is inaccurate for relatively high temperatures. Taking into account this small discrepancy between both schemes, we are expecting to perform several ST simulations as a useful way to contrast the relation $g_r - g_{r'}$ with both methods in the near future.

6.2 Entropy for the BEG model

Here we present the entropy values as temperature function calculated from two equations, as shown in the right graph of figure 6.3. The values of the constants used in the simulations are the same as those used in the references [51, 82, 88]. A good agreement between both ways confirms the validity of the TMM in calculating entropies.

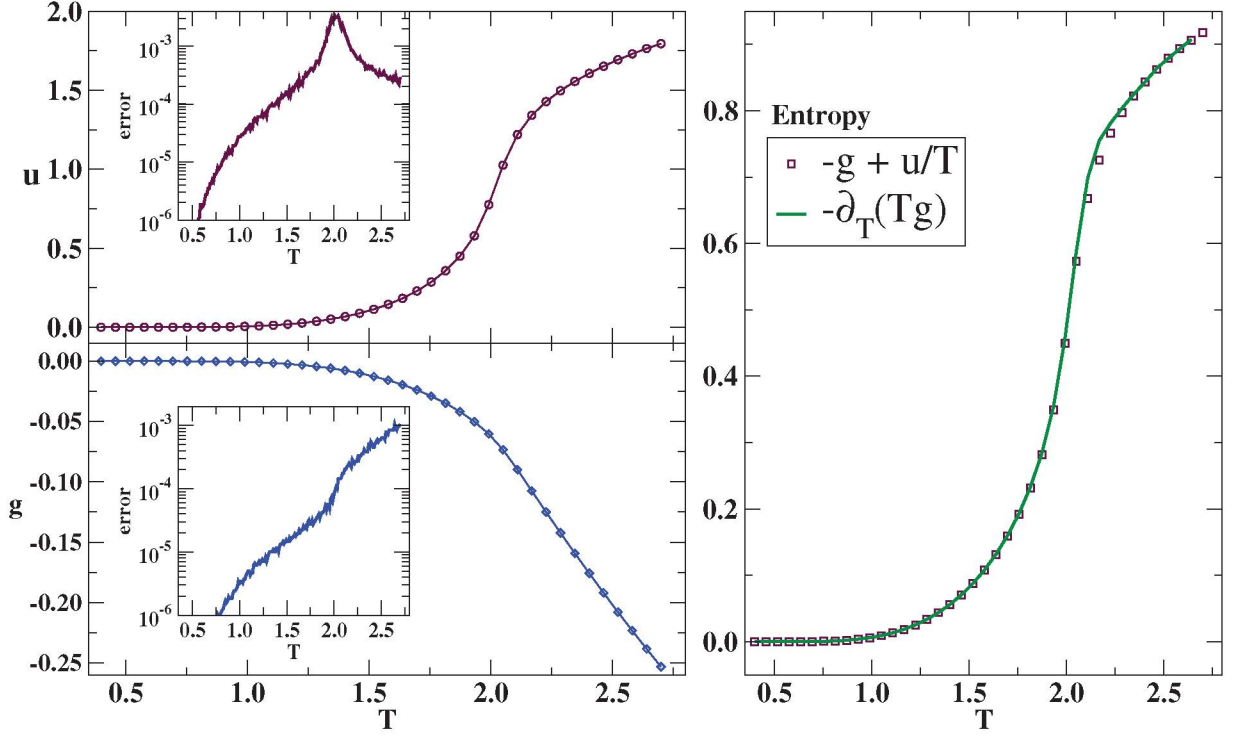


Figure 6.3: Results obtained for the BEG model by using SA simulations and the TMM, with $K = 3$, $J = 1$, $H = 0$, $\mu = -8$ and $N = 18 \times 18$. Note that the chosen values for the coupling constants satisfied the equation $-\mu/2 = J + K$, thus, the phases should coexist in the system at the steady state. The weights $g = -\ln(\lambda_0)/L$ were calculated by the averages of diagonal elements of \mathcal{T} and the coincidences between two subsequent layers (equation 3.29). The derivative of g was computed as $\partial_T g \approx (g_{r+1} - g_r)/(T_{r+1} - T_r)$ for $r = 1, \dots, 30$. In each r -point the steady state was reached with 10^6 MC steps. The value of λ_0 was obtained by the averages in 10^4 different configurations of the lattice.

Mild effects due to the discretization of the entropy $S = -\frac{\partial(Tg)}{\partial T} \approx -g - T \frac{\Delta g}{\Delta T}$ are observed around $T = 2.2$. The change of entropy $\Delta g|_{T \approx 2.2}$, in this case, is more pronounced than in other cases. Note that for this lattice model, there is a strong concordance between $-\frac{\partial(Tg)}{\partial T}$ and $-g + u/T$ at high temperatures. Also, as we can see for $T > 2$, the weights g decrease linearly with T , or equivalently $-f \propto T^2$ (typical behavior of ^3He - ^4He mixtures at the disorder phase [113]).

An important point here is that equation $S = -\frac{\partial(Tg)}{\partial T}$ does not depend on the internal energy U . Consequently, in order to determine Υ_R by means of the CE method, the knowledge of $g(T)$ -curve is enough to compute each T_r -value, if the TMM is implemented.

6.3 Gibbs–Duhem integration for the BL model

Similarly than the BEG model, we compute the internal energy $u(T)$ and weights $g(T)$ for the BL model using the TMM in SA simulations, which are presented in the left graph of figure 6.4.

SA simulations varying the chemical potential were performed to verify the Gibbs–Duhem relation. In the right graph of figure 6.4, we compare some values of the pressure $p = -\psi$ (where $\psi = g/\beta$ is the free energy) calculated from the transfer matrix approach with those obtained from numerical integration of the Gibbs–Duhem equation

$$SdT - Vdp + Nd\mu = 0, \quad (6.6)$$

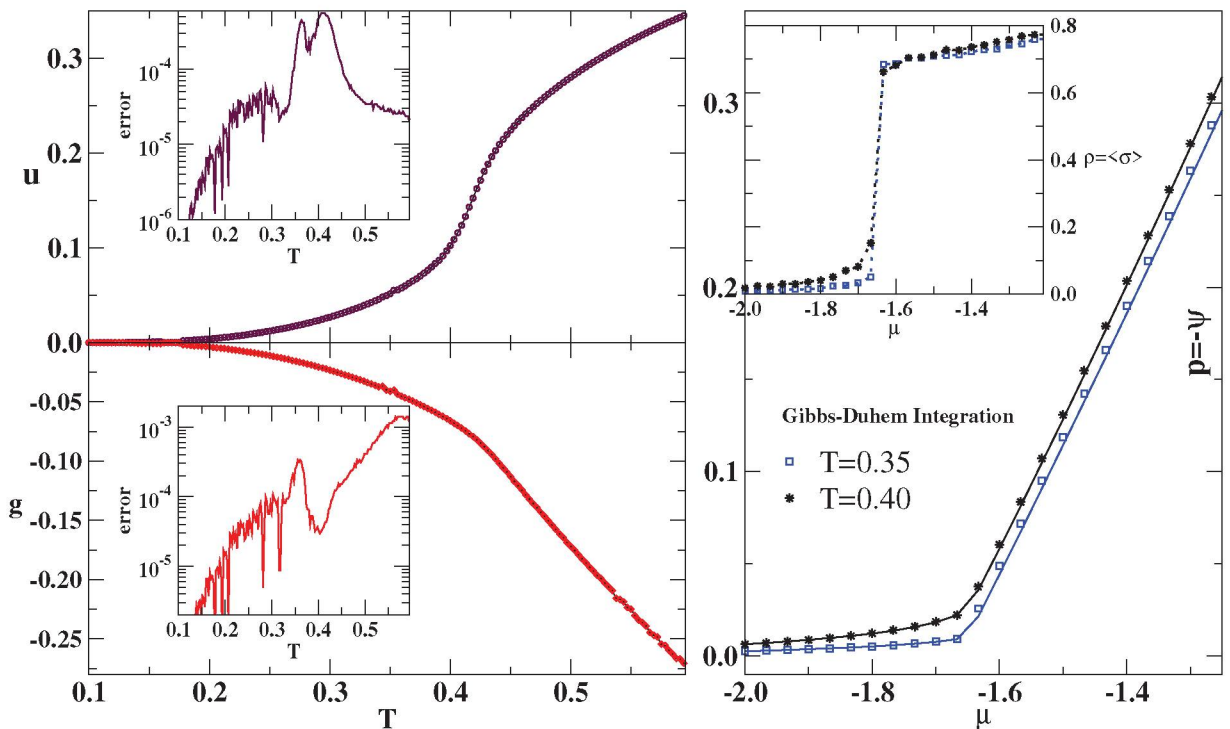


Figure 6.4: Results obtained for the BL model by using SA simulations (10^8 MC steps in each point) and the TMM, with $\epsilon_{\text{hb}} = 1$, $\epsilon_{\text{vdw}} = 0.1$ and $N = 18 \times 18$. The left graphs were obtained at $\mu = -1.65$, which is a value close to the phase coexistence ($\mu^* = -1.6528$ [89]). In order to compare our results with the Gibbs–Duhem relation, we have plotted the particle density ρ versus the chemical potential μ (the inside graph) to computed the cumulative integral of this curve, such as is shown in the right graphs. The solid lines are the results of the numerical integration in equation 6.7 from $\mu = -2.0$ (where $\rho \approx 0$) to μ 's that they correspond to $p-\mu$ graph.

at fixed temperatures. Thus,

$$p(\mu) = p(\mu_o) + \int_{\mu_o}^{\mu} \rho d\mu, \quad (6.7)$$

where the density is computed as $\rho(\mu) = \rho_1 + \rho_2 + \rho_3$ (see section 5.2) and $p(\mu_o)$ is a known value of pressure at $\mu = \mu_o$. As it can be seen, even for a small size of the lattice $V = N$ and low temperatures, the agreement is relatively good.

6.4 Pressure for the BEG, BL and Potts model

In figure 6.5 we present a comparison of the pressure computed by means of the transfer matrix method (TMM, equation 3.33, in points) and by direct thermodynamic integration (DTI, equation 4.9, in solid line) for the BEG, BL and Potts models. Once known the internal energy $u(T)$ and u_o , the DTI is a standard method to determine thermodynamics properties such as the pressure. Thus, numerical measurements obtained through the DTI are good reference points to comparing values obtained by means of other methods. In this sense, there is a good agreement for BEG model, meaning that the TMM is a reasonably good approach to compute the free energy.

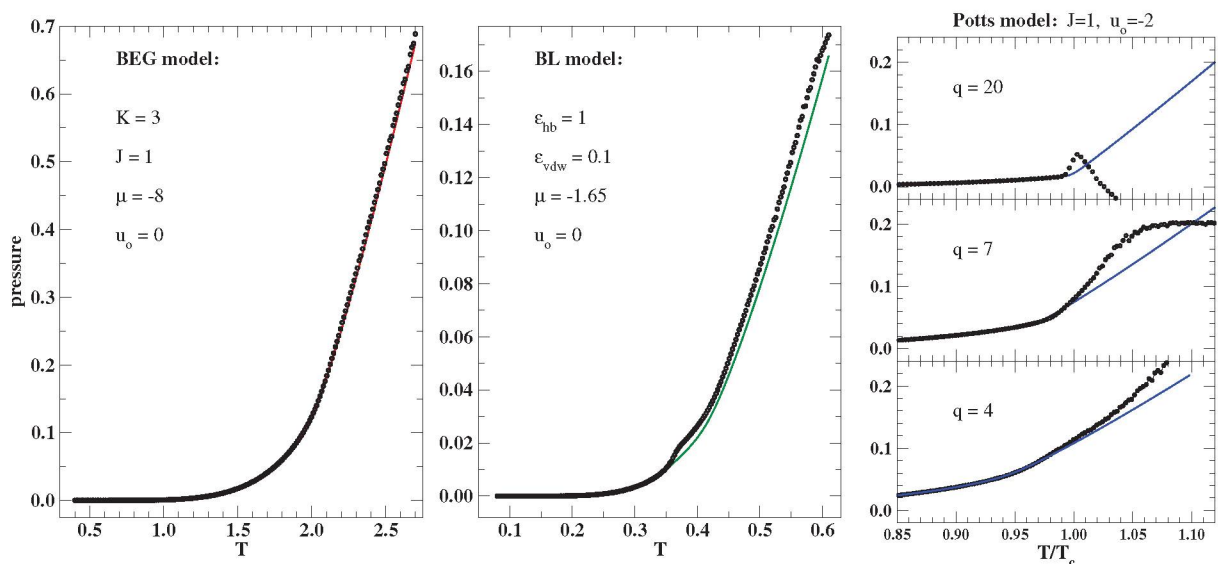


Figure 6.5: Pressure computed by two ways for the three lattice models with volume equal to $N = 18 \times 18$. The values of g , in points (\bullet), were calculated by means of the TMM, which was averaged 300 times over 10^4 configurations. The *solid lines* were built by using direct thermodynamic integration (equation (4.9)).

For the BL model, we can observe a slight discrepancy around $T \approx 0.36$. This happens because it can appear spontaneously particles without being linked to the network in the formation of hexagonal structures like as figure 5.2. This phenomenon can be interpreted as a metastable phase formation, and it is also observed in references [34, 110]. This metastable phase is a consequence of the BL model, due to there is not repulsion between the “arms” ($\tau_i^{ij} \tau_j^{ji} \geq 0$). Namely, the molecules with $\tau_i^{ij} \tau_j^{ji} = 0$ generate instability in the hexagonal structure from $T \geq 0.36$, where the bonding energy is relatively low. The average $\langle \delta_{\mathcal{L}_k, \mathcal{L}_{k'}} \rangle$ (see equation 3.29) is reduced as a consequence of the instability, and thus, the calculation of the pressure by means of TMM is slightly increased.

The results for the Potts shows a wide difference for $T > T_c$. Even more, when the number of microstates q is equal to 20, the pressure has negative values. In this case the TMM fails to predict the right free energy values, as it was explained in section 4.1 and commented in Ref. [88]_{§II}.

6.5 Exchange frequencies and probabilities

Once the weights $g_r - g_{r'}$ were obtained (by means of the TMM or the DTI), the simulated tempering simulations can be performed. The weights that have been implemented in the following simulations belong to figure 6.5 (computed by TMM and DTI). The figure 6.6 shows some contours of a map of the exchange frequencies $f_{r \rightarrow r'}$, which was built as follows: (1) setting only two values of temperature T_r and $T_{r'}$, (2) executing N_{ST} times the ST algorithm described in section 3.3 with $\Upsilon_2 = \{T_r, T_{r'}\}$, (3) accounting the $N_{r \rightarrow r'}$ times when temperature changes occurs ($T_r \rightarrow T_{r'}$) in the step 2, and (4) computing the exchange frequency as [51, 52]

$$f_{r \rightarrow r'} = \frac{N_{r \rightarrow r'}}{N_{ST}}. \quad (6.8)$$

The differences between the exchange frequencies obtained using the TMM and DTI methods (figure 6.6) are in accordance with the variations found in the previous section. On the other hand, domains where $f_{r \rightarrow r'} \approx 0$ were found in the maps. This implies that certain microstates can be accessed only from a limited set of states.

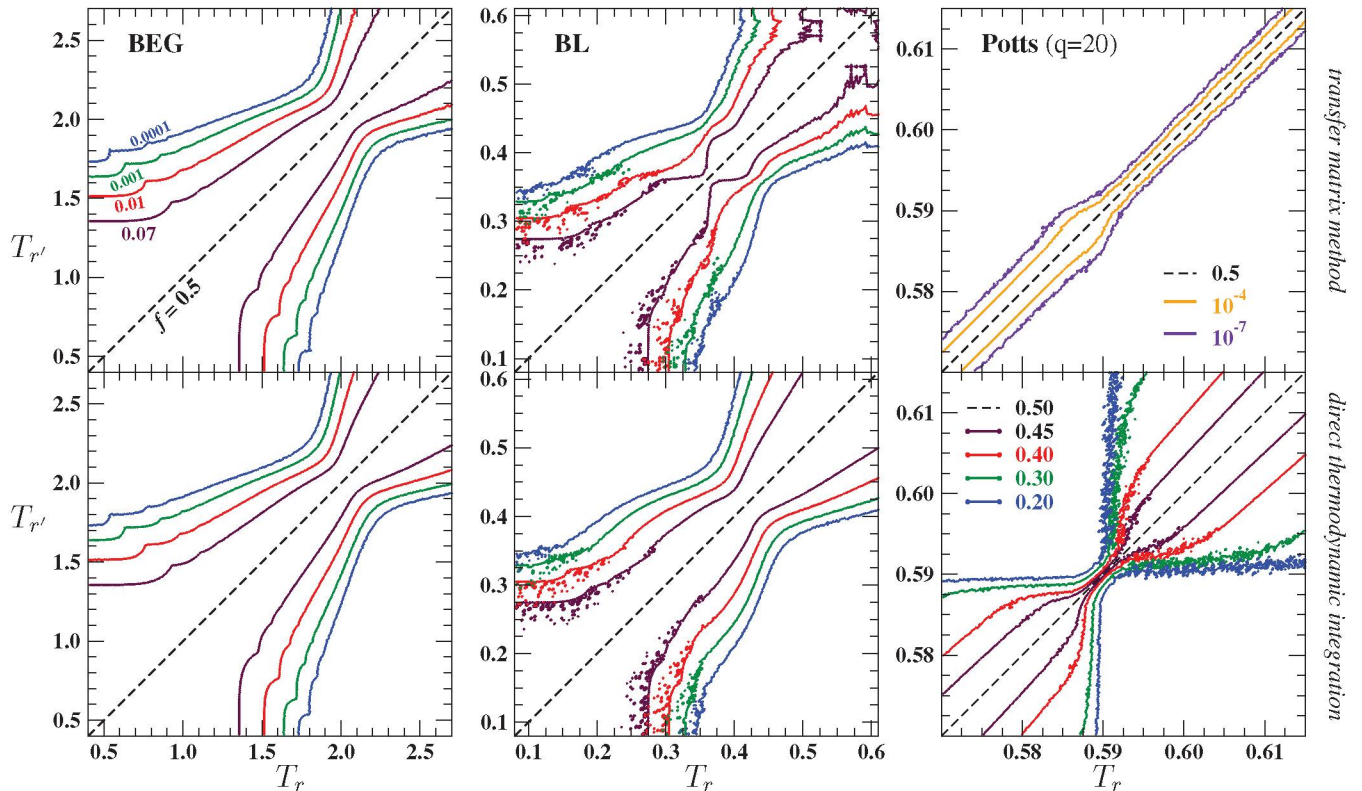


Figure 6.6: Contours map for different exchange frequencies $f_{r \rightarrow r'}$ (between two replicas T_r and $T_{r'}$) for the BEG, BL and Potts models with volume $N = 18 \times 18$. In top graphs, the transfer matrix method was used to calculate the weights $g_r - g_{r'}$, whereas that the direct thermodynamic integration was implemented in below graphs. In each model, we have computed $n_* \times n_* = 200 \times 200$ frequencies and their values were put in a map, which were interpolated to build all the contours. From each frequency contour the set $\Upsilon_R = \{T_1, T_2, \dots, T_R\}$ can be determined (see figure 4.1).

Namely, it is almost impossible to access a state with temperature T_r to a state with temperature $T_{r'}$, where the difference $\Delta T_{r,r'} \equiv |T_r - T_{r'}|$ is relatively large. We can identify an area in each map with a bottleneck shape at $T \approx T_b$ (BEG: 2.1, BL: 0.42, Potts_{q=20}: 0.59), which can be interpreted as a second order phase transition, because in this area $\Delta T_{r,r'}$ is minimum for any frequency (approximately).

Also, maps with exchange probabilities can be built too. In figure 6.7 we present those maps where an area with the bottleneck shape can also be observed. The contours here were determined by fixing the exchange probability $\exp(M_{r,r'})$ where the values of $M_{r,r'}$ are shown in the graphs for each contour. It is important to note that the temperatures T_b (where $\Delta T_{r,r'}$ is minimum) obtained in these graphs match with the values found in the exchange frequencies maps (figure 6.6). Thus, we can ensure that the exchange frequency $f_{r \rightarrow r'}$ should be strongly related with the exchange probability

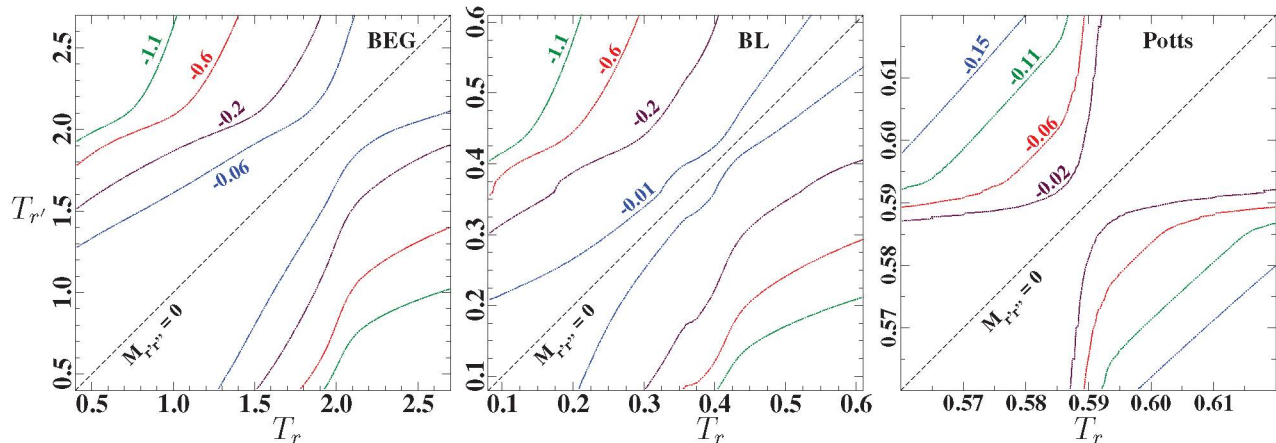


Figure 6.7: The plots show the contours map of logarithm of the exchange probability $\exp(M_{r,r'})$ between two replicas T_r and $T_{r'}$, for the BEG, BL and Potts models with volume $N = 18 \times 18$. The values of $M_{r,r'}$ were calculated by using equation 4.17. The Hamiltonian parameters used here correspond to figure 6.5 (for the Potts model we have used $q = 20$). Since the discontinuous line is to $M_{r,r'} = 0$ or $\Delta T_{r,r'} \equiv |T_r - T_{r'}| = 0$ (similar to figure 6.6), there is a point in each contour with $\Delta T_{r,r'}$ minimum. The contours move away to discontinuous line as $\exp(M_{r,r'})$ decreases, in the same way that $f_{r \rightarrow r'}$ decreases.

$\exp(M_{r,r'})$.

The values of temperature T_r or $T_{r'}$, whereby $\Delta T_{r,r'}$ is minimum in each contour (located over the bottleneck), yield a maximum value of the heat capacity

$$C_V = \left. \frac{\partial U}{\partial T} \right|_V \approx \frac{\Delta U}{\Delta T_{r,r'}}. \quad (6.9)$$

This fact is a condition of a continuous phase transition that it occurs across the temperatures T_r and $T_{r'}$ [114].

6.6 Replicas

As mentioned above, it is only by means of the maps of exchange frequencies or exchange probabilities that the set of replicas $\Upsilon_R = \{T_1, T_2, \dots, T_R\}$ can be calculated (see Figure 4.1). In order to have a comparative point of view, we have computed and plotted the replicas T_r by means of figures 6.6 (FEF method) and 6.7 (FEP method). The results for the combinations BEG \times (CE, FEF) \times (TMM, DTI) are shown in figure 6.8, BL \times (CE, FEF) \times (TMM, DTI) in figure 6.9, and (BEG, BL) \times FEP in figure 6.10.

As one can see, there are many similarities between the results obtained with FEF and FEP, especially when $f \rightarrow 1^+$ and $M_{r,r'} \rightarrow 0^-$. On the other hand, the range

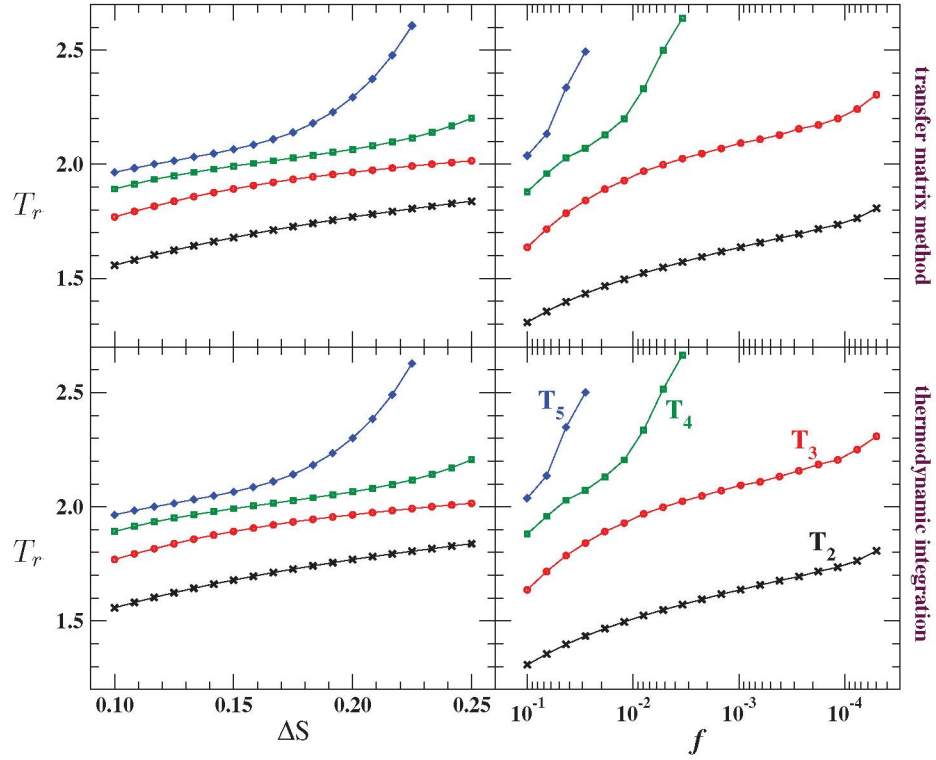


Figure 6.8: Replicas for the BEG model ($N = 18 \times 18$) with two methods: constant entropy (CE, *graphics on the left*) and fixed exchange frequency (FEF, *graphics on the right*). The weights were calculated by using the transfer matrix method (TMM, *upper graphics*) and direct thermodynamic integration (DTI, *down graphics*).

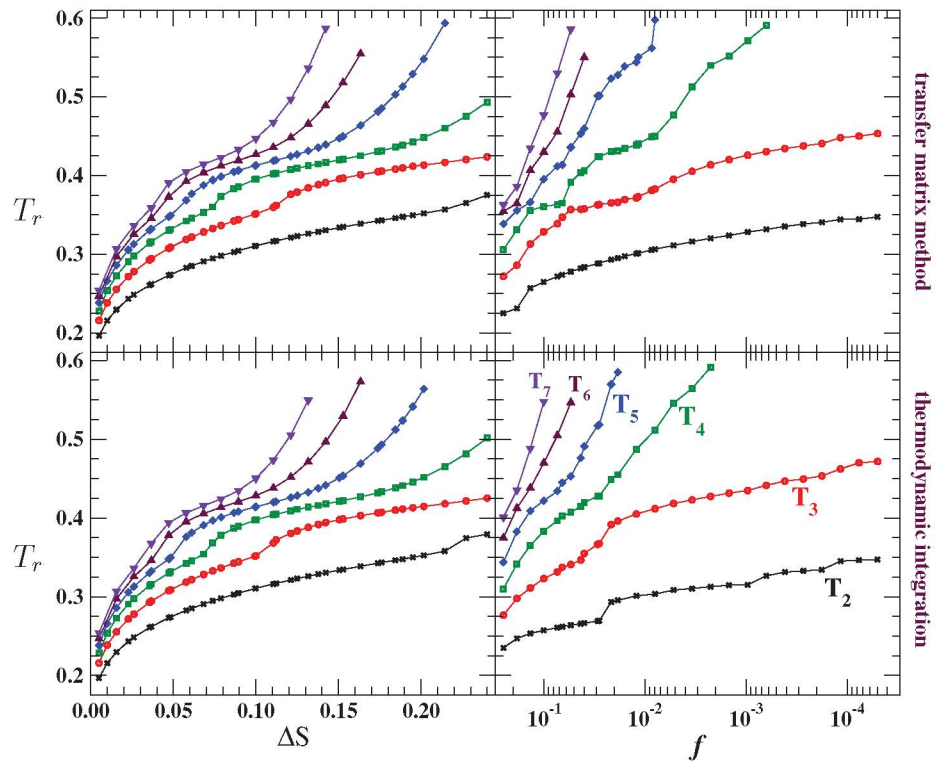


Figure 6.9: The same as in Fig.6.8, but for the BL model.

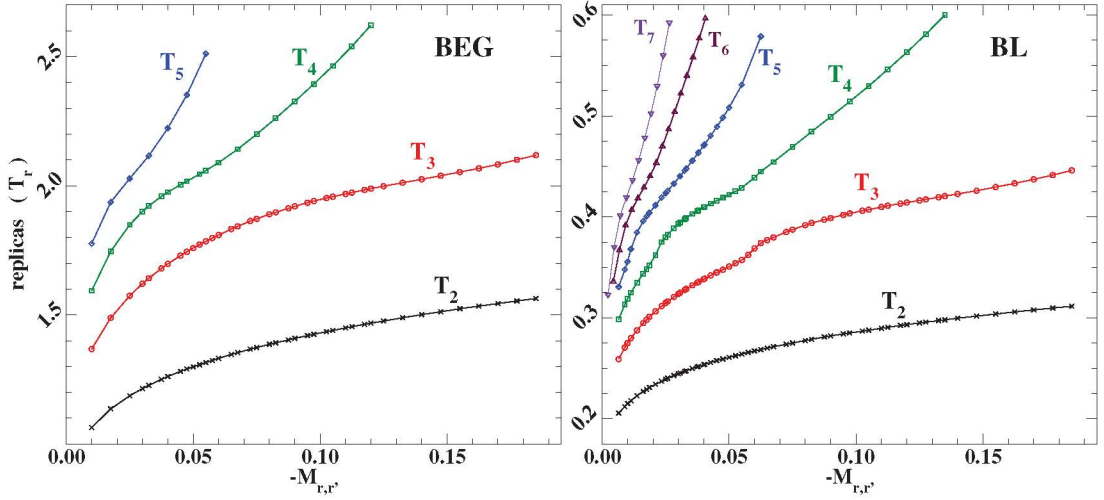


Figure 6.10: Values of the replicas T_r computed by means of fixed exchange probability method (FEP) with $N = 18 \times 18$. This method, and thus T_r , does not depend on the thermodynamics weights g_r . While on the contrary, the CE and FEF methods depend on the accuracy of g_r , which are computed by using other methods (TMM or DTI).

of the difference $\Delta T_{r+1,r} \equiv |T_{r+1} - T_r|$ obtained by means of CE method (especially with $r = 2, 3$) are very different with the other two methods (for the BEG and BL models). Namely, the differences $\Delta T_{3,2}$ and $\Delta T_{4,3}$ are approximately constant with Δs varying, whereas $\Delta T_{r+1,r}$ increase as f or $\exp(M_{r,r'})$ decreases.

Values of T_r for the Potts model were computed also, as shown in figure 6.11. Here, the replicas was computed with DTI only, because the thermodynamic weights calculated by means of the TMM proved to be inaccurate in this work (see figures 6.5 and 6.6). For the Potts model, the differences $\Delta T_{3,2}$ and $\Delta T_{4,3}$ are observed approximately constant with f or $M_{r,r'}$ varying, contrary to the BEG and BL models.

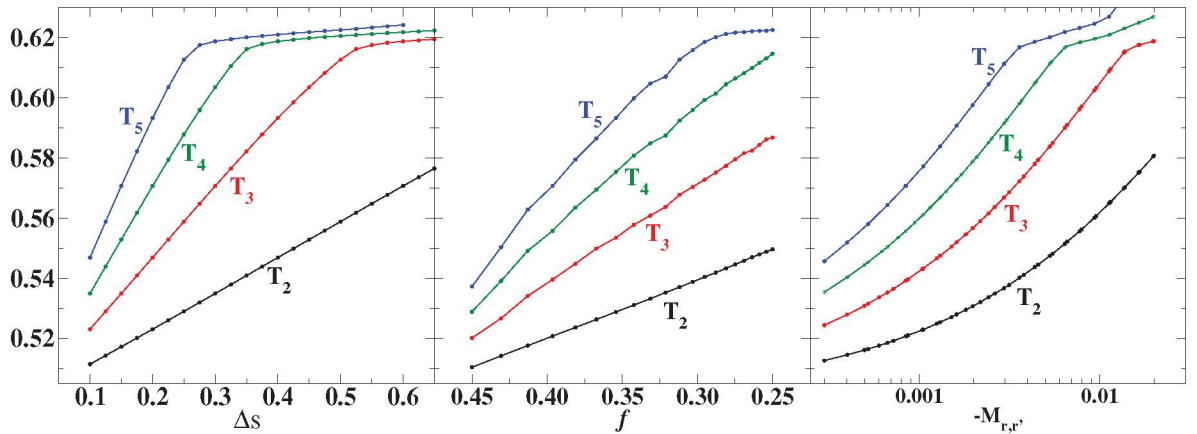


Figure 6.11: For the Potts model with $q = 16$, replicas T_r calculated with the DTI method and the three schemes to compute Υ_R (CE, FEF, FEP).

6.7 ST simulations for the BEG and BL models

The next step is to perform ST simulation with already known Υ_R . To determine which set Υ_R is the best one, in figure 6.12 is presented the results obtained for the BEG model with $T_1 = 0.5$, $R = 3$ and three values of Δs , f and $M_{r,r'}$. The figure 6.12 shows the density and magnetization evolutions (ρ and m) towards the steady value $\rho_{ss} = 2/3$. For this model, we start from a typical initial configuration, a lattice totally filled of particles $\sigma_i = +1$ (this is a ordered phase at steady state).

There is no convergence when the CE method is implemented to calculate Υ_R . Also, for relatively larger f 's (> 0.01) or smaller $-M_{r,r'}$'s (< 0.1), despite more frequent temperature exchanges, the system gets trapped in the initial configuration as a consequence of a too low T_3 . On the other hand, for much lower f 's (< 0.0001) or larger $-M_{r,r'}$'s (> 0.18), the resulting T_3 's become high enough to cross the entropy

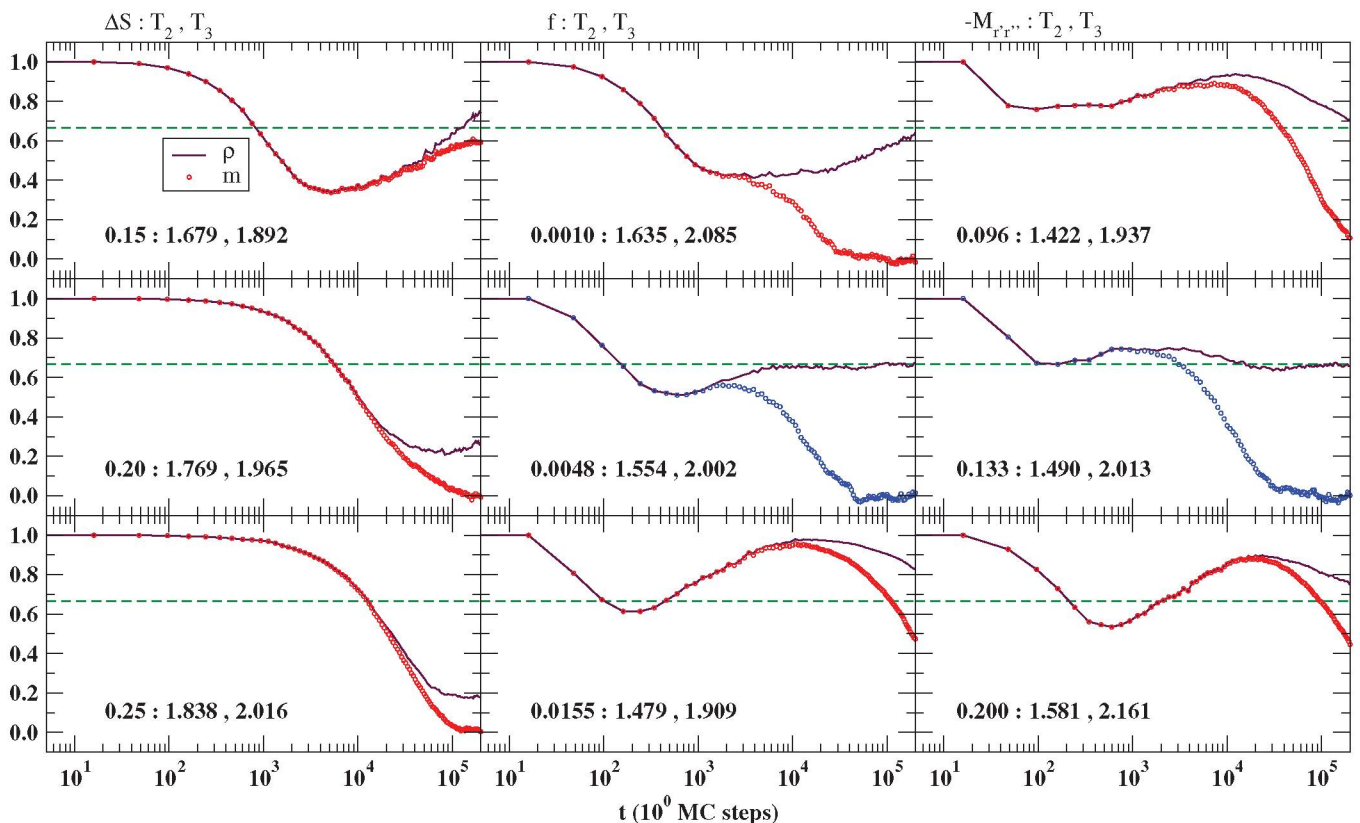


Figure 6.12: For the BEG model ($N = 18 \times 18$) at the phase coexistence (see figure 6.3), ρ and m simulated with the ST algorithm for $\Upsilon_{R=3}$ ($T_1 = 0.5$) obtained from three distinct values of Δs , f and $M_{r,r'}$. The best convergence towards the steady value $\rho_{ss} = 2/3$ (see equation 5.4) and $m_{ss} = 0$ is obtained for $f = 0.0048$ or $M_{r,r'} = 0.133$. The thermodynamics weights g_r used here were calculated by using the transfer matrix method in the first instance, as in references [51, 87].

barrier, but then exchanges hardly take place. As a consequence, there is an optimal intermediate value of f , yielding the best convergence to the correct ρ_{ss} .

Since the convergence is limited by the technique to compute Υ_R and a control parameter, a conclusion in advance is the fact that the MA is not the best algorithm to include in ST methods. A simple Monte Carlo step with the MA is not enough to guarantee a partial convergence, which is necessary to change the temperature with probability $\mathcal{P}_{r \rightarrow r'}$ (see equation 3.15).

Simulations with other initial configurations were performed too. For this case, we start from a empty lattice for the BEG and BL models. The evolution of ρ and m by means of ST ($R = 3, 4, 5$) are shown in figures 6.13 (BEG) and 6.14 (BL). The simulations presented in figures 6.13 and 6.14 were performed by implementing the calculation of $g_{r'} - g_r$ with DTI method, and computing the averages as (cumulative time averages)

$$\langle \Psi \rangle_t = \sum_{i=0}^t \Psi_i = \left(1 - \frac{1}{t}\right) \langle \Psi \rangle_{t-1} + \frac{\Psi_t}{t}, \quad (6.10)$$

where t is the Monte Carlo step (iteration) and $\Psi = \rho, m$. Two important aspects can

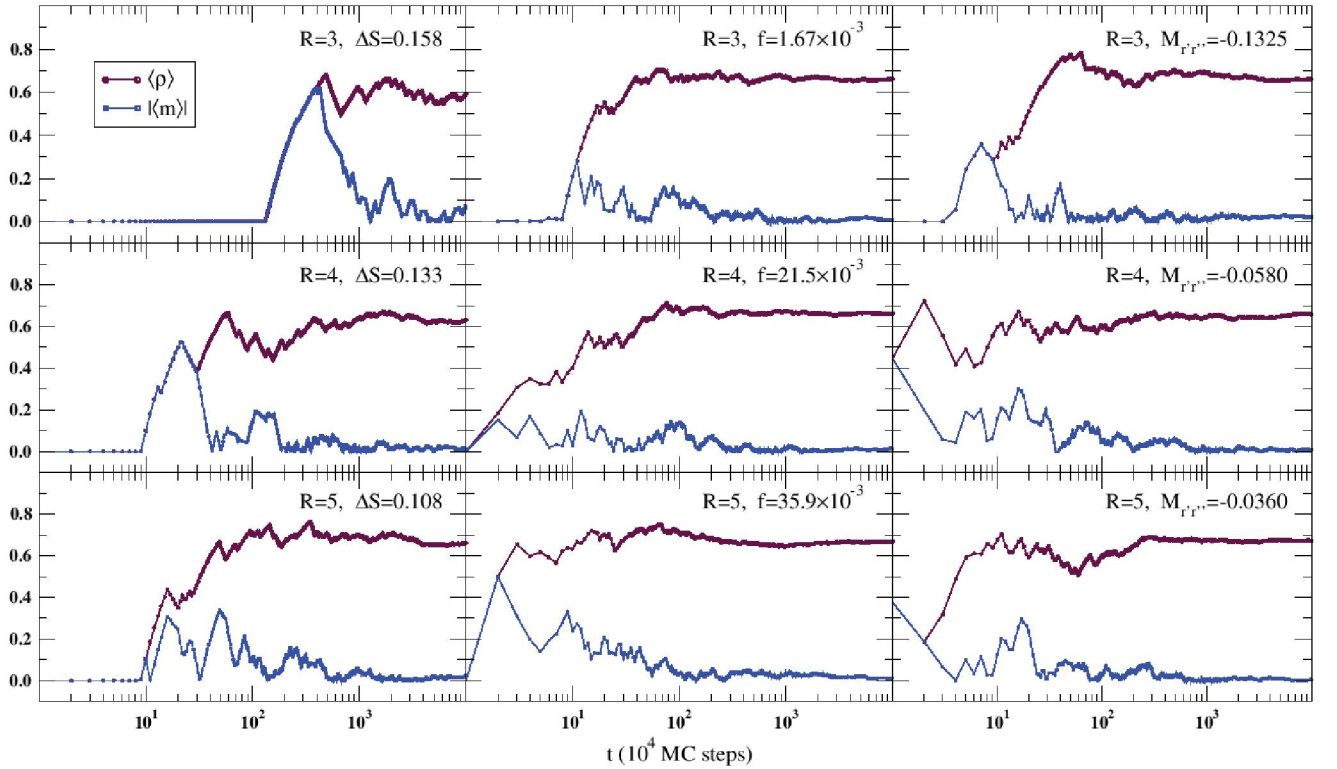


Figure 6.13: Evolutions of ρ and $|m|$ in ST simulations for the BEG model ($N = 18 \times 18$) and distinct values of R and with the optimal values of Δs , f and $-M_{r,r'}$.

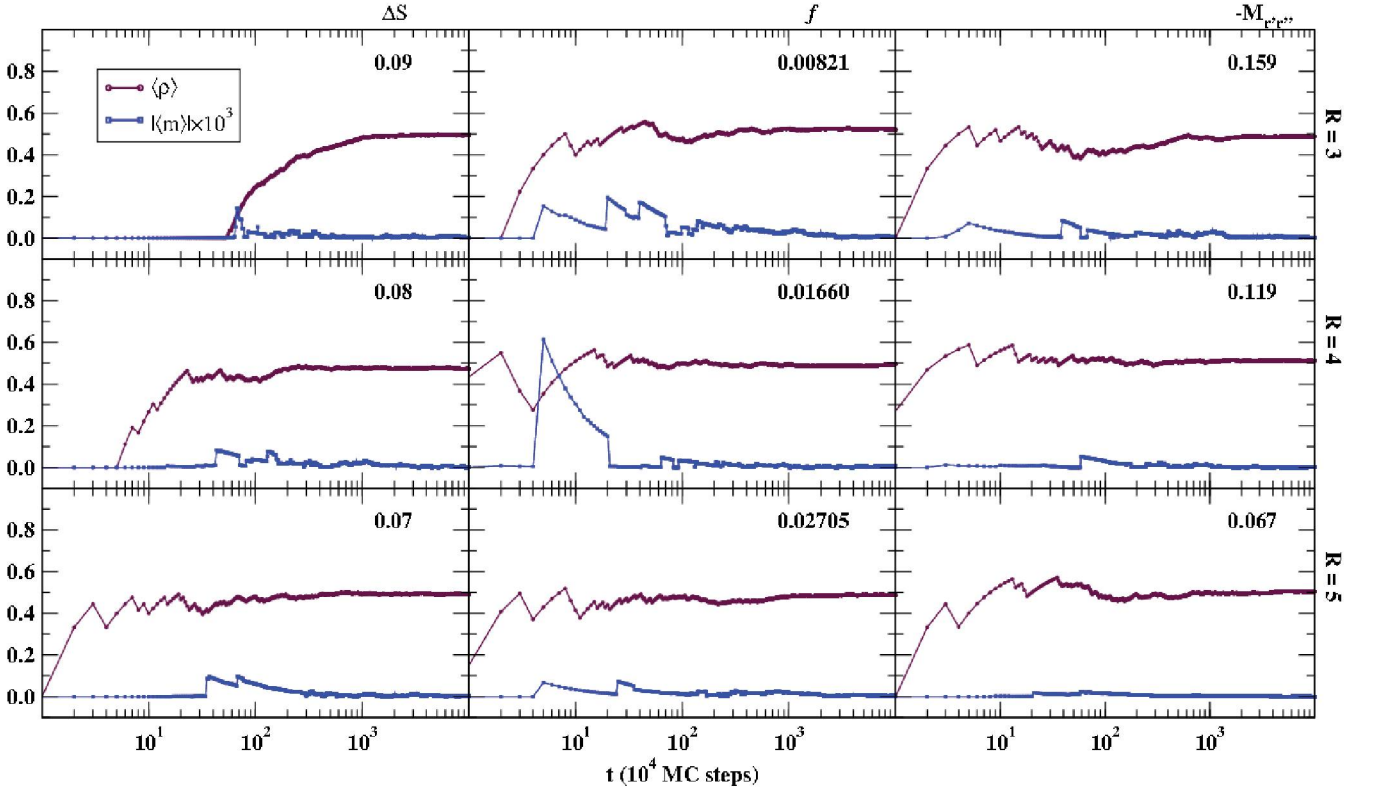


Figure 6.14: The same as in Fig.6.13, but for the BL model with $T_1 = 0.1$.

be observed in figures 6.13-6.14: (1) The convergences of ρ and m are faster as R is greater [95,115]. (2) The FEF and FEP methods reproduce significantly equal results.

In order to determine the effects of the TMM and DTI implementations in the simulated tempering algorithm, we have performed simulations for large number of iterations (Monte Carlo steps). They are shown in figures 6.15 (for BEG with the TMM), 6.16 (for BEG with the DTI) 6.17 (for BL with the TMM) and 6.18 (for BL with the DTI). For the four cases (BEG,BL) \times (TMM,DTI), the values of the density ρ and the average particle orientation m were computed by means of typical averages between intervals δt , that is, $\langle \Psi \rangle_t = \sum_{i=t}^{t+\delta t} \Psi_i$, where $\delta t = 10^7$ and $\Psi = \rho, m$. Also, for these cases the initial configuration was a lattice with random values of the microstate $\sigma_i = 0, \pm 1$.

When comparing figures 6.17 (BL with TMM) and 6.18 (BL with DTI), one can see a significant difference, namely, ρ is more stable (best tunneling) when DTI is used. The values of $g_{r'} - g_r$ computed by DTI are more close to $\beta_{r'} \psi_{r'} - \beta_r \psi_r$ (where ψ_r is the “correct” free energy), in such a way that the transition occurs with more intensity than with TMM at the steady state.

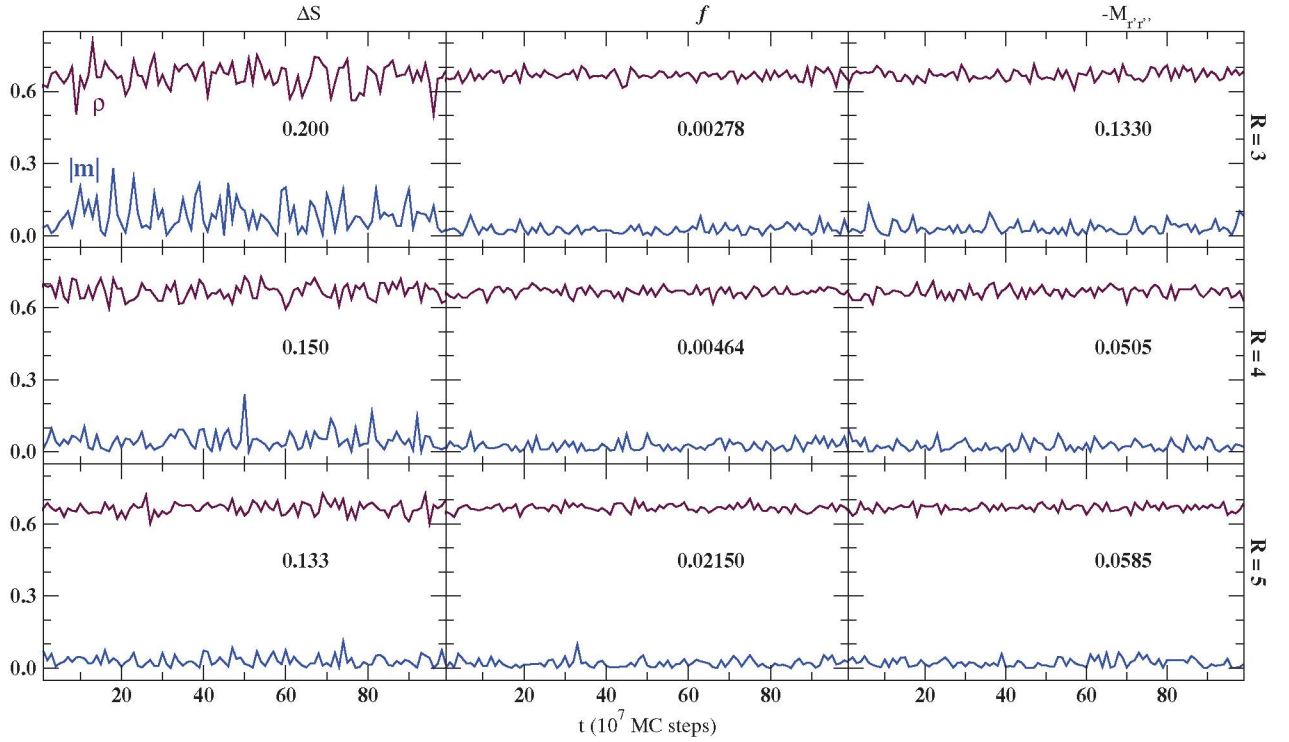


Figure 6.15: Long evolutions of ρ and m in the ST simulations with $T_1 = 0.5$, $R = 3, 4, 5$ for the BEG model ($N = 18 \times 18$) with TMM and for the three methods to determine Υ_R (CE, FEF and FEP). The graphs only show the ST simulations with the optimal parameter.

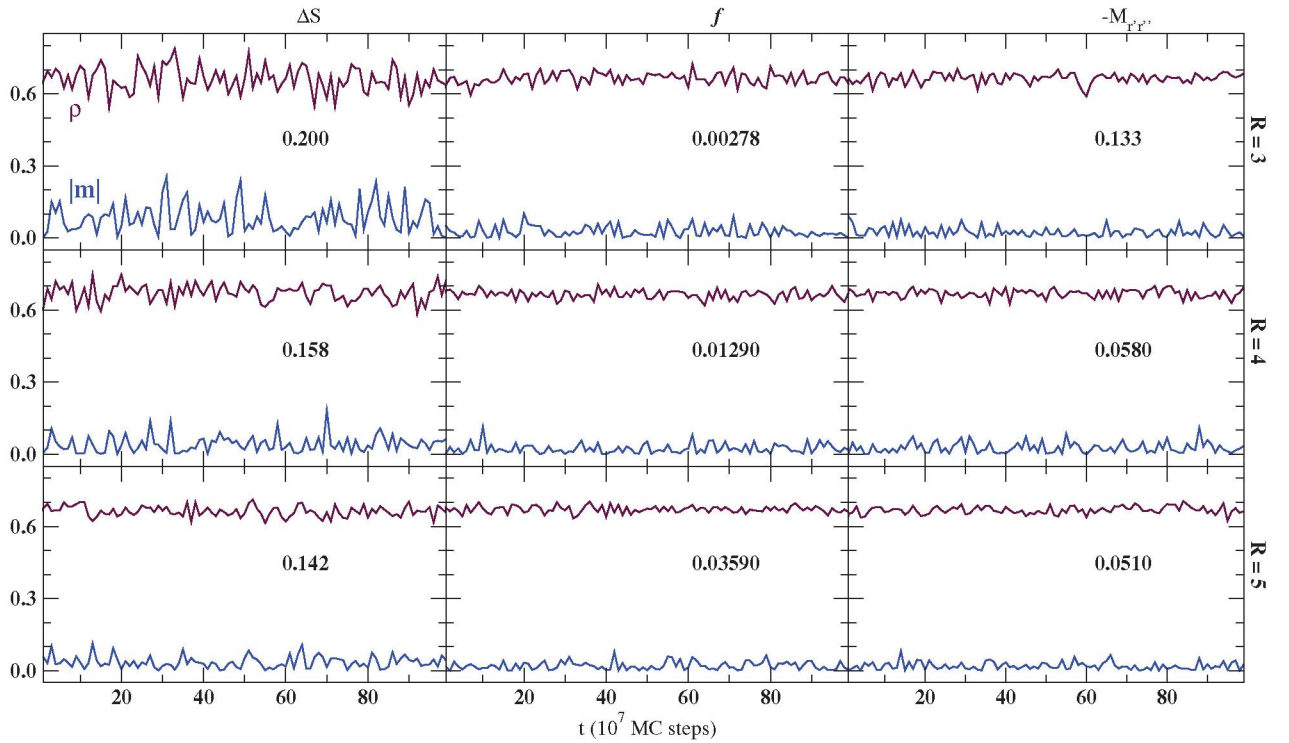


Figure 6.16: The same as in figure 6.15, but for the BEG model with DTI. It can not see a significant difference with respect to the TMM.

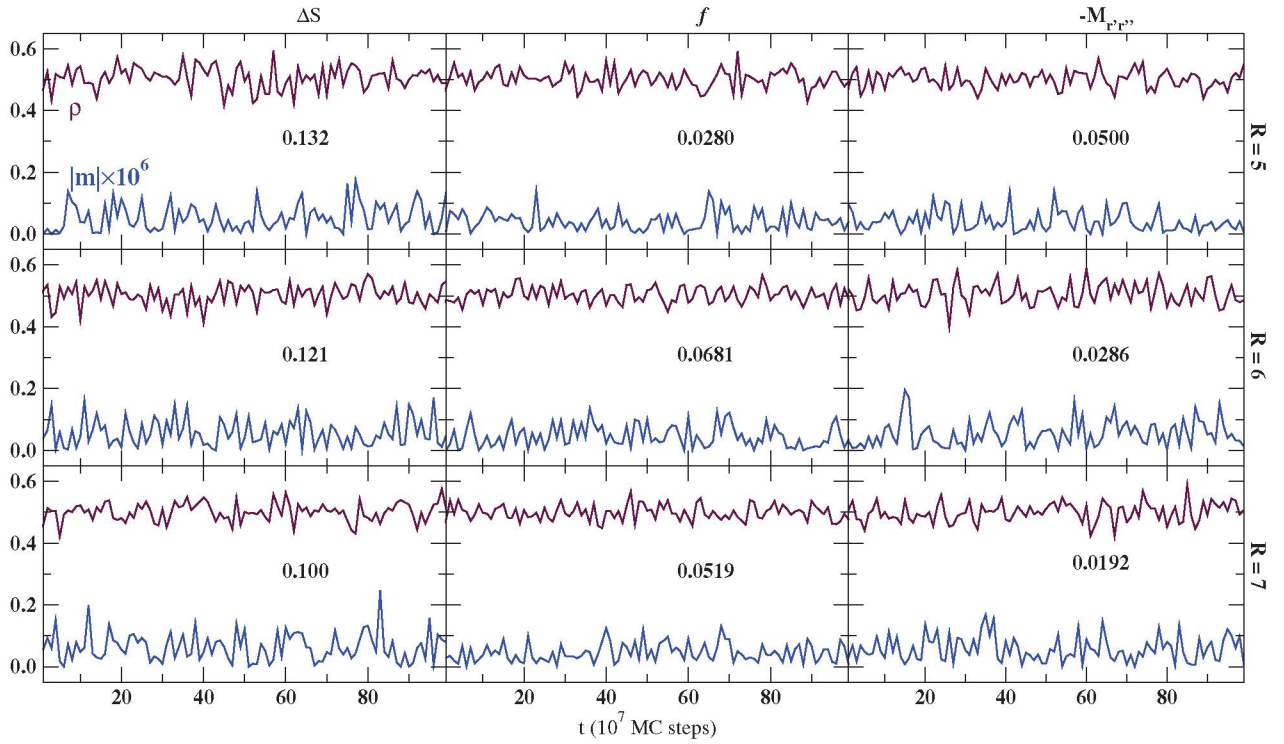


Figure 6.17: The same as in figure 6.15, but for the BL model with TMM, $T_1 = 0.1$ and $R = 5, 6, 7$. The values obtained for the magnetization m turned out to be very small (10^{-7}), and for this reason, we have rescaled these values in the graphs.

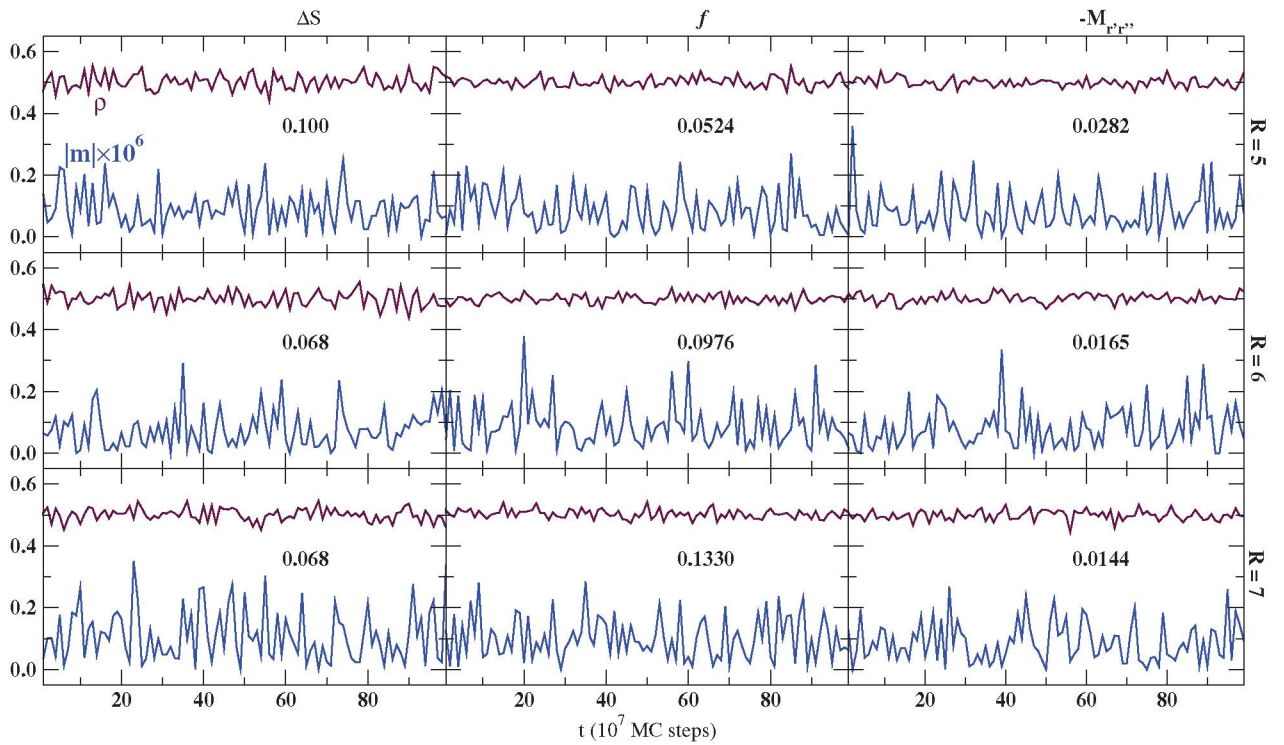


Figure 6.18: The same as in figure 6.17, but for the BL model with DTI.

6.8 Probability distributions

For the simulations presented in figures 6.16 and 6.18 (namely, thermodynamic weights calculated with DTI), we have computed averages over the probability distributions for the CE, FEF and FEP methods. The results are displayed in figure 6.19 for BEG ($R = 3$) and figure 6.20 for BL ($R = 5$).

The tunneling is observed through the peaks in the probability curves which point out the equilibrium phases. From this analysis, in the three cases (CE, FEF and FEP) the best tunneling is observed when the replicas Υ_R are determined using the FEP method. This fact is evidenced in the P_2 -values, which are more pronounced, first by FEP, second by FEF, and third by CE.

Also, it is important to note that for the BL model the distributions P_R ($R = 5$) are significantly different between the CE, FEF and FEP methods. In particular, the FEP method yield the distribution P_5 with more dispersion than with CE or FEF. This means that more configurations can be obtained in the firsts replica when Υ_R is computed through the FEP scheme.

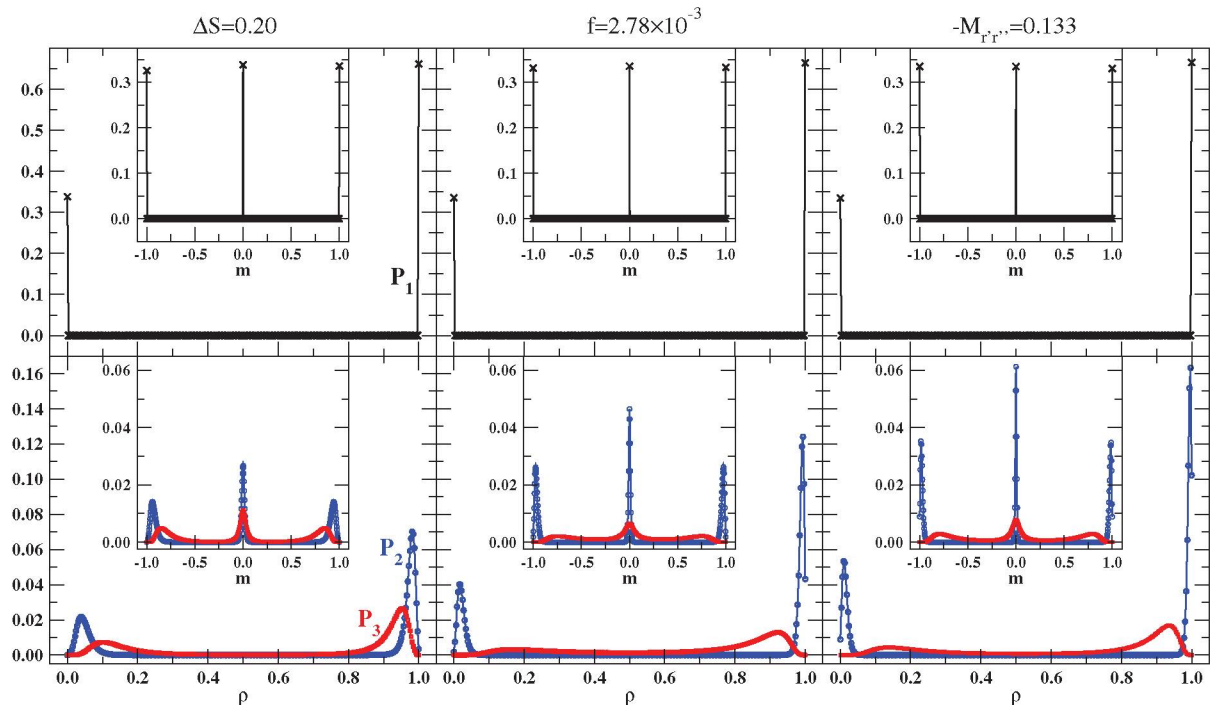


Figure 6.19: For the BEG model ($N = 18 \times 18$) and $R = 3$, the probability distribution histogram of the order parameters ρ and m in each replica at the coexistence for the CE, FEF and FEP methods. The distribution for the replica T_r are indicated as P_r . Maximum values reveal the phase coexistence in each replica given by ρ_{ss} .

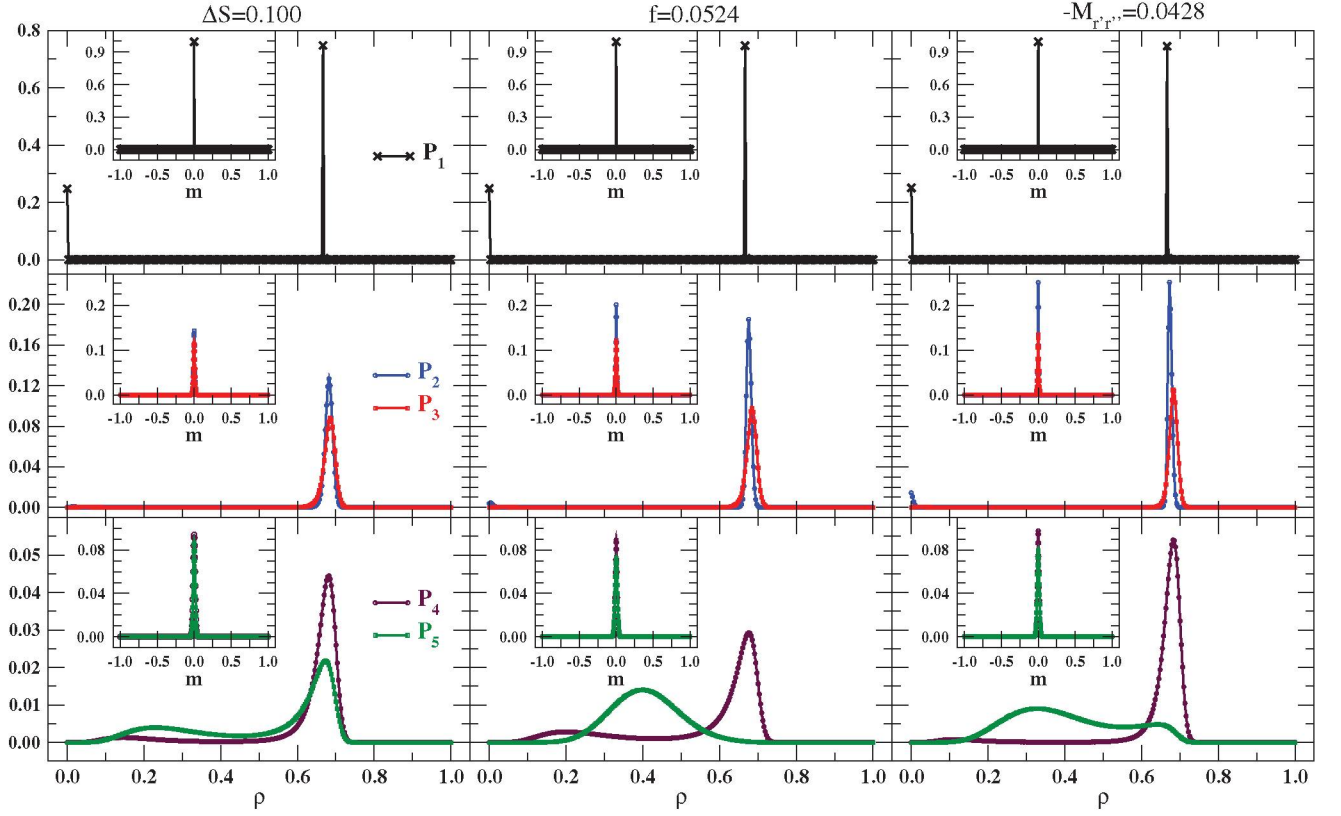


Figure 6.20: The same as in figure 6.19, but for the BL model with $R = 5$.

6.9 FOPT for the BEG and BL models

As such is presented in section 2.4, the order parameter close to the coexistence is not depend on V . From the theory developed by Fiore and da-Luz [81,82], the partition function can be decomposed as a sum of exponential functions where one can derive an analytical expression of the order parameter, which depends on few coefficient. The volume $V = N$ is one of the parameter that disappears in the derivation.

Then, by using the FEF protocol with $R = 3$ and the optimal values of f present in figures 6.15 and 6.17 (transfer matrix method), we have run ST simulations with different chemical potentials μ (for BEG and BL), H (for BEG) with fixed values of volumes V . In figure 6.21 are shown these results with three different values of V . The behavior of the particle density ρ and the internal energy u close to the coexistence (equation 5.10 for BEG and equation 5.15 for BL), presents an intersection for the three values of V , revealing a FOPT and corroborating the formulation made by Fiore and da-Luz. Also, we can observe that, in the range $\mu + 8 > 0$ for BEG and $\mu + 1.65 > 0$ for BL, u decreases linearly.

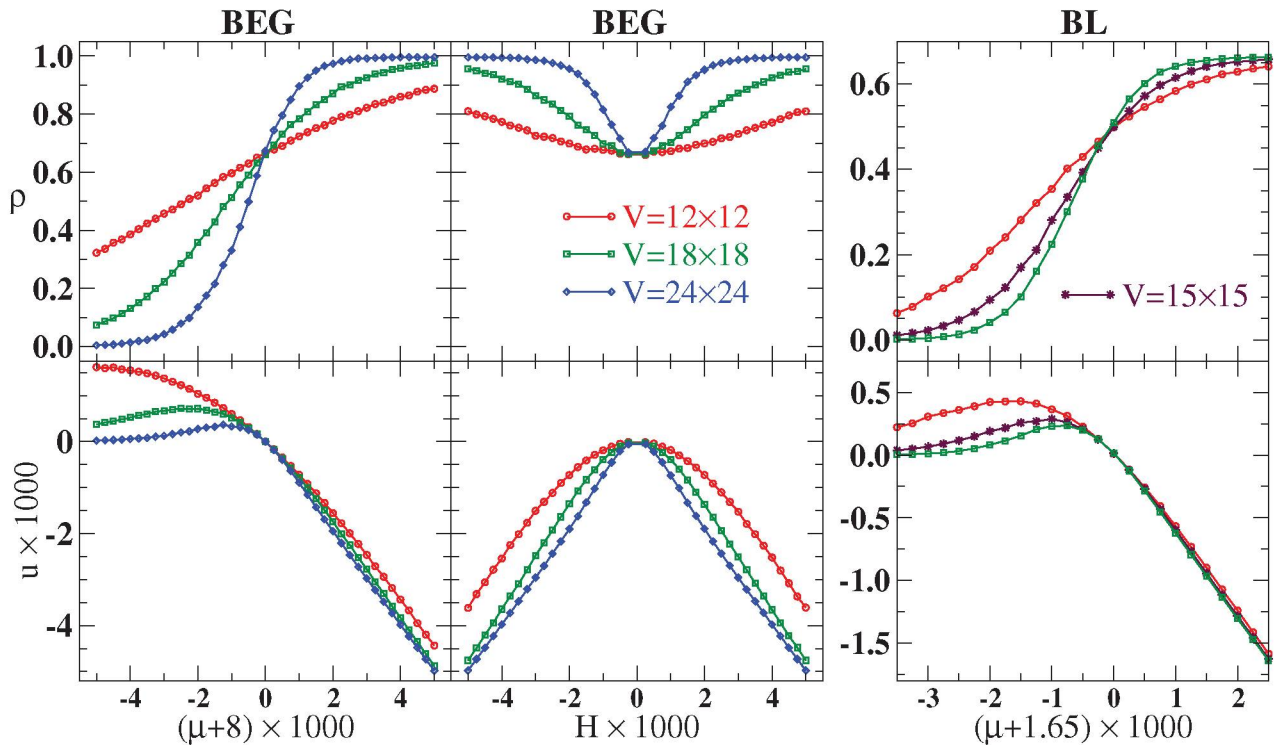


Figure 6.21: Recognition of a first order phase transition through the intersection of ρ or u versus μ (BEG and BL) and H (BEG) for three different values of volume $V = N$.

6.10 ST simulations for the Potts model

Finally, in this section we present results for the Potts model with $q = 5$ ($T_c \approx 0.85$). In order to determine V_{max} (see equation 5.19), a recursive algorithm that visit successive neighbors has been developed. First that all, a SA simulation was performed to determine $u(T)$ -curve (see figure 6.22). Later, by means of the DTI and FEP schemes, we run some ST simulations varying the control parameter $-M_{r,r'}$, as shown in figure 6.23. In this figure we present the evolutions of the pseudo-magnetization m , the order parameter ϕ and the internal energy u , with $R = 3$. The results shown that for $-M_{r,r'} = 0.0347$ the evolution of m present the best tunneling towards the steady value $m_{ss} = 2$ (see equation 5.24).

The scattering of m -values in figure 6.23 is in agreement with that observed for the BEG an BL order parameters. It can be obtained an optimal value of $-M_{r,r'}$ allowing substantially more frequent tunneling between phases, and thus, much better statistics to calculate relevant thermodynamic quantities. However, values of ϕ and $-M_{r,r'}$ show the same scattering for the three values of $-M_{r,r'}$. This fact point out that the pseudo-magnetization is more effective to percieve a FOPT.

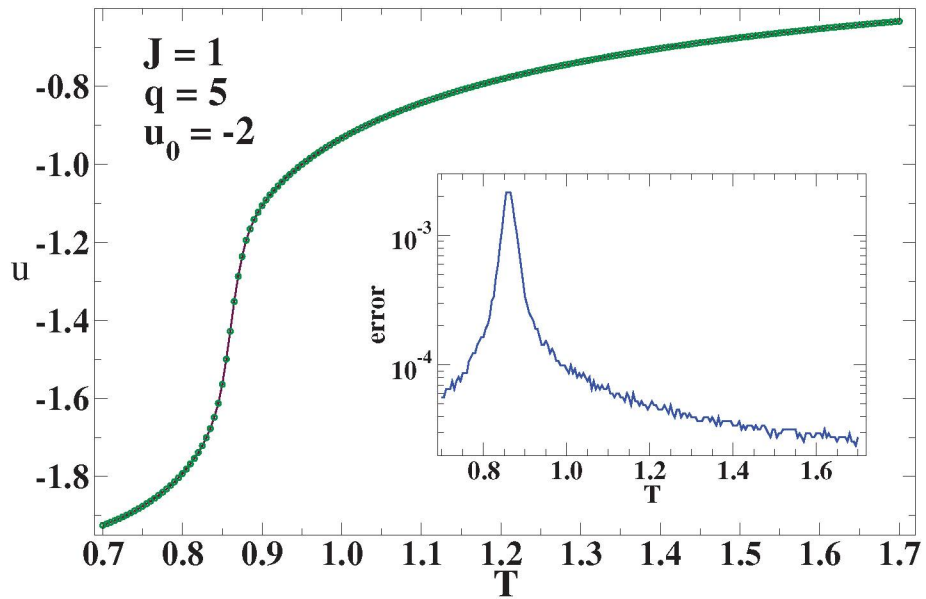


Figure 6.22: For the Potts model ($N = 18 \times 18$), internal energy u versus temperature T . This curve was obtained by through a SA simulation with 200 points of temperature.

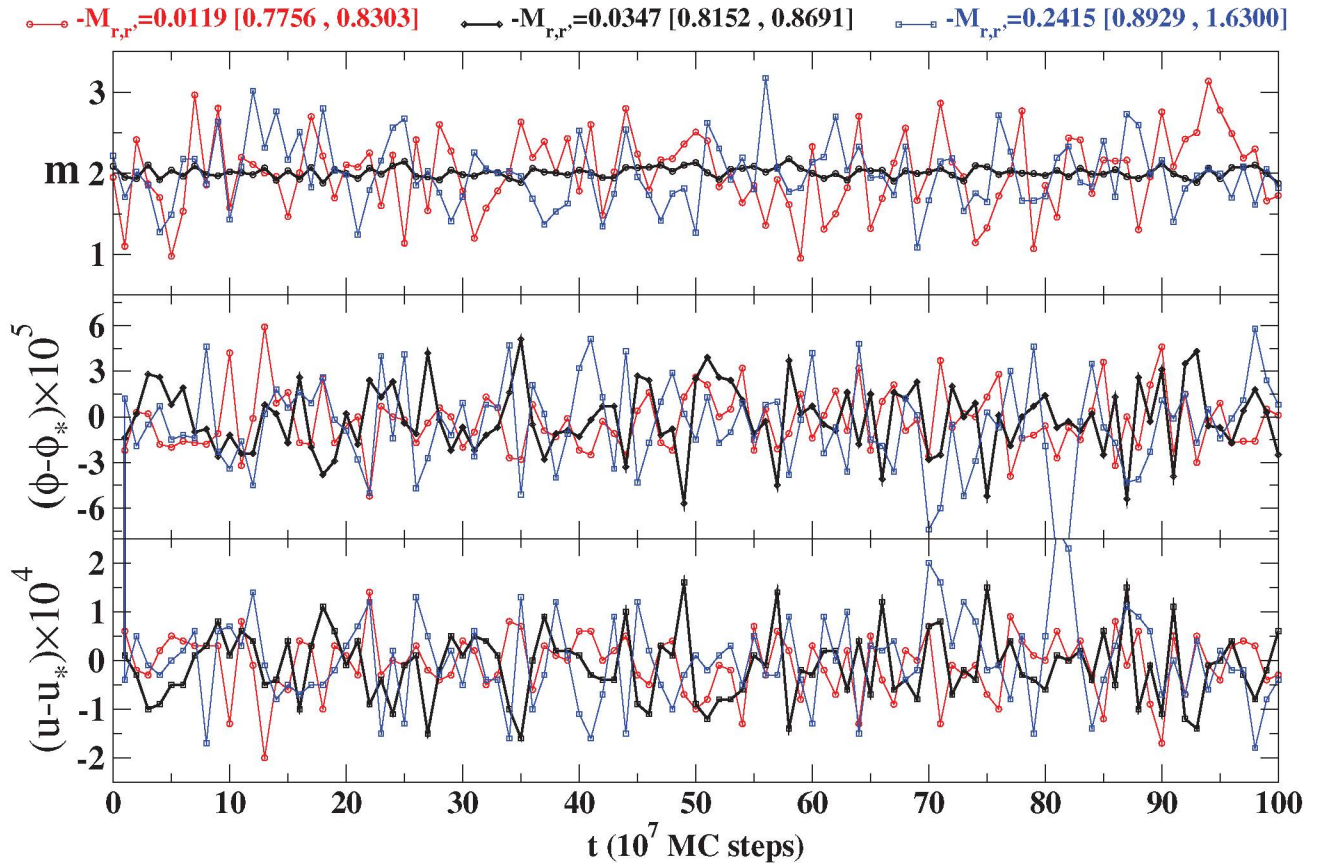


Figure 6.23: For the Potts model, m , ϕ and u evolutions (as function of ST iterations, t) with $R = 3$, $T_1 = 0.7$ and three values of $-M_{r,r'}$. The averages of each estimator for each value of t were calculated by means of equation 6.10 (cumulative time averages). The T_2 and T_3 replicas are pointed out in the brackets as $[T_2, T_3]$. For the temperature $T = T_1$, the critical values $\phi_* \approx 0.97891$ and $u_* \approx -1.9253$ have been obtained from the same simulations.

Chapter 7

Conclusions

The innovative idea in simulated tempering (**ST**) is to treat the temperature T as an additional dynamic parameter. As a consequence, the system is defined on an augmented space $\Omega_s \times \Omega_T$ where Ω_s is the original phase space and Ω_T denotes the one-dimensional temperature space. Through Ω_T , namely, by varying the temperature ladder T_r ($r = 1, 2, \dots, R$), more places of Ω_s can be visited, allowing to detect phase coexistence and phase transitions. In our simulations we have been able to verify the phase coexistences through the numeric calculation of averages over \mathcal{N} phases: $\rho_{ss} = 2/3$ (BEG), $\rho_{ss} = 1/2$ (BL) and $m_{ss} = 2$ (Potts).

The efficiency of ST schemes strongly depend on (1) the number of replicas R , (2) the accuracy of weight factors $g_{r'} - g_r$ and the set $\Upsilon_R = \{T_1, T_2, \dots, T_R\}$. In this sense, two contributions were developed and implemented in this work,

1. The values of the thermodynamic weights ($g_{r'} - g_r$) computed directly from the internal energy (DTI) were analyzed and compared with values obtained from the transfer matrix method for the Ising, BEG, BL and Potts models. The theory described in section 4.1 includes internal energy of the ground state u_o , which is non zero for the Ising and Potts models (the same scheme with $u_o = 0$ is described in reference [43]). These weights were implemented in ST simulation for BEG, BL and Potts models. For the BEG model, there is no distinction in the tunneling between TMM and DTI. However, for the BL model, better tunnelings were found regardless of the technique to determine Υ_R . It was impossible to implement the TMM for the Potts model, since there is a strong phase transition

for $q > 4$ [111, 116], and thus $\langle \delta_{\mathcal{L}_k, \mathcal{L}_{k'}} \rangle \rightarrow 0$ (see equation 3.29).

2. A new method to determine the set $\Upsilon_R = \{T_1, T_2, \dots, T_r\}$ has been formulated and partially tested. For a given number of replicas R , adjacent T_r 's are chosen in such a way that the changes of temperature (from T_r to T_{r+1} , for any $r = 1, 2, \dots, R-1$) occur with a fixed probability $\exp(M_{r,r'}) = \mathcal{P}_{r \rightarrow r'} \mathcal{P}_{r' \rightarrow r}$ (see equation 4.17). Note that this probability does not depend on g_r or previous simulations, while FEF does depend on it [51]. However, in most of the results with FEF and FEP the tunneling was almost the same (in few ST simulations the FEP is slightly better). The main advantage here was the simple implementation of $g_{r'} - g_r$ (once known $u(T)$).

On the other hand, the search for the optimal values of X [where X is equal to Δs (CE), f (FEF) or $-M_{r,r'}$ (FEP)], demands preliminary numerics. Namely, we needed to perform some simulations (say \mathcal{N}) fixing the parameter X from X_1 to X_2 . Later, it was necessary define a magnitude $\Delta\mathcal{W}$ that would establish the difference between the simulated order parameter and the theoretical value at the steady state (ρ_{ss} or m_{ss}). Then, the optimal simulation (with $X = X_{opt}$) was the one with $\Delta\mathcal{W}$ minimum. For this reason, we suggest to research new analytically methods to know the optimal value of X . We are convinced that the temperature where the continuous phase occurs T_b should be the minimum value of T_R , because to $T_R < T_b$ the simulations would not change the state.

We have evaluate the ST method with new ingredients and we could detected the phase coexistence when observing the tunneling of the order parameter towards ρ_{ss} or m_{ss} . The first-order phase transition (**FOPT**) was simulated for the BEG and BL models. However, the FOPT for the Potts model is a pending work. Such as in section 6.9, in references [51, 81, 82, 94] the FOPT is evidenced by varying some Hamiltonian parameter, such as μ , H , and others (say ψ). Then, by performing simulation with different V (volume), and plotting the order parameter versus ψ , the point where all curves cross is a FOPT. Therefore, in a near future, it will be necessary to perform more simulations for the Potts model.

Finally, we recommend to perform ST by means of an adaptative algorithm to determine the weights $g_r - g_{r'}$. As we explained before the ST algorithm requires

these values to be executed. The methodology implemented in this work (and previous works [51,52,81,87–89]) was to determine the weights by means of previous simulations, namely by performing simulated annealing (**SA**) simulations. In these SA simulations were obtained the internal energy $u(T)$ and $g(T)$ (by using the transfer matrix method). In this sense, we consider possible to design and implement an ST algorithm where $u(T)$, and latter $g(T)$, would be computed in each Monte Carlo step, before the attempt to change the temperature. The weights required to change the temperature should be update in each Monte Carlo step, and initial values of $g_r - g_{r'}$ will be necessary for each replica. Obviously, the first attempts of temperature will be “loose” because the initial values of $g_r - g_{r'}$ are unknown (or incorrectly initialized). However, in the evolution of these values, the correct free energy should be obtained.

Chapter 8

References

- [1] J.M. Yeomans. *Statistical mechanics of phase transitions*. Oxford University Press, Great Britain, 1992.
- [2] H.E. Stanley. *Introduction to phase transitions and critical phenomena*. Clarendon Press, MIT, 1971.
- [3] N. Metropolis, A.W. Rosenbluth, M.N. Rosenbluth, A.H. Teller, and E. Teller. Equation of state calculations by fast computing machines. *J.Chem.Phys.*, 21:1087–1092, 1953.
- [4] D.T. Gillespie. *Markov Processes: An introduction for physical scientists*. Academic Press, California, 1992.
- [5] D.P. Landau and K. Binder. *A guide to Monte Carlo simulations in statistical physics*. Cambridge University Press, New York, 3 edition, 2009.
- [6] K. Binder. Applications of Monte Carlo methods to statistical physics. *Rep.Prog.Phys*, 60(5):487, 1997.
- [7] M. Kastner. Monte Carlo methods in statistical physics: Mathematical foundations and strategies. *Commun.Nonlinear Sci.Numer.Simul.*, 15(6):1589–1602, 2010.
- [8] Y. Wang. Quantum Monte Carlo simulation. *Ann.Appl.Stat.*, 5(2A):669–683, 2011.

- [9] M. Creutz and B. Freedman. A statistical approach to quantum mechanics. *Ann.Phys.*, 132:427–462, 1981.
- [10] W.M.C. Foulkes, L. Mitas, R.J. Needs, and G. Rajagopa. Quantum Monte Carlo simulations of solids. *Rev.Mod.Phys*, 73(1):33, 2001.
- [11] J. Seco and F. Verhaegen. *Monte Carlo techniques in radiation therapy*. Taylor & Francis, Minnesota, 2013.
- [12] D.W.O. Rogers. Fifty years of Monte Carlo simulations for medical physics. *Phys.Med.Biol.*, 51:R287–R301, 2006.
- [13] F. Sánchez-Doblado, A. Leal, M. Perucha, R. Arráns, L. Núñez, J.V. Roselló, B. Sánchez-Nieto, E. Carrasco, A. Gonzalez, J.C. Medrano, L. Errazquin, and J.A. Sánchez-Calzado. Monte Carlo clinical dosimetry. *Rep.Pract.Oncol.Radiother.*, 7(2):43–51, 2002.
- [14] M. Kulkarni, R. Dendere, F. Nicolls, S. Steiner, and T.S. Douglas. Monte Carlo simulation of a slot-scanning x-ray imaging system. *Phys.Med.*, 32:284–289, 2016.
- [15] G. Tirao, C. Quintana, F. Malanoa, and M. Valente. X-ray spectra by means of Monte Carlo simulations for imaging applications. *X-Ray Spectrom.*, 39:376–383, 2010.
- [16] J. Doll and D.L. Freeman. Monte Carlo methods in chemistry. *IEEE Comput.Sci.Eng.*, 1(1):22–32, 1994.
- [17] G.D. Cohen. Monte Carlo simulation of reactions kinetics. *Ind.Eng.Chem.Fundam.*, 4(4):471–475, 1965.
- [18] T. Houska, S. Multsch, P. Kraft, H.-G. Frede, and L. Breuer. Monte Carlo-based calibration and uncertainty analysis of a coupled plant growth and hydrological model. *Biogeosciences*, 11:2069–2082, 2014.
- [19] M. Matsuoka, H. Nagare, and T. Fujiwara. Simulation of the collection of catch crops for the recovery of agricultural resources using geographic and statistical data. *Transactions in GIS*, 20(2):221–239, 2016.

- [20] P. Glasserman. *Monte Carlo methods in financial engineering*. Springer, New York, 2003.
- [21] J.D. Annan and J.C. Hargreaves. Efficient estimation and ensemble generation in climate modelling. *Philos.Trans.Royal Soc.A*, 365:2077–2088, 2007.
- [22] L. Bramer. *Methods for modeling and forecasting wind characteristics*. PhD thesis, Iowa State University, Iowa, 2013.
- [23] C. Moglestue. *Monte Carlo Simulation of Semiconductor Devices*. Springer, Freiburg im Breisgau, 1 edition, 1993.
- [24] C.J. Mode. *Applications of Monte Carlo Methods in Biology, Medicine and Other Fields of Science*. InTech, California, 2011.
- [25] S. Mark and S. Mordechai. *Applications of Monte Carlo Method in Science and Engineering*. InTech, Croatia, 2011.
- [26] J.M. Hammersley and D.C. Handscomb. *Monte Carlo methods*. John Wiley & Sons, New York, 1964.
- [27] S. Friedli and Y. Velenik. *Statistical mechanics of lattice systems: A concrete mathematical introduction*. Cambridge University Press, 1 edition, 1993.
- [28] A.D. Mackie, A.Z. Panagiotopoulos, D. Frenkel, and S.K. Kumar. Constant-pressure Monte Carlo simulations for lattice models. *EPL*, 27(7):549–554, 1994.
- [29] S.G. Brush. History of the Lenz-Ising model. *Rev.Mod.Phys*, 39:883, 1967.
- [30] G.R. Schreiber. Frustrated Blume-Emery-Griffiths model. *EPJ B*, 9:479–490, 1999.
- [31] V.O. Öz celik and A.N. Berker. Blume-Emery-Griffiths spin glass and inverted tricritical points. *Phys.Rev.E*, 78:031104, 2008.
- [32] M. Weigel and M.J.P. Gingras. Zero-temperature phase of the xy spin glass in two dimensions: Genetic embedded matching heuristic. *Phys.Rev.B*, 77:104437, 2008.

- [33] A.P. Young and D.A. Lavis. Critical behavior of a two-dimensional bonded lattice model. *J.Phys.A*, 12(2):229, 1979.
- [34] C.E. Fiore, M.M. Szortyka, M.C. Barbosa, and V.B. Henriques. Liquid polymorphism, order-disorder transitions and anomalous behavior: A Monte Carlo study of the Bell-Lavis model for water. *J.Chem.Phys.*, 131:164506, 2009.
- [35] A.J. Schultz and D.A. Kofke. Algorithm for constant-pressure Monte Carlo simulation of crystalline solids. *Phys.Rev.E*, 84:046712, 2011.
- [36] D. Buta, K.F. Freed, and I. Szleifer. Thermodynamic properties of lattice polymers: Monte Carlo simulations and mean-field theories. *J.Chem.Phys.*, 112(13):6040, 2000.
- [37] A. Ibenskas, M. Šimėnas, and E.E. Tornau. Numerical engineering of molecular self-assemblies in a binary system of trimesic and benzenetribenzoic acids. *J.Phys.Chem.C*, 120:6669–6680, 2016.
- [38] M.M. Szortyka, C.E. Fiore, M.C. Barbosa, and V. Henriques. Hydration and anomalous solubility of the Bell-Lavis model as solvent. *Phys.Rev.E*, 86:031503, 2012.
- [39] Y. Gandica, E. Medina, and I. Bonalde. A thermodynamic counterpart of the Axelrod model of social influence: The one-dimensional case. *Physica A*, 392(24):6561–6570, 2013.
- [40] M.E. Tuckerman. *Free energy calculations theory and applications in chemistry and biology*. Springer, New York, 2007.
- [41] R.Q. Topper, D.L. Freeman, D. Bergin, and K.R. LaMarche. Computational techniques and strategies for Monte Carlo thermodynamic calculations, with applications to nanoclusters. In *Reviews in Computational Chemistry*, volume 19, chapter 1. John Wiley & Sons, 2003.
- [42] R.S. Barcikowski and J.P. Stevens. A Monte Carlo study of the stability of canonical correlations, canonical weights and canonical variate-variable correlations. *Multivar.Behav.Res.*, 10(3):353–364, 2010.

- [43] C.E. Fiore. Simulações numéricas de modelos de monocamadas de Langmuir. Master's thesis, Universidade de São Paulo, 2003.
- [44] A.K. Hartmann and H. Rieger. *New optimization algorithms in physics*. Wiley VCH, Germany, 2004.
- [45] B.A. Berg and T. Neuhaus. Multicanonical algorithms for first order phase transitions. *Phys.Lett.B*, 267:249–253, 1991.
- [46] B.A. Berg and T. Neuhaus. Multicanonical ensemble: A new approach to simulate first-order phase transitions. *Phys.Rev.Lett.*, 68:9, 1992.
- [47] W. Janke. Multicanonical Monte Carlo simulations. *Physica A*, 254:164–178, 1998.
- [48] F. Wang and D.P. Landau. Efficient, multiple-range random walk algorithm to calculate the density of states. *Phys.Rev.Lett.*, 86(10):2050–2053, 2001.
- [49] D.J. Earl and M.W. Deem. Parallel tempering: Theory, applications, and new perspectives. *Phys.Chem.Chem.Phys.*, 7:3910–3916, 2005.
- [50] E. Marinari and G. Parisi. Simulated tempering: A new Monte Carlo scheme. *EPL*, 19(6):451–458, 1992.
- [51] A. Valentim, M.G.E. da Luz, and C.E. Fiore. Determining efficient temperature sets for the simulated tempering method. *Comp.Phys.Comm.*, 185:2046–2055, 2014.
- [52] A. Valentim. *Algoritmos de Monte Carlo: Eficiência, adequabilidade e comparação*. PhD thesis, UFPR–Física, Curitiba, 2015.
- [53] M. Mézard, G. Parisi, and R. Zecchina. Analytic and algorithmic solution of random satisfiability problems. *Science*, 297:812, 2002.
- [54] C.P. Gomes and B. Selman. Satisfied with physics. *Science*, 297:784, 2002.
- [55] S. Gogioso. Aspects of statistical physics in computational complexity. 2014.

- [56] M. Finger and G. De-Bona. Probabilistic satisfiability: Logic-based algorithms and phase transition. *Proceedings of the Twenty-Second International Joint Conference on Artificial Intelligence*, page 528, 2011.
- [57] M.A. Arroyo, S. Cannon, J.J. Daymude, D. Randall, and A.W. Richa. A stochastic approach to shortcut bridging in programmable matter. *23rd International Conference on DNA Computing and Molecular Programming (DNA)*, 10467:122–138, 2017.
- [58] D. Gillman and D. Randall. Slow convergence of Ising and spin glass models with well-separated frustrated vertices. In *29th International Conference on Probabilistic, Combinatorial and Asymptotic Methods for the Analysis of Algorithms (AofA 2018)*, volume 110 of *Leibniz International Proceedings in Informatics (LIPIcs)*, pages 24:1–24:17, Dagstuhl, Germany, 2018. Schloss Dagstuhl–Leibniz-Zentrum fuer Informatik.
- [59] M. Mézard and R. Zecchina. The random k-satisfiability problem: from an analytic solution to an efficient algorithm. *Phys.Rev.E*, 66:056126, 2002.
- [60] A. Braunstein, M. Mézard, and R. Zecchina. Survey propagation: an algorithm for satisfiability. *Random Structures & Algorithms*, 27(2):201–226, 2005.
- [61] S. Mertens, M. Mézard, and R. Zecchina. Threshold values of random K-SAT from the cavity method. *Random Structures & Algorithms*, 28(3):340–373, 2006.
- [62] H.T. Davis. *Statistical mechanics of phases, interfaces and thin films*. Wiley VCH, Minnesota, 1996.
- [63] C.L. Wang, J.C. Li, M.L. Zhao, M.I. Marqués, C. Aragó, and J.A. Gonzalo. Monte Carlo simulation of first order phase transitions. *Ferroelectrics*, 401(1):3–8, 2010.
- [64] I.F. Lyuksyutov, V.L. Pokrovskii, and D.E. Khmel'nitskii. Intersection of lines of second-order transitions. *J.Exp.Theor.Phys.*, 42(5):923, 1975.
- [65] R.J. Baxter. *Exactly solved model in statistical mechanics*. Academic Press, San Diego, 1989.

- [66] I. Todoshchenko. Finite-size effects in thermodynamics: Negative compressibility and global instability in two-phase systems. *Phys.Rev.B*, 97:134101, 2018.
- [67] J.W. Cahn and J.E. Hilliard. Free energy of a nonuniform system. i. interfacial free energy. *J.Chem.Phys.*, 28:258–267, 1958.
- [68] R. Evans. The nature of the liquid-vapour interface and other topics in the statistical mechanics of non-uniform, classical fluids. *Adv.Phys.*, 28(2):143–200, 1979.
- [69] B.F. McCoy and H.T. Davis. Free-energy theory of inhomogeneous fluids. *Phys.Rev.A*, 20:1201, 1979.
- [70] S. Puri. Kinetics of phase transitions. *Phase Transit.*, 77(5-7):407–431, 2004.
- [71] P. Papon, J. Leblond, and P.H.E. Meijer. *The physics of phase transitions: Concepts and applications*. Springer, Paris, 2 edition, 2002.
- [72] X. Liang, M.L. Michelsen, and G.M. Kontogeorgis. A density gradient theory based method for surface tension calculations. *Fluid Ph.Equilibria*, 428(25):153–163, 2016.
- [73] X. Liang and M.L. Michelsen. General approach for solving the density gradient theory in the interfacial tension calculations. *Fluid Ph.Equilibria*, 451(15):79–90, 2017.
- [74] D.I. Uzunov. *Introduction to the theory of critical phenomena*. World Scientific, Salerno, 2002.
- [75] M. Schrauth, J.A.J. Richter, and J.S.E. Portela. Two-dimensional Ising model on random lattices with constant coordination number. *Phys.Rev.E*, 97:022144, 2018.
- [76] A.M. Ferrenberg, J. Xu, and D.P. Landau. Pushing the limits of Monte Carlo simulations for the three-dimensional Ising model. *Phys.Rev.E*, 97:043301, 2018.
- [77] L. Onsager. Crystal statistics. i. A two-dimensional model with an order-disorder transition. *Phys.Rev.*, 65:117, 1944.

- [78] R. Guida and J. Zinn-Justin. 3d Ising model: The scaling equation of state. *Nucl.Phys.B*, 489(FS):626–652, 1997.
- [79] D. Sornette. *Critical phenomena in natural sciences. Chaos, fractals, selforganization and disorder: Concepts and tools*. Springer, UCLA and Nice, 2 edition, 2003.
- [80] K. Binder. Theory of first-order phase transitions. *Rep.Prog.Phys.*, 50:783, 1987.
- [81] C.E. Fiore and M.G.E. da Luz. General approach for studying first-order phase transitions at low temperatures. *Phys.Rev.Lett.*, 107:230601, 2011.
- [82] C.E. Fiore and M.G.E. da Luz. Exploring a semi-analytic approach to study first order phase transitions. *J.Chem.Phys.*, 138:014105, 2013.
- [83] C. Borgs and R. Kotecký. A rigorous theory of finite-size scaling at first-order phase transitions. *J.Stat.Phys.*, 61(1/2):79, 1990.
- [84] C. Borgs and R. Kotecký. Finite-size effects at asymmetric first-order phase transitions. *Phys.Rev.Lett.*, 68(11):1734, 1992.
- [85] M. Henkel, H. Hinrichsen, and S. Lübeck. *Non-equilibrium phase transitions. Absorbing phase transitions*. Springer, Würzburg, 2 edition, 2008.
- [86] R.D. Schram and G.T. Barkema. Monte Carlo methods beyond detailed balance. *Physica A*, 418:88–93, 2015.
- [87] C.E. Fiore and M.G.E. da Luz. Comparing parallel- and simulated-tempering-enhanced sampling algorithms at phase-transitions regimes. *Phys.Rev.E*, 82:031104, 2010.
- [88] C.E. Fiore and M.G.E. da Luz. A simple protocol for the probability weights of the simulated tempering algorithm: Applications to first-order phase transitions. *J.Chem.Phys.*, 133:244102, 2010.
- [89] C.E. Fiore. Comparing different protocols of temperature selection in the parallel tempering method. *J.Chem.Phys.*, 135:114107, 2011.

- [90] C.E. Fiore and C.E.I. Carneiro. Obtaining pressure versus concentration phase diagrams in spin systems from Monte Carlo simulations. *Phys.Rev.E*, 76:021118, 2007.
- [91] M.P. Nightingale. Non-universality for Ising-like spin systems. *Phys.Lett.*, 59A(6):486–488, 1977.
- [92] M. Plischke and B. Bergersen. *Equilibrium statistical physics*. World Scientific Publishing, Vancouver, 3 edition, 2006.
- [93] S. Park and V.S. Pande. Choosing weights for simulated tempering. *Phys.Rev.E*, 76:016703, 2017.
- [94] A. Valentim, C.J. DaSilva, and C.E. Fiore. Efficient simulated tempering with approximated weights: Applications to first-order phase transitions. *Comp.Phys.Comm.*, 196:212–220, 2015.
- [95] Ch. Zhang and J. Ma. Comparison of sampling efficiency between simulated tempering and replica exchange. *J.Chem.Phys.*, 129:134112, 2008.
- [96] C. Marcoux, Z. Byington, T.W. Qian, P. Charbonneau, and J.E.S. Socolar. Emergence of limit-periodic order in tiling models. *Phys.Rev.E*, 90:012136, 2014.
- [97] Y. Liu and H. Yan. Modular self-assembly of dna lattices with tunable periodicity. *Small*, 1:327–330, 2005.
- [98] D. Sabo, M. Meuwly, D.L. Freeman, and J.D. Doll. A constant entropy increase model for the selection of parallel tempering ensembles. *J.Chem.Phys.*, 128:174109, 2008.
- [99] D.A. Kofke. On the acceptance probability of replica-exchange Monte Carlo trials. *J.Chem.Phys.*, 117(15):6911–6914, 2002.
- [100] I. Bloch. Quantum gases. *Science*, 319(5867):1202–1203, 2008.
- [101] M. Blume, V.J. Emery, and R.B. Griffiths. Ising model for the λ transition and phase separation in He^3 - He^4 mixtures. *Phys.Rev.A*, 4:1071, 1971.

- [102] J. Sivardière and J. Lajzerowicz. Spin-1 lattice-gas model. iii. tricritical points in binary and ternary fluids. *Phys.Rev.A*, 11:2101, 1975.
- [103] M. Keskin, M.A. Pınar, A. Erdinç, and O. Canko. Multicritical behavior of the antiferromagnetic spin- $\frac{3}{2}$ Blume-Emery-Griffiths model. *Physica A*, 364:263, 206.
- [104] M. Schick and W.-H. Shih. Spin-1 model of a microemulsion. *Phys.Rev.B*, 34:1797, 1986.
- [105] J.M. Kosterlitz. The critical properties of the two-dimensional xy model. *J.Phys.C*, 7:1046–1060, 1974.
- [106] W. Kwak, J. Jeong, J. Lee, and D.-H. Kim. First-order phase transition and tricritical scaling behavior of the Blume-Capel model: A Wang-Landau sampling approach. *Phys.Rev.E*, 92:022134, 2015.
- [107] A. Crisanti and L. Leuzzi. Thermodynamic properties of a full-replica-symmetry-breaking Ising spin glass on lattice gas: The random Blume-Emery-Griffiths-Capel model. *Phys.Rev.B*, 70(1):014409, 2004.
- [108] H. Ez-Zahraouy, L. Bahmad, and A. Benyoussef. Phase diagrams of the Blume-Emery-Griffiths thin films. *Braz.J.Phys.*, 36(2B):557, 2006.
- [109] G.M. Bell and D.A. Lavis. Two-dimensional bonded lattice fluids ii. Orientable molecule model. *J.Phys.A*, 3:568, 1970.
- [110] M. Šimėnas, A. Ibenskas, and E.E. Tornau. Phase transition properties of the Bell-Lavis model. *Phys.Rev.E*, 90:042124, 2014.
- [111] F.Y. Wu. The Potts model. *Rev.Mod.Phys.*, 54:235, 1982.
- [112] A.E. Ferdinand and M.E. Fisher. Bounded and inhomogeneous Ising models. i. specific-heat anomaly of a finite lattice. *Phys.Rev.*, 185:832, 1969.
- [113] G. Chaudhry and J.G. Brisson. Thermodynamic properties of liquid ^3He - ^4He mixtures between 0.15 k and 1.8 k . *J.Low Temp.Phys.*, 155(5-6):235–289, 2009.

- [114] J.A. Souza, Yi-K. Yu, J.J. Neumeier, H. Terashita, and R.F. Jardim. Method for analyzing second-order phase transitions: Application to the ferromagnetic transition of a polaronic system. *Phys.Rev.Lett.*, 94:207209, 2005.
- [115] A. Mitsutake and Y. Okamoto. Replica-exchange extensions of simulated tempering method. *J.Chem.Phys.*, 121:2491, 2004.
- [116] J-Ch.A. d'Auriac and F. Iglói. Phase transition in the 2d random Potts model in the large- q limit. *Phys.Rev.Lett.*, 90:190601, 2003.